The Thesis Committee for Zachary David Webb
Certifies that this is the approved version of the following thesis:

EXPERIMENTAL INVESTIGATION OF

ASR/DEF-INDUCED REINFORCING BAR FRACTURE

Approved by
Supervising Committee:

Oguzhan Bayrak, Co-Supervisor

Jinying Zhu, Co-Supervisor

James O. Jirsa

EXPERIMENTAL INVESTIGATION OF ASR/DEF-INDUCED REINFORCING BAR FRACTURE

by

Zachary David Webb, B.S.C.E.

Thesis

Presented to the Faculty of the Graduate School of

The University of Texas at Austin

in Partial Fulfillment

of the Requirements

for the Degree of

Master of Science in Engineering

The University of Texas at Austin

December 2011

Dedication

To my wife, Lindsay

Acknowledgements

First and foremost, I would like to thank the faculty of the structural engineering department. The wealth of knowledge that one is exposed to through your advice and teachings is truly what makes the program at The University of Texas at Austin so remarkable. I would like to extend a special thanks to the project faculty members: Dr. Folliard, Dr. Zhu, and Dr. Bayrak. In particular, Dr. Bayrak, I would not have been given this extraordinary opportunity without your confidence and support. Your practical approach to structural engineering and your pursuit of simple, straightforward answers will leave a lasting impression on me for years to come. I would also like to thank Dr. Jirsa for his interest in my work and his willingness to participate on my thesis committee.

Additional thanks go to the students and staff at Ferguson Structural Engineering Laboratory. I cannot recall a time when someone was not around to lend a much needed helping hand. Special thanks to project team members, Kerry Kreitman and Eric Giannini, for their contributions to all aspects of the experimental research. In addition, I would like to thank Dean Deschenes for his invaluable technical knowledge and his enthusiasm to assist me along the way. Finally, the laboratory staff members deserve special mention. The dedication of Blake Stassney, Dennis Fillip, Andrew Valentine, Eric Schell, Mike Wason, Barbara Howard, and Jessica Hanten is what keeps the lab running and operating safely and smoothly.

Lastly, I would like to thank my friends and family. My work is a direct reflection of your love and support. To my best friend and wife, Lindsay, your love and encouragement will always give me the drive that I need to succeed.

August 18, 2011

EXPERIMENTAL INVESTIGATION OF ASR/DEF-INDUCED REINFORCING BAR FRACTURE

Zachary David Webb, M.S.E
The University of Texas at Austin, 2011
SUPERVISORS: Oguzhan Bayrak, Jinying Zhu

Numerous cases of premature concrete deterioration due to alkali-silica reaction and/or delayed ettringite formation have developed within highway infrastructure in the state of Texas over the past two decades. Although experimental research and in-situ load testing on an international scale has indicated that moderate levels of deterioration are unlikely to pose a threat to structural safety, the discovery of reinforcing bar fracture in Japan due to ASR-related expansion has called into question the integrity of heavily damaged structures.

A two-part experimental program was conducted at The University of Texas at Austin relating to ASR/DEF-induced reinforcing bar fracture. Work conducted under TxDOT Project 0-6491 included the fabrication and monitoring of four concrete specimens. Methods were employed to simulate a fracture of the transverse reinforcement within the time frame of the study and the applicability of various NDT monitoring techniques to detect bar fracture was evaluated. Furthermore, a number of reinforcing bar samples were tested and analyzed to investigate (1) the development of reinforcing bar cracking due to the bending operation and (2) the progression of cracks after application of an expansive opening force on bars with 90° bends. Research findings and conclusions form a preliminary assessment on the potential for reinforcing bar fracture within affected infrastructure in Texas.

Table of Contents

List of Tables

List of Figures

CHAPTER 1
Introduction

1.1 MOTIVATION

Numerous occurrences of alkali-silica reaction (ASR) and/or delayed ettringite formation (DEF) over the past two decades are responsible for premature concrete deterioration within highway infrastructure in the state of Texas. The Texas Department of Transportation (TxDOT) has sponsored a number of research efforts, both in-house and through funding of university research programs, to address materials specifications and resolve the issue of ASR/DEF in new concrete construction. However, the evaluation and maintenance of existing deteriorated structures is of further concern for TxDOT bridge engineers.

Appropriately, multiple research programs have been conducted to establish the structural implications of ASR/DEF deterioration. Primarily, recent research conducted at The University of Texas at Austin has focused on the potential loss in shear and flexural capacity of reinforced concrete members with ASR/DEF-related damage. Preliminary results from these studies, in agreement with additional laboratory research and in-situ load testing of field structures throughout the world, have indicated that the deterioration mechanisms are unlikely to pose a threat to structural safety. However, the discovery of ASR-induced brittle reinforcing bar fracture within deteriorated structures in Japan (Figure 1-1) has called into question the integrity of heavily damaged structures. Thus, an assessment of the potential for reinforcing bar fracture is critical for the evaluation of ASR/DEF-affected infrastructure within Texas.

Figure 1-1: Examples of ASR-Induced Reinforcing Bar Fracture in Japan (Torii et al. 2008)

1.2 OBJECTIVES AND SCOPE

The primary objectives of the experimental work contained in this thesis are: (1) to investigate the use of various non-destructive test (NDT) methods in the evaluation process of existing deteriorated structures and (2) to assess the potential for ASR/DEF-induced reinforcing bar fracture within affected infrastructure. Two independent, yet related, experimental programs were conducted at Ferguson Structural Engineering Laboratory to carry out the aforementioned goals.

Research conducted under TxDOT Project 0-6491 included the use of several non-destructive test (NDT) methods on a variety of test specimens deteriorated by ASR and DEF. Specific to the task at hand, four reinforced concrete specimens, representative of a segment from the large-scale bent cap specimens to be tested as part of Project 0-6491 (see Kreitman (2011) for details relating to large-scale specimens) were constructed and monitored throughout this study. The potential of each NDT technique to detect the loss in confinement through the fracture of transverse reinforcement in a single reinforced concrete specimen was evaluated (Objective 1).

Furthermore, an extensive review of background material highlighted the discovery of ASR-induced bar fracture in Japan and an evaluation of the circumstances that led to the development of such fractures. A comparison of reinforcing bar standards from the United States and Japan formed the basis for an additional experimental study. The reinforcing bar bend tests program was conducted to assess the potential for bar fracture within existing deteriorated structures (Objective 2).

1.3 THESIS ORGANIZATION

Following this brief introduction, a thorough review of relevant background material is presented within Chapter 2. First, a description of the two concrete deterioration mechanisms (i.e. ASR and DEF) is presented. The behavior of reinforced concrete beams affected by ASR/DEF is discussed, and the role of confinement reinforcement in the maintenance of structural capacity is emphasized. Attention is then diverted toward topics relating to the discovery of reinforcing bar fracture within Japan. A review of field investigations and laboratory studies contained in the literature are analyzed, and the presumed mechanisms of ASR-induced reinforcing bar fracture are highlighted. An initial evaluation of the potential for such fractures in existing deteriorated infrastructure is assessed through a comparison of reinforcing bar standards within the United States to the Japanese standards. Finally, a brief background of the NDT techniques evaluated during monitoring of the concrete specimens, and the parameters measured from each, is provided.

Experimental methods relating to the concrete *beam segment* specimens is outlined in Chapter 3. First specimen design is presented, followed by details of the fabrication process. A discussion of the experimental methods used to trigger rapid development of concrete deterioration is provided. The use of various monitoring techniques throughout the experimental program are examined. Finally, the procedures used to simulate ASR/DEF-induced bar fracture of a transverse stirrup is examined. All measurements and observations made during the study of the concrete specimens are discussed in Chapter 4.

Chapter 5 includes an overview of the experimental reinforcing bar bend tests. Two different series of bend tests were produced to investigate (1) the development of cracking during the bending process and (2) the progression of cracking after a simulated ASR/DEF-induced opening force on 90° bends at stirrup corners. Selection of test variables and testing procedures are provided in detail. Observations from the reinforcing bar tests and a discussion of the effects of each test variable on the results obtained are presented in Chapter 6.

In Chapter 7, a summary of the work reported in this thesis is presented. Research findings and conclusions made from the independent experimental programs conducted during the course of this research study are summarized.

CHAPTER 2
Background

2.1 OVERVIEW

An examination of previous research relating to the effects of alkali-silica reaction (ASR) and delayed ettringite formation (DEF), in a structural context, is presented in this chapter. In addition, a critical evaluation of Japan's experiences with ASR-induced reinforcing bar fractures is presented. The topics reviewed will assist in an assessment of the potential for ASR/DEF-induced reinforcing bar fracture and will form the basis for the experimental research programs in the remainder of this thesis.

The organization of this chapter is as follows: A summary of the chemical and physical processes of the premature concrete deterioration (PCD) mechanisms of ASR and DEF are presented first. The effects of ASR/DEF on the behavior of reinforced concrete beams are then considered. In particular, the role of confining reinforcement in the maintenance of structural integrity is explored. Details pertaining to the discovery of reinforcing bar fracture in Japan are then reviewed and constitute the majority of the background material. Relevant literature is reviewed to provide a description of the presumed mechanisms of bar fracture. Next, a comparison of the reinforcement standards within Japan and the United States is presented to aid in the assessment of potential PCD-induced bar fracture. Finally, a brief explanation of the parameters measured from non-destructive test (NDT) monitoring of the concrete specimens is provided.

2.2 PREMATURE CONCRETE DETERIORATION MECHANISMS

The chemical and physical processes of alkali-silica reaction (ASR) and delayed ettringite formation (DEF) are reviewed in this section. A limited summary is provided only to establish a background of the premature distress mechanisms. A more detailed explanation of the deterioration mechanisms and processes can be found in TxDOT Project 0-4085 technical report.

2.2.1 (ASR) Alkali-Silica Reaction

ASR, a common form of alkali-aggregate reaction (AAR), is a chemical reaction that occurs in concrete that, when advanced, results in severe concrete cracking. The mechanisms of the reaction are illustrated in Figure 2-1. Initially, hydroxyl ions in the cement pore solution react with certain forms of silica in the aggregate. The resulting alkali-silicate gel forms on the surfaces of the aggregate. The gel will expand if a sufficient supply of moisture is available until the tensile strength of the material is reached, resulting in internal micro-cracking. As the deterioration progresses throughout the cement paste and aggregate, the reaction can self-propagate and produce bulk expansion of the concrete and a network of surface cracking.

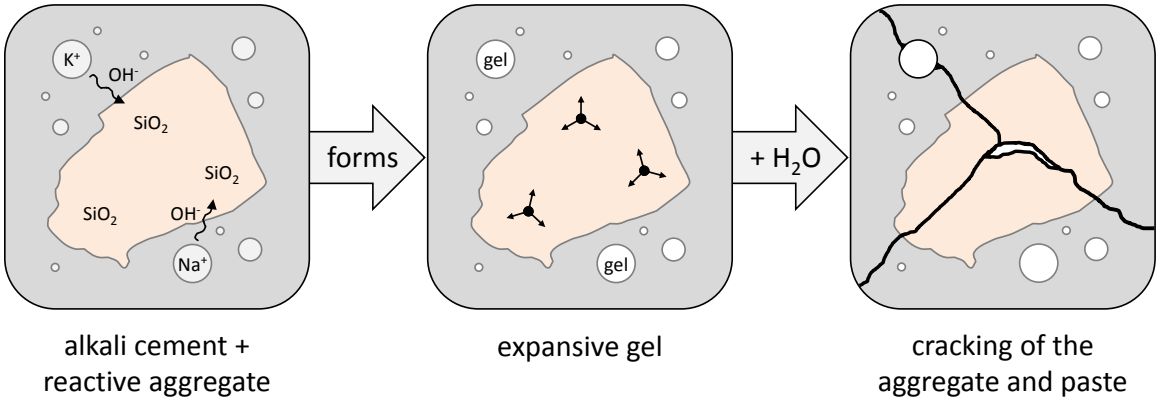

Figure 2-1: Alkali-Silica Reaction (Deschenes 2009)

The development of ASR-induced expansion is dependent on three conditions: (1) a reactive form of silica is available within the aggregate, (2) sufficient supply of alkalis are present in the cement pore solution, and (3) a sufficient supply of moisture is present

in the hardened concrete. Efforts to prevent ASR in new concrete, and arrest the development in damage structures, are focused primarily on preventing any of the three conditions. Additionally, the use of supplementary cementing materials (SCMs) in appropriate mix proportions has been shown to prevent the development of ASR in new concrete through modification of the hydration processes (Folliard et al. 2006).

2.2.2 (DEF) Delayed Ettringite Formation

Delayed ettringite formation is an alternate distress mechanism that can result in concrete expansion and cracking. The development of DEF, depicted in Figure 2-2, is, however, a different chemical process than ASR. The formation of ettringite, a natural product of a reaction between sulfates and aluminates that occurs during cement hydration, is hindered when curing temperatures exceed 158°F (70°C). Instead, the high temperatures trap the sulfates and aluminates within the hydration products. Over time, the constituents diffuse out into the pore solution of the hardened cement paste to react and form ettringite. The re-formation of ettringite produces expansion of the cement paste and the development of cracks within the hardened concrete.

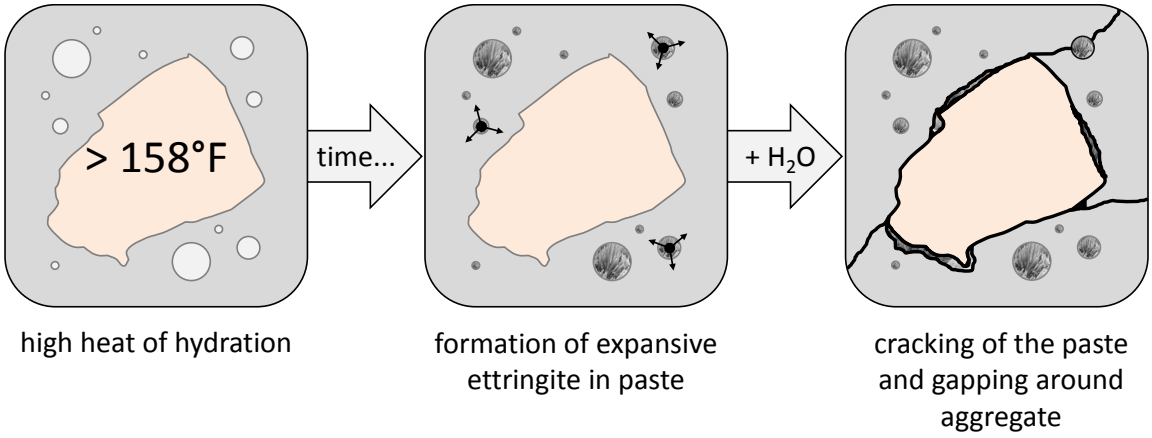

Figure 2-2: Delayed Ettringite Formation (Deschenes 2009)

The possibility for damaging DEF is dependent on (1) early curing temperatures in excess of 158°F (70°C) for an extended period of time and (2) the availability of sufficient moisture in the hardened concrete to allow for the development of ettringite.

Prevention of late ettringite is accomplished by limiting the curing temperature below the DEF threshold. Similarly, the proper proportions of SCMs in the fresh concrete mixture can prohibit delayed ettringite formation (Folliard et al. 2006).

Up to this point, the two distress mechanisms have been discussed independently. However, it should be acknowledged that the development of both ASR and DEF distress often coincide in actual structures. Additionally, the deleterious effects of each (bulk expansion of the concrete body and cracking at the concrete surface) are indistinguishable from the perspective of a structural engineer and no distinction will be made between the two mechanisms for the remainder of this thesis.

2.3 THE BEHAVIOR OF REINFORCED CONCRETE BEAMS AFFECTED BY ASR/DEF

Damaging ASR and DEF lead to internal microcracking, expansion of the concrete core, and eventually severe cracking on the concrete surface. As a result, the mechanical properties (i.e. compressive strength, modulus, tensile strength) of the material are typically reduced, and it has been widely assumed that ASR/DEF-induced expansion and cracking is related to a loss in structural capacity. In most cases, however, results of laboratory studies and in-situ load tests have indicated that the structural integrity of ASR/DEF affected beams is not seriously compromised.

Deschenes et al. (2009) conducted an extensive literature review of experimental research over the last three decades, to give an explanation for the behavior of reinforced concrete beams in both flexure and shear affected by ASR/DEF (reference TxDOT technical report No. 12-8XXIA006 for further details). Of the 144 laboratory tests summarized, failure loads of the damaged beams were 0.93 to 1.47 times the measured capacities of the undamaged beams. In addition, the stiffness of many of the damaged beams was unchanged relative to that of the undamaged specimens.

Moreover, Deschenes et al. (2009) constructed six-large-scale reinforced concrete specimens in an effort to establish a relationship between in-situ deterioration and nominal shear capacity of affected bridge bent caps. Three of the specimens (one non-reactive and two reactive, representing undamaged to moderate levels of deterioration)

were tested in shear after an extended exposure period and load conditioning. In agreement with observations made during the literature review conducted by Deschenes et al. (2009), the shear strength of the damaged specimens was not compromised by ASR/DEF distress.

The behavior of ASR/DEF affected beams (little to no loss in strength and stiffness) is a result of the confinement provided by the stressed reinforcement as illustrated in Figure 2-3. As the hardened concrete expands, the confining reinforcement is actively engaged as significant tensile strains (and stresses) are generated. The tensile forces within the reinforcement are equilibrated by compression in the concrete, resulting in a multi-axial state of compression within the concrete core. The ASR/DEF-related confining stresses are analogous to prestressing the affected beam. The imposed compression compensates for the loss in material properties due to microstructural damage (i.e. internal microcracking), and the strength and stiffness of the damaged beam are largely unaffected.

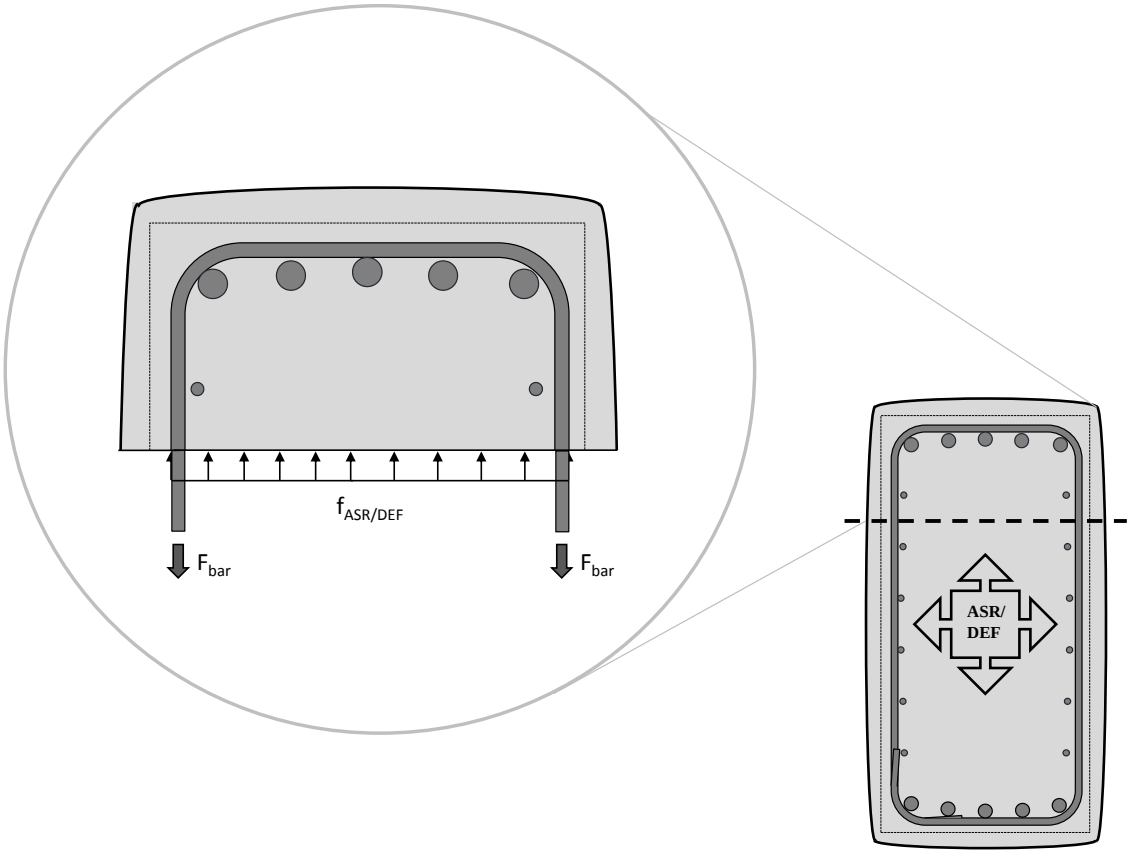

Figure 2-3: ASR/DEF-Induced Confining Stresses

It should be acknowledged that this discussion is limited to the behavior of conventionally reinforced concrete beams, properly detailed to avoid undesirable anchorage or bearing failure. Additionally, beams unreinforced in shear are excluded from this discussion because the lack of transverse reinforcing would result in a rapid deterioration of the unconfined concrete. Similarly, "the loss of confinement through fracture of the reinforcement, [as experienced in Japan (see Section 2.4)], would lead to a rapid deterioration of the structural core and unquestionable loss of structural safety (Deschenes et al. 2009)."

2.4 REINFORCING BAR FRACTURE IN JAPAN

In 1979, routine inspections of bridge piers on the Hanshin Expressway in Japan revealed surface cracking indicative of premature concrete deterioration. Large cracks (approximately 0.2 inches wide) were discovered in 1982 and subsequent inspections exposed over 100 bridge piers, mostly constructed in the 1970s and 1980s, that were damaged by alkali-silica reaction. Nationwide investigations, including in-situ load tests of damaged bridge piers in 1984, concluded that ASR damage did not significantly affect the structural performance (Clark 1989). Subsequent work was focused on measures to mitigate ASR damage and repair affected structures. In particular, application of surface coatings and treatments as well as crack injection was employed to prevent moisture penetration and arrest the development of ASR damage.

In the late 1990s and early 2000s fractured reinforcing bars were discovered in a number of highway and railway structures in Japan with 20 to 30 years of continuous ASR damage. In many cases the structures had been previously repaired with surface coatings and treatments; however, repairs failed to halt ASR-induced expansions. The discovery of reinforcing bar fractures led Japanese researchers to reevaluate their assessment of ASR damaged structures and the impact on structural safety.

> *As long as reinforcing steels are not broken due to ASR-caused expansion, the safety of a structure is considered not to be seriously compromised. However, the safety of a structure becomes questionable when the confinement of the concrete becomes degraded due to fracture of reinforcing steel bars (Miyagawa 2006).*

The Japan Society of Civil Engineers (JSCE) launched a task force in 2003 to investigate (1) the scope of ASR-induced reinforcing bar fractures, (2) to determine the mechanisms of the fractures, (3) to assess the safety of structures with fractured reinforcing steel, and (4) to evaluate repair and strengthening measures. Sections 2.4.1 and 2.4.2 summarize the results from an extensive literature search of field investigations and laboratory studies aimed at determining the causes and mechanisms of ASR-induced reinforcing bar fracture.

2.4.1 Field Investigations

2.4.1.1 Kubo et al. (2003)

Kubo et al. investigated a 5 m wide by 1.8 m thick by 5 m long (16.4 ft x 5.9 ft x 16.4 ft) strip footing of a 20 year old bridge pier. The pier had previously been repaired with surface treatments to mitigate damage to the superstructure resulting from alkali-silica reaction. Excavation of the footing revealed extensive surface cracking and a "large gap" running horizontally the full length of the footing. Chipping back the cover concrete along the gap exposed fractures at the bent portion of all D16 (No. 5) top bars (Figure 2-4).

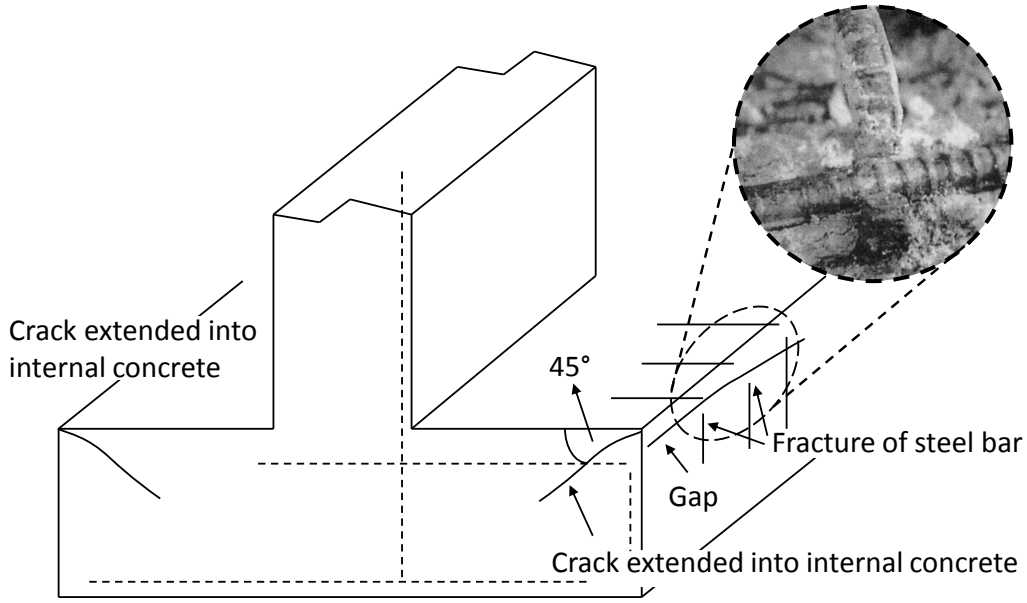

Figure 2-4: Condition of Damaged Footing and Associated Bar Fracture (Adapted from Kubo et al. 2003)

The bar fracture surface indicated a brittle fracture. The fractures occurred at a location on the footing with very low stress in the steel bars under loading from the pier. In addition, a lack of corrosion products on the steel bars was observed. Investigators hypothesized that the brittle reinforcing bar fractures were due to a prolonged period of ASR activity that induced concentrated tensile stresses at the bent portion of the bar.

Model specimens of the footing were constructed in the laboratory to confirm the hypotheses (Section 2.4.2.1).

2.4.1.2 Nomura et al. (2004)

In 2000, fractures at the bent portion of D32 (No. 10) primary longitudinal reinforcing steel were discovered during repair work of a railway bridge pier. The T-shaped pier, illustrated in Figure 2-5, had experienced significant ASR damage since construction in 1974. Subsequent inspections of structures along the railway viaduct with similar cracking patterns revealed five additional piers with fractured bars. In total, 168 of the 228 bars inspected were fractured at the bend. The condition of the fracture surface was similar to that reported by Kubo et al. (i.e. brittle surface, minimal corrosion product). Nomura et al. recognized that the initiation point of the fracture was located on the inside of the bend. Reinforcing bar samples were taken from the structure and analyzed to investigate the cause of fracture (Section 2.4.2.2).

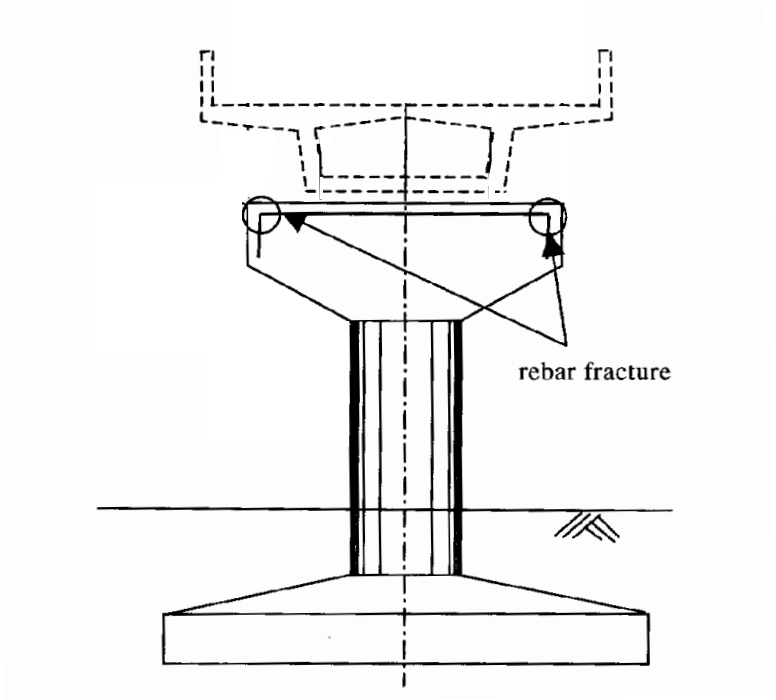

Figure 2-5: Location of Fractured Longitudinal Reinforcing (Nomura et al. 2004)

2.4.1.3 Miyagawa et al. (2006)

Miyagawa reported 30 highway and railway structures in Japan, damaged by alkali-silica reaction, confirmed to have reinforcing bar fractures. A reactive aggregate prone to volumetric expansion was used in the concrete mixture for all of the structures. No distinction was made as to the location on the structures of the fractures (i.e. beam, column, footing); however, "fractures occurred at many bent sections of steel bars in pier beams, and similar cases have been reported to occur in footings" (p. 339). Additionally, the severity of fractured bars increased at locations with direct access to moisture (such as a pier cap directly under a bridge deck joint) and sections with low reinforcement ratios.

As a case example of reinforcing bar fracture, Miyagawa reported on the precast beam of a T-shaped pier with fractured stirrups shown in Figure 2-6. The pier was constructed in 1979 and had been repaired with surface coatings twice, once in 1989 and again in 1992, after ASR-induced surface cracking continued to develop. A 1999 inspection revealed wide cracks running parallel to the longitudinal reinforcement and after chipping back the corner concrete fractured stirrups were discovered. The fractures were brittle in nature (no reduction in cross section) and occurred exclusively at the bent portion of the stirrups. Stirrup fracture was more likely where the transverse reinforcement ratio was "low". Further investigation exposed fractures at the bent portion of the longitudinal reinforcement at the pier ends, where exposure to moisture was also severe.

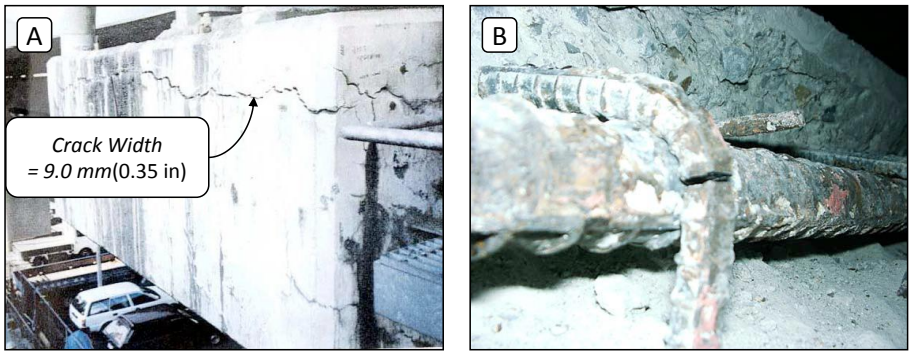

Figure 2-6: (A) Example of Pier Damage (B) Fracture of Reinforcing Bar (Miyagawa et al. 2006)

2.4.1.4 Daidai & Torii (2008)

Daidai and Torii investigated heavily deteriorated concrete piers of a seven span bridge to determine the degree of reinforcing bar fracture and develop an appropriate repair procedure. The piers, constructed in 1972, were repaired in 1989 using epoxy crack injection and waterproofing coating. Within five years the surface coating was cracked on two piers at locations where the deck drained directly onto the concrete piers, providing for a supply of water required for continuous ASR deterioration. Figure 2-7 shows the condition of one heavily damaged pier, with confirmed bar fractures, before the concrete cover was removed for the investigation.

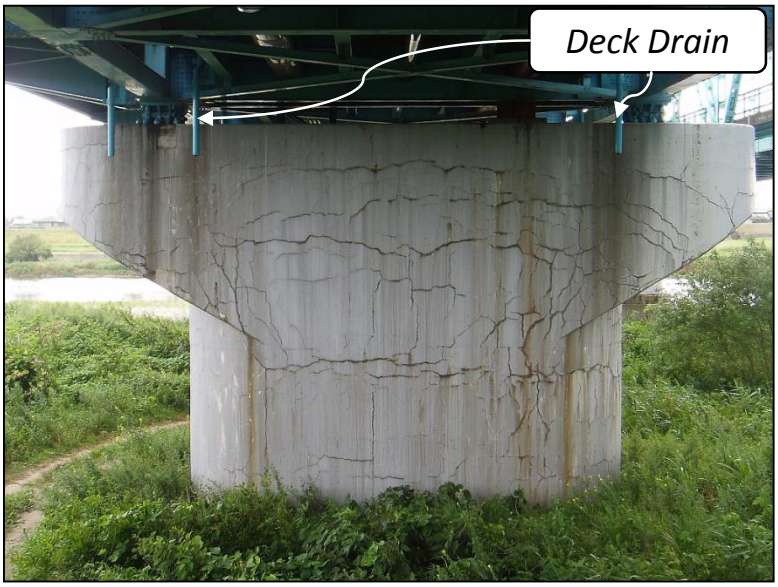

Figure 2-7: Heavily Damaged Bridge Pier with Confirmed Reinforcing Bar Fractures (Daidai and Torii 2008)

Fracture percentages as high as 43% for the D16 (No. 5) stirrups and 63% for the primary longitudinal steel bars were discovered after demolition of the bent cap. Although several bars were damaged during demolition work, it was concluded that the majority of the characteristic brittle fractures occurred due to ASR-induced expansive forces. The highest percentage of fractures occurred along the beam soffits under the deck drains. Unfortunately, details of the reinforcement (reinforcement ratio, type,

bending radius, etc.) were not reported; however, it was reported that all fractures occurred at a 90° or 135° bend.

2.4.1.5 Torii et al. (2008)

Torii et al. conducted a large scale investigation of 19 bridge piers on the Noto Expressway in Japan with moderate to severe levels of ASR deterioration. A reactive coarse aggregate prone to high volumetric expansion was used in the construction of the approximately 30 year old concrete highway structures. Fractures were discovered at the bent portion of reinforcing bars in 13 of the 19 affected bridge piers at locations where cracks as large as 5 mm (0.2 inches) were discovered. In addition, bar fractures tended to occur in "structural element[s] with a low reinforcement ratio" (p.1141).

A flat and smooth fracture surface with no reduction in cross section and little to no products of corrosion were a typical feature of the inspected bars. Torii et al. described the fracture mechanism as a three stage process (see Figure 2-8 for a description of process). First an initial crack formed on the inside of the bar at the base of a deformation during bending. Second, the initial crack progressed due to the tensile stresses induced at the bend by ASR expansion and the altered mechanical properties of the steel due to cold bending (i.e. strain aging, residual stresses). Finally, the second stage of cracking developed and eventually the steel bar fractured under the continuous application of tensile stresses due to ASR expansion. Torii concluded that reinforcing bar fractures resulting from ASR deterioration can only occur when the reinforcing steel is initially cracked during bending.

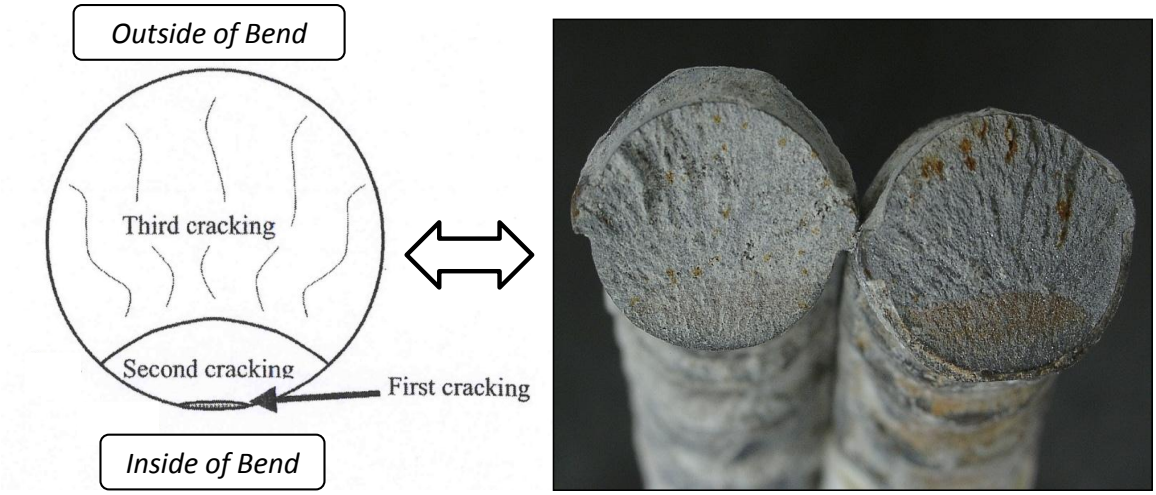

Figure 2-8: Three-Stage Process of Brittle Reinforcing Bar Fracture (Adapted from Torii et al. 2009 and Daidai and Torii 2008)

2.4.2 Laboratory Studies

2.4.2.1 Kubo et al. (2003)

Motivated by field investigations of a damaged bridge pier footing with fractured reinforcing bars (Section 2.4.1.2), Kubo et al. constructed three scaled model footings, using an expansive concrete mix, to investigate the relationship between concrete strain and the strain along reinforcing bars. Details of the 0.3 m wide by 0.3 m high by 0.9 m long (1.0 ft x 1.0 ft x 3.0 ft) specimens are included in Figure 2-9. The area of top steel was varied between the three specimens so that the reinforcement ratios in the axial direction were 0.4%, 0.5%, and 0.6%. Concrete mixture proportions included the use of a reactive volcanic coarse aggregate and the addition of sodium hydroxide ions to maximize alkali-silica reactivity. After initial curing, the specimens were located outdoors for exposure to the environment.

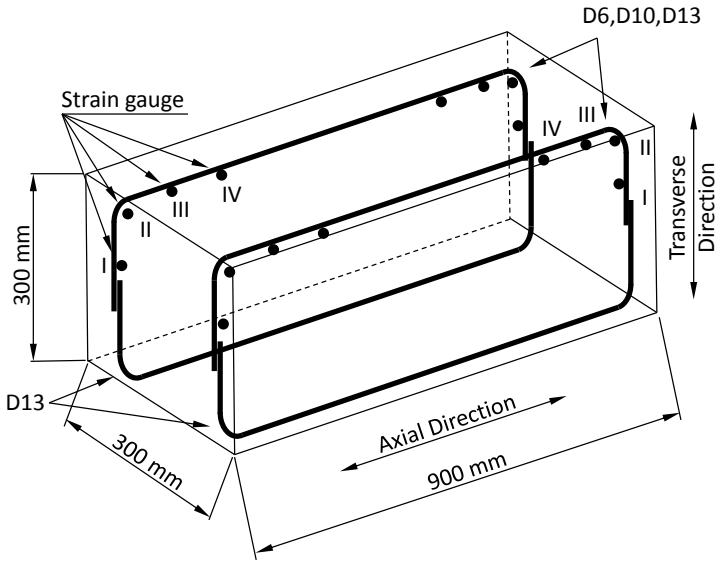

Figure 2-9: Details of Laboratory Specimen (Adapted from Kubo et al. 2003)

Steel strains were measured at four points along the length of the bar, denoted I, II, III, and IV in Figure 2-9, using strain gauges attached to the inside of the reinforcement. Strains were reported after 160 days of exposure. Steel strain measurements at gauge point II indicated that ASR induced concrete expansions resulted in large tensile forces at the bend of the reinforcing bars. Regardless of the reinforcement ratio, the steel strain at the bend exceeded the yield point; while away from the bend in both the axial and transverse directions the steel was not yielded. Kubo et al. concluded that the tensile strains imposed at the bend due to ASR expansion, combined with altered bar properties as a result of the bending operation (see Section 2.5), were the cause of the fractured reinforcing bars in the bridge pier footings.

2.4.2.2 Nomura et al. (2004)

Nomura et al. removed D32 (No. 10) reinforcing bar samples from a damaged bridge pier (Section 2.4.1.2) for inspection and analysis to investigate the cause of fracture. Chemical composition of the samples indicated no "abnormality in its ingredient" and the requirements of the Japanese Industrial Standard (JIS) for reinforcing bar composition were satisfied. Additionally, results from tensile testing were well

within acceptable limits of JIS standards. Results from the materials tests provided no evidence of deficiencies in the mechanical properties.

Inner radius measurements of the bent portion of the bar samples were 15 to 40 percent smaller than the minimum bending radius allowed by JIS standards. Microscopy of the fractured surface revealed intense deformations and plastic flow on the interior of the bent bars. The hardness of the steel samples, from Vickers hardness testing, was significantly greater on the inside portion of the bar near the fractured surface. It was concluded that the ASR-induced steel fractures were an effect of "weakened" steel at the bent portion of the bar as a result of the bending operation.

2.4.2.3 Miyagawa et al. (2006)

Miyagawa et al. summarized a number of reinforcing bar materials tests aimed at investigating the cause of bar fracture in structures due to ASR. D16 (No. 5) reinforcing bar samples (Grade SD295A equivalent to 40ksi yield strength) were obtained from damaged structures for comparison with newer, identical samples from the same manufacturer. The materials tests considered the effects of bending and of delayed deterioration (e.g. strain ageing, stress corrosion, and hydrogen embrittlement) as influential in fracturing the bars.

Results of the materials testing suggested that the development of cracking at the base of the deformations during bending was the most significant factor that influenced the sensitivity to reinforcing bar fracture. Cracking only occurred when samples were bent around a pin with a radius equal to the diameter of the bar and/or on bars taken from the damaged structures. Researchers proposed the mechanisms of Figure 2-10 to explain the cause of reinforcing bar fracture in structures heavily deteriorated due to ASR.

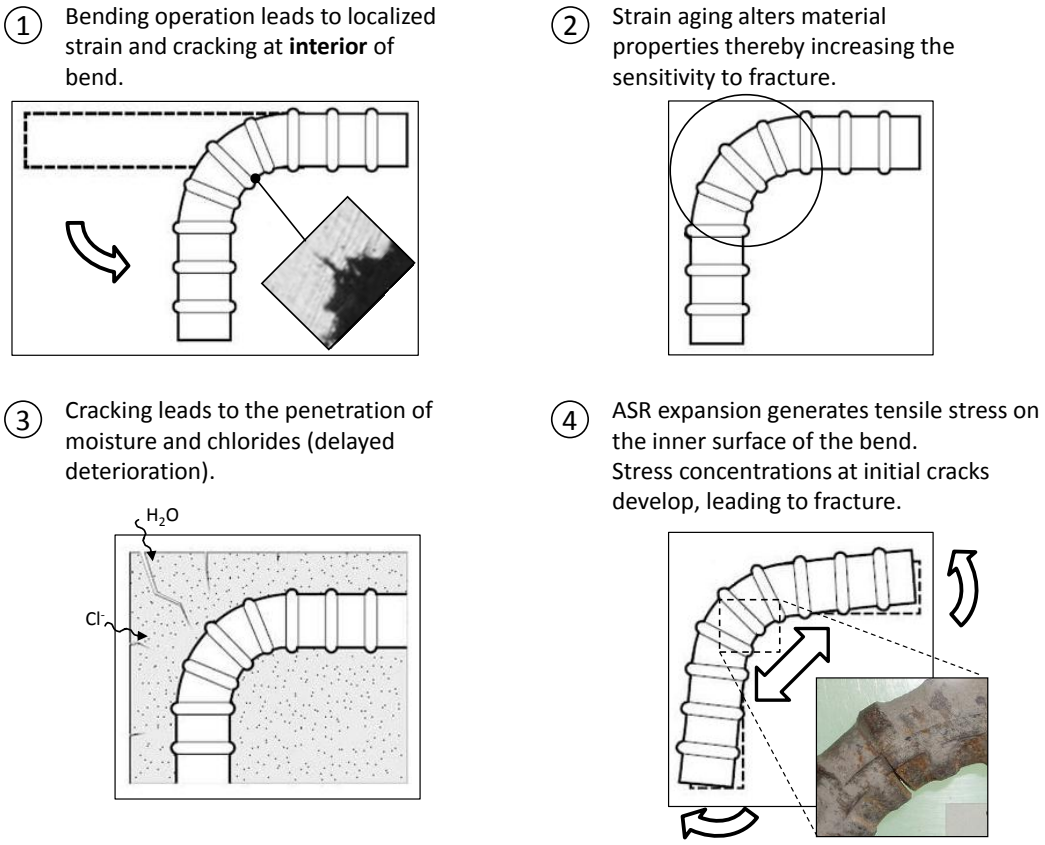

Figure 2-10: Presumed Mechanism of Reinforcing Bar Fracture (Adapted from Miyagawa et al. 2006 and Daidai and Torii 2008)

2.4.2.4 Kawashima et al. (2008)

Kawashima et al. constructed scaled specimens of a bridge pier in an effort to simulate brittle reinforcing bar fracture in the laboratory. Specimens were made using a highly expansive mortar that was poured into a blocked out internal cavity to simulate ASR-induced core expansions. The effects of bar type (bars from the damaged structure referred to as old bars vs. modern bars), bar size, bending radius, and corrosiveness of the environment were investigated to verify mechanisms of fractured reinforcing bars.

The development of cracking on the reinforcing bars was assessed by comparing crack depth measurements immediately after bending with the depth of cracks after progressive expansion. Experimental results revealed that the old-type bars were

particularly prone to cracking during bending because the radius at the base of the rolled on deformations was much smaller than the more modern bars. The progression of crack development was considerably larger for bars bent to small bend diameter (on the order of one times the bar diameter) and from bars taken from the damaged structure. The effect of bars placed in a corrosive environment had no impact on the development of reinforcing bar cracking.

Additionally, one of the bars fractured during the course of the experiment in a brittle fashion, similar to bar fractures discovered in existing structures. Kawashima et al. concluded that the processes responsible for the fracture of the reinforcing bars are as follows: "1) the generation of large initial cracks during bending, influenced by the use of old-type reinforcing bars and small bending radii, 2) embrittlement caused by strain aging, and 3) the development of cracks by the application of expansive pressure (2008)."

2.5 THE EFFECTS OF BENDING REINFORCING BARS

The background of Japanese field and laboratory investigations provided insight on the mechanisms of brittle reinforcing bar fracture. It was found that the formation of initial cracks during bending developed into a brittle fracture after decades of ASR-induced tensile forces at the bend. The effects of bending reinforcing bars are reviewed here to provide further explanation of the fracture mechanisms discovered within the Japanese investigations. The discussion provided in this section is largely a summary of work conducted in New Zealand by Erasmus (1981). Erasmus's work was conducted after numerous cases of brittle reinforcing bar fracture occurred during construction as a result of re-straightening previously made design bends.

As illustrated in Figure 2-11, when a reinforcing bar is bent the outside of the bend is elongated and the inside of the bend is compressed. Moreover, the contact of the transverse ribs with the bending pin flattens the inside ribs. This effectively decreases the radius between the bar and the deformations at the rib base and results in large stress concentrations. When the bending radius is small, sharp notches at the base of the inside ribs can form and, in an extreme case, will result in the formation of compression cracks.

The likelihood of crack formation is dependent on the bar size, the bending radius, and the rib geometry.

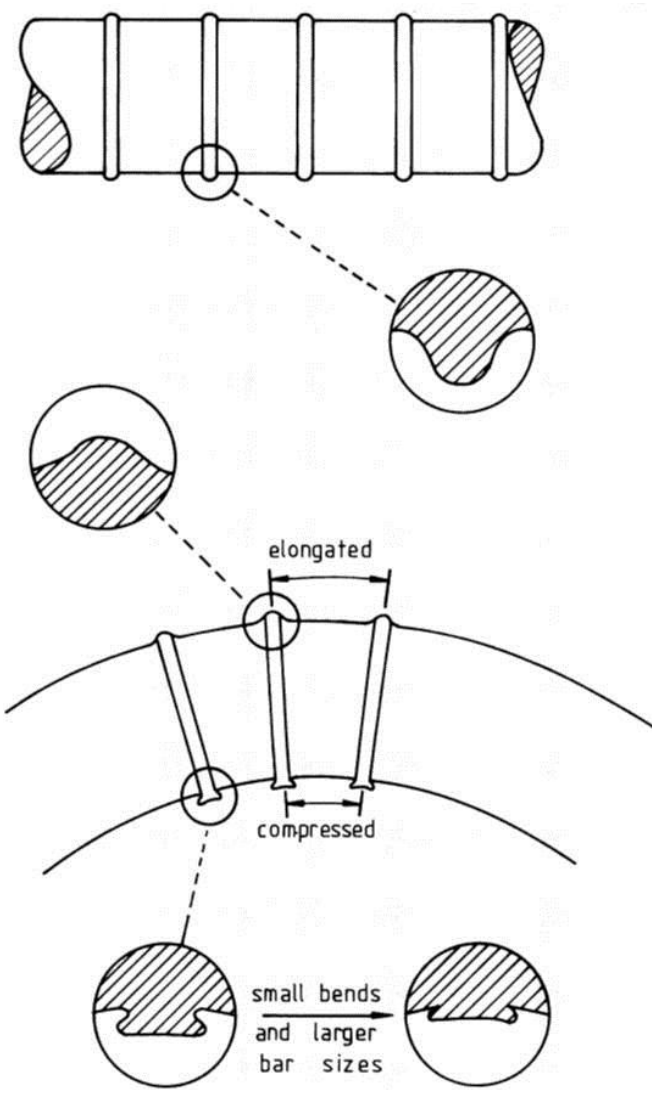

Figure 2-11: Change in Rib Geometry from Bending (Erasmus 1981)

Over a period of time when the bent portion of the bar is subjected to tensile forces, such as those induced by ASR, localized plastic straining occurs at the base of these sharp notches and the mechanical properties of the steel are altered. This phenomenon, referred to as strain aging, is a result of straining the steel into the plastic

range during bending (i.e. permanently deforming the bar) and is a property of low carbon steel. These property changes can be further divided into strain age hardening and strain age embrittlement. Strain age hardening results in an increase of the tensile strength of the steel and a reduction in ductility after the steel has been plastically deformed and then "aged". The ageing process continues even after the reinforcing bar is embedded in concrete. Strain age embrittlement refers to a transition of the failure mode from one that is predominately ductile to a brittle one and is a function of the stress state and the strain rate (Erasmus 1981). Combined with the formation of initial cracks during the bending operation, the manifestation of ASR-induced tensile forces at the "weakened" bent portion of the bar can lead to the development of brittle reinforcing bar fracture.

2.6 COMPARISON OF REINFORCING BAR STANDARDS

A comparison of the material and design standards for Japanese and American reinforcing bars are summarized here to aid in the assessment of the potential for bar fracture within highway infrastructure affected by ASR and/or DEF in Texas (and United States). In addition, the provisions reviewed here will serve as the basis for the selection of test variables in the experimental reinforcing bar bend tests (Chapter 5 & 6).

2.6.1 Material Standards

2.6.1.1 Mechanical Properties

In the United States the exclusive use of Grade 60 reinforcing steel is quite common in reinforced concrete construction. In Japan, however, the use of a reinforcing steel equivalent to Grade 40 is more commonly used in substructures and as stirrups and ties. A comparison of the mechanical properties for both Grade 40 and Grade 60 reinforcement and the Japanese counterpart is summarized in Tables 2-2 and 2-3, respectively. For each respective type of steel the Japanese standards require slightly stronger and much more ductile steel. Primarily, this is due to the fact that the chemical composition of the Japanese steel more closely resembles steel manufactured under

ASTM A706 (2009) within the United States. Regardless, the comparison suggests that the weaker and less ductile steel from the U.S. would be more prone to develop a crack during bending and eventually fracture, as it is less deformable.

Table 2-1: Mechanical Properties of Grade 40 Reinforcement or Equivalent

Standard	Type	Grade 40 Reinforcement or Equivalent		
		Yield Strength Min.	Tensile Strength Min.	Elongation Min.
JIS G 3112:2004	SD295A	42.8 ksi	63.8 to 87.0 ksi	16.0 %
ASTMA615:2009	GR40	40.0 ksi	60.0 ksi	11.0 % (No. 3) 12.0 % (No. 4-6)

Table 2-2: Mechanical Properties of Grade 60 Reinforcement or Equivalent

Standard	Type	Grade 60 Reinforcement or Equivalent		
		Yield Strength Min.	Tensile Strength Min.	Elongation Min.
JIS G 3112:2004	SD390	56.6 to 74.0 ksi	81.2 ksi	16.0 %
ASTMA615:2009	GR60	60.0 ksi	90.0 ksi	9.0% (No. 3-6) 8.0% (No. 7-8) 7.0% (No. 9-11)

2.6.1.2 Geometric Properties

A crucial factor of the fracture mechanisms proposed in the Japanese studies was the potential for cracks to develop during bending at the base of a transverse deformation (rib). Poor details of the deformations (also referred to as a knot in Japanese literature) in the "old" reinforcing bars was recognized as a location of high stress concentration and an initiation point for cracking that led to brittle bar fractures. A comparison of the deformation geometry required by U.S. and Japanese standards, shown in Table 2-3, reveals, with one exception, little difference between the two standards. The JIS standard requires a range for the rib height (i.e. minimum and maximum) while the ASTM standard requires only a minimum value. Thus, the U.S. standards potentially allow for a

very deep and steep rib that would increase the stress concentration at the base during bending.

Perhaps more important, is the fact that neither standard makes requirements for the angle of the rib with the bar or the radius at the base of the ribs. These quantities refer to the "steepness" and "sharpness" of the rib and are known to affect the stress concentration at the base of a deformation (Stecich et al. 1984). As observed by Japanese researchers (see Section 2.4.2.4), the radius was much smaller on the "old" reinforcing bars as compared to the newer bars, which in turn maximized the likelihood of compression cracking at the inner portion of the bent bar. It should be noted that these properties are difficult to control during manufacturing due to ageing and wear of the rollers used for production of the deformations on the bars; hence, this is the reason why they are not included in the materials specifications.

Table 2-3: Requirements for Reinforcing Bar Deformation Geometry

Bar Size	JIS G 3112:2004		ASTMA615:2009	
	Average Spacing Max	Average Height Min - Max	Average Spacing Max	Average Height Min
3 [10]	0.264 in.	0.016 - 0.031 in.	0.262 in.	0.015 in.
4 [13]	0.350 in.	0.020 - 0.039 in.	0.350 in.	0.020 in.
5 [16]	0.437 in.	0.028 - 0.055 in.	0.437 in.	0.028 in.
6 [19]	0.528 in.	0.039 - 0.079 in.	0.525 in.	0.038 in.
7 [22]	0.610 in.	0.043 - 0.087 in.	0.612 in.	0.044 in.
8 [25]	0.701 in.	0.051 - 0.102 in.	0.700 in.	0.050 in.
9 [29]	0.787 in.	0.055 - 0.110 in.	0.790 in.	0.056 in.
10 [32]	0.878 in.	0.063 - 0.126 in.	0.889 in.	0.064 in.

2.6.1.3 Bend Tests

Materials specifications for deformed bars require a sample to be bent to a specified degree around a pin with a specified diameter slightly smaller than the code minimum bend diameter as a measure of the "bendability" of the bar. Bend-test requirements for reinforcing bar manufactured under ASTM A615 (2009) reads:

> *10.1 The bend-test specimen shall withstand being bent around a pin without cracking on the outside radius of the bent portion.*

A similar test is required within the Japanese reinforcing bar specifications. Of particular interest is the fact that the failure criterion is based on cracks or open defects on the exterior of the bend, however, the fracture of reinforcing bars in Japan originated at the interior of the bend. Consequently, it is possible that bars manufactured under previous or current code specifications passed a bend-test even if the bars were prone to cracking at the interior. If this were the case, it is also possible that these bars are currently in place within structures affected by premature concrete deterioration and are susceptible to fracture.

2.6.2 Design Standards

2.6.2.1 Minimum Bend Diameter

A comparison of Japanese and American bending standards is included in Table 2-4. Note that ACI provisions specify the minimum bend diameter by bar size and use; while, Japanese code dictates the bend diameter by type (grade) of reinforcement. The minimum bend diameter from ACI provisions is equal to or greater than Japanese standards with the exception of No. 4 and No. 5 stirrups and ties of Grade 60 reinforcing. Although the minimum bend diameter is two times greater than bend diameters subject to fracture within the Japanese studies, the smaller bend diameter, combined with weaker and less ductile steel, suggests that these bars are the most prone to fracture within the U.S.

Table 2-4: Code Specified Minimum Bend Diameter

Bar Size	Minimum Bend Diameter					
	JSCE Guidelines:2002				ACI 318-08	
	Grade 40 Equivalent		Grade 60 Equivalent		All Grades	
	Standard Hooks	Stirrups and Ties	Standard Hooks	Stirrups and Ties	Standard Hooks	Stirrups and Ties
3 [10]	$5d_b$	$3d_b$	$6d_b$	$3d_b$	$6d_b$	$4d_b$
4 [13]	$5d_b$	$4d_b$	$6d_b$	$5d_b$	$6d_b$	$4d_b$
5 [16]	$5d_b$	$4d_b$	$6d_b$	$5d_b$	$6d_b$	$4d_b$
6 [19]	$5d_b$	$4d_b$	$6d_b$	$5d_b$	$6d_b$	$6d_b$
7 [22]	—	—	$6d_b$	$5d_b$	$6d_b$	$6d_b$
8 [25]	—	—	$6d_b$	$5d_b$	$6d_b$	$6d_b$
9 [29]	—	—	$6d_b$	—	$8d_b$	—
10 [32]	—	—	$6d_b$	—	$8d_b$	—

d_b = Nominal Diameter of Reinforcing Bar

Current ACI and JSCE provisions dictate the use of a much larger bending diameter than was consistently discovered within structures with fractured bars, and a rationale for such small bend diameters was not publicized in the literature. However, a review of the history of the U.S. concrete building code reveals that before the adoption of the 1971 code, ACI provisions allowed for bend diameters as low as two times the bar diameter for stirrups and ties (Table 2-5). Furthermore, the minimum bend diameters specified by ACI in 1971 were not adopted into the AASHTO code until 1977 (AASHTO 1977). Alarmingly, highway structures built prior to the adoption of the 1977 AASHTO code are clearly at more risk for ASR-induced bar fractures. Fortunately, the outbreak of ASR/DEF within TxDOT owned infrastructure occurred much later than the time period when such small bend diameters were allowed. The development of premature concrete deterioration elsewhere in the United States is unknown, however, and a more definitive assessment of the history of a structure's construction should be considered when evaluating the potential for reinforcing bar fracture.

Table 2-5: ACI Provisions for Minimum Bend Diameter (1963-Present)

Bar Size	Minimum Bend Diameter			
	ACI 318-63		ACI 318-71 – Present	
	Standard Hooks	Stirrups and Ties	Standard Hooks	Stirrups and Ties
No. 3 – No. 5	$5d_b$	$2d_b$	$6d_b$	$4d_b$
No. 6 – No. 8	$6d_b$	$2d_b$	$6d_b$	$6d_b$
No. 9 – No. 11	$8d_b$	—	$8d_b$	—

d_b = Nominal Diameter of Reinforcing Bar

2.6.2.2 Reinforcement Ratio

The results of Japanese investigations indicate the location where the fracture of reinforcing bars is initiated, the distribution of reinforcement was "low". The term "low" is in reference to the percentage of reinforcement in a particular area of the structure as opposed to another region of the structure (Nakamura 2011). Little information of the actual reinforcement percentages within the affected structures is provided in the literature. Considering the fact that most of Japan is within a seismic zone, it is possible that a "low" reinforcement ratio is considerably higher than, or at minimum equivalent to, the minimum requirements for reinforcement within Texas and the United States. Clearly, knowledge of the actual distribution of fractured reinforcement would be necessary to make a valid comparison.

In summary, a lack of information and general inconsistencies in the material specifications make it difficult to directly compare results from Japanese studies on the mechanisms of ASR-induced fracture with structural elements in the United States. Additional experimental work, such as the experimental program of Chapter 5 & 6, is necessary for accurately determining the future potential for reinforcing bar fracture within TxDOT affected highway infrastructure.

2.7 NON-DESTRUCTIVE TESTING (NDT) METHODS EVALUATED

Several NDT techniques are being evaluated as part of TxDOT Project 0-6491 to monitor the progress of ASR/DEF deterioration in large scale specimens and assess the applicability of incorporating NDT methods into the evaluation of deteriorated structures. In the same way, for the Beam Segment Specimens (Chapters 3 & 4) constructed as part of this study, the use of these NDT methods to monitor the deterioration process was assessed. Primarily, it was of interest to explore the use of the NDT techniques evaluated to detect the loss in confinement through the fracture of the transverse reinforcement.

A total of four testing methods were used to monitor the deterioration throughout this experimental project: (1) ultrasonic pulse velocity, (2) impact echo, (3) spectral analysis of surface waves, and (4) surface wave energy transmission. The following simplified summary is intended to give a background on the NDT parameters measured for use when interpreting the experimental results (Chapter 4). A detailed evaluation and background on each of these methods can be found in additional theses from this project, namely Kreitman (2011).

2.7.1 Ultrasonic Pulse Velocity (UPV)

The UPV method is a technique that is commonly used to evaluate concrete properties and assess the uniformity of concrete within a structural element. The testing setup, illustrated in Figure 2-12, consists of an ultrasonic pulser/receiver and two transducers. The pulse travel time is measured and the velocity of the compression wave (travel time ÷ distance traveled) is computed.

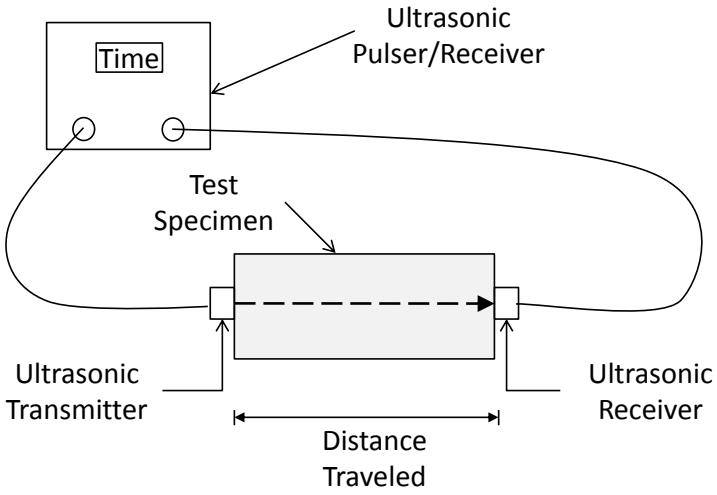

Figure 2-12: Ultrasonic Pulse Velocity Test Setup (Kreitman 2011)

In general, a decrease in velocity from that of an undamaged specimen indicates deterioration as the wave takes longer to travel through cracks than a homogeneous concrete matrix. A wide range of concrete mixture composition, materials, exposure conditions, load conditions, and varying degrees of deterioration within a single concrete element leads to significant variation of UPV test results. Therefore, interpretation of testing results is difficult without a baseline measurement.

2.7.2 Impact Echo

The impact echo was originally developed for detecting voids in concrete slabs; however, it has also been used for evaluating deterioration in concrete structures when UPV measurements are not possible due to limitations of access to both sides of the structure. Surface displacements imparted by a short-term mechanical impact (e.g. via a ball-pein hammer) are recorded via a displacement transducer (Figure 2-13). The presence of internal micro-cracking causes reflections of the induced stress waves that alter the received signal. The velocity of the compression wave can be computed from analysis of the measured surface displacements. Similar to UPV evaluation, a decrease in velocity is indicative of increasing damage.

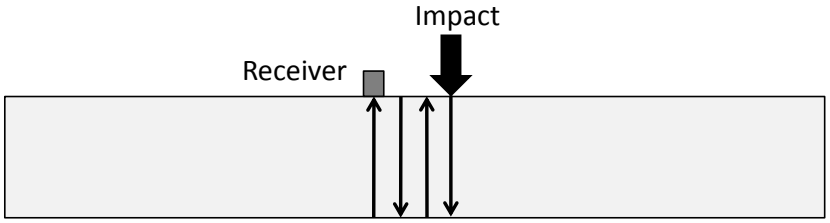

Figure 2-13: Impact Echo Test Setup

2.7.3 Surface Wave Methods

Both spectral analysis of surface waves (SASW) and surface wave transmission (SWT) testing methods utilize the transmission of surface waves, rather than compression waves, in an effort to quantify deleterious concrete deterioration. The test setup shown in Figure 2-14 is used for data collection of both methods. A set of receivers, placed on each side of the test region, measures the surface displacement initiated by a mechanical impact in line with the receiver. The velocity of the surface wave and the energy transmission are determined from analyses of the propagating surface wave using the SASW method and SWT method, respectively. Like the compression wave methods, a loss in surface wave velocity (SASW method) should indicate deterioration as the velocity decreases when the wave travels through cracks. Similarly, for the SWT method a decrease in energy transmission is indicative of damage as energy is attenuated due to the presence of cracks.

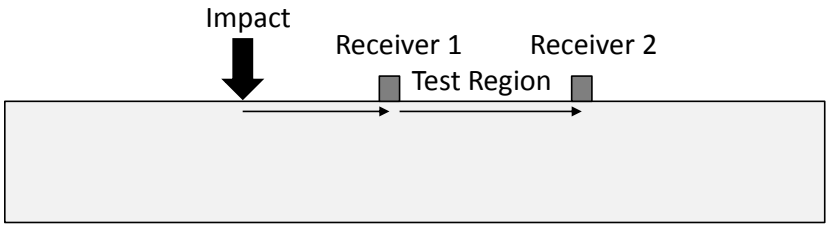

Figure 2-14: Surface Wave Test Setup (Kreitman 2011)

2.8 SUMMARY

In this chapter, the chemical and physical processes of ASR and DEF were introduced. Within affected structures, both deterioration mechanisms result in bulk expansion of the concrete body and a network of surface map cracking, and it is commonly assumed that structural safety is compromised. However, a review of laboratory testing revealed little to no loss in strength and stiffness due to the interaction between the highly stressed reinforcement and the confined concrete core. Still, the loss of confinement through the fracture of reinforcing bars, as experienced in Japan, was highlighted as a serious compromise to structural safety.

Literature relating to Japan's experiences with the discovery of reinforcing bar fracture within highway and railway infrastructure affected by ASR was reviewed. Emphasis was placed on field investigations and laboratory studies aimed at defining the scope and mechanisms of bar fractures. The potential for ASR-induced bar fracture within Texas and the United States was assessed by comparing Japanese and U.S. reinforcing standards and typical details. Circumstances that led to reinforcing bar fracture in Japan, combined with a lack of information and inconsistencies in the materials standards, make a direct comparison difficult and the need for additional research was highlighted.

Finally, a brief background of measured parameters of the four NDT methods used in the monitoring of the concrete specimens was provided. The background information included within this chapter will serve as the basis for the experimental program detailed in Chapter 3 and the reinforcement bend tests discussed in Chapter 5.

CHAPTER 3
Experimental Program: Beam Segments

3.1 OVERVIEW

In accordance with the research objectives identified in Chapter 1, two beam segment specimens were constructed at the Ferguson Structural Engineering Laboratory (FSEL) as part of this experimental program. These specimens were continuously examined for approximately ten months to evaluate the applicability of various monitoring techniques to detect the loss of confinement through the simulated fracture of the transverse reinforcement. Furthermore, two additional specimens were constructed as a supplementary experiment to investigate the use of fly ash to arrest the development of ASR/DEF expansions. Details relating to the design, fabrication, and monitoring of the four beam segment specimens are reviewed in this chapter.

3.2 SPECIMEN DETAILS

Impetus for the design of the beam segments originated from the large scale bent cap specimens tested in shear as part of a TxDOT IAC (Reference Deschenes et al. 2009) and the flexural test specimens from Project 0-6491. Numerous details relating to the geometry, reinforcing layout, and concrete mixture design borrowed from these respective programs are discussed in this section. Table 3-1 includes a summary of the beam segment design variables and leads to the discussion that follows.

Table 3-1: Overview of Beam Segment Specimens

Identification	Stirrup Spacing	Concrete Mixture
Specimen 1	20 in	Reactive
Specimen 2	9.5 in	Reactive
Specimen 3	9.5 in	25% Fly Ash Replacement
Specimen 4	9.5 in	25% Fly Ash Addition

3.2.1 Geometry & Reinforcing Layout

The geometry and reinforcement layout of the beam segments were selected with three objectives in mind: (1) to fully develop the longitudinal bars in the testing region to ensure that the directionality of PCD-induced expansion was primarily oriented in the transverse direction, (2) to maintain compatibility with the large scale bent cap specimens, while (3) minimizing the overall specimen size for constructability purposes (see Section 3.3) and storage (Section 3.4). The geometry of the cross section and longitudinal reinforcement layout is shown in Figure 3-1. A cross sectional width of twenty-one inches (b=21") and height of forty-two inches (h=42") was determined from the large scale specimens. Additionally, the distribution of longitudinal reinforcement was unchanged from the large scale flexural test specimens. The section was reinforced with five No. 11 bars serving as the primary tension and compression reinforcement and a total of twelve (six per side) No. 5 bars that were originally designed as crack control reinforcement.

The spacing of transverse reinforcement was also based on the large scale bent cap specimens. Two different stirrup spacings, 9.5 inches and 20 inches, were used for the beam segment specimens, corresponding to 0.31 and 0.15 percent transverse reinforcement. The list of specimens and the corresponding stirrup spacing is included in Table 3-1. An elevation of the beam segment specimens is shown in Figure 3-2.

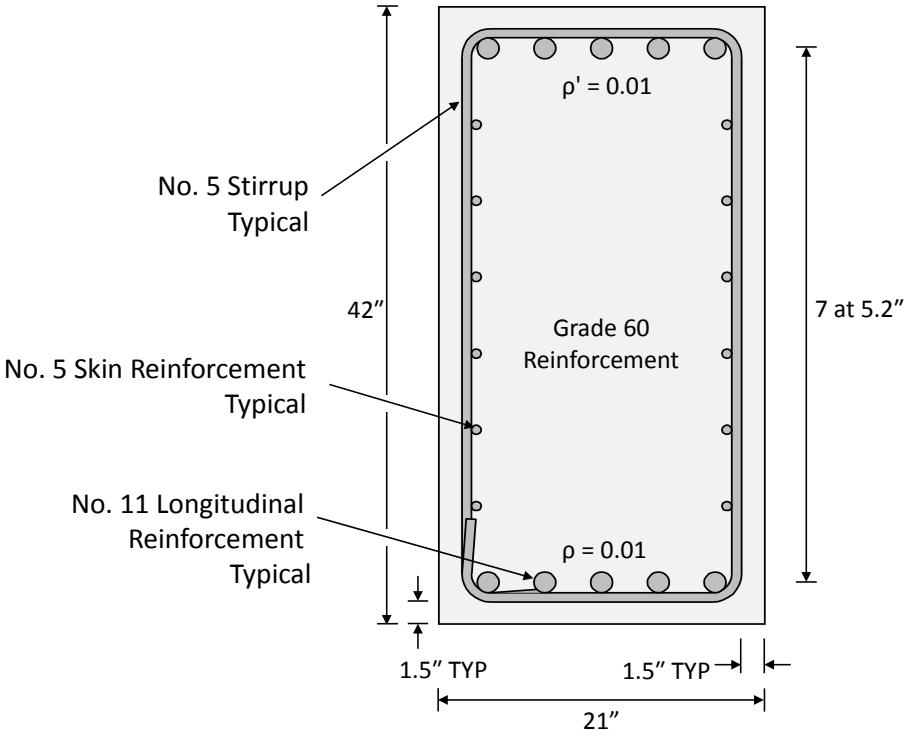

Figure 3-1: Beam Segment Cross Section

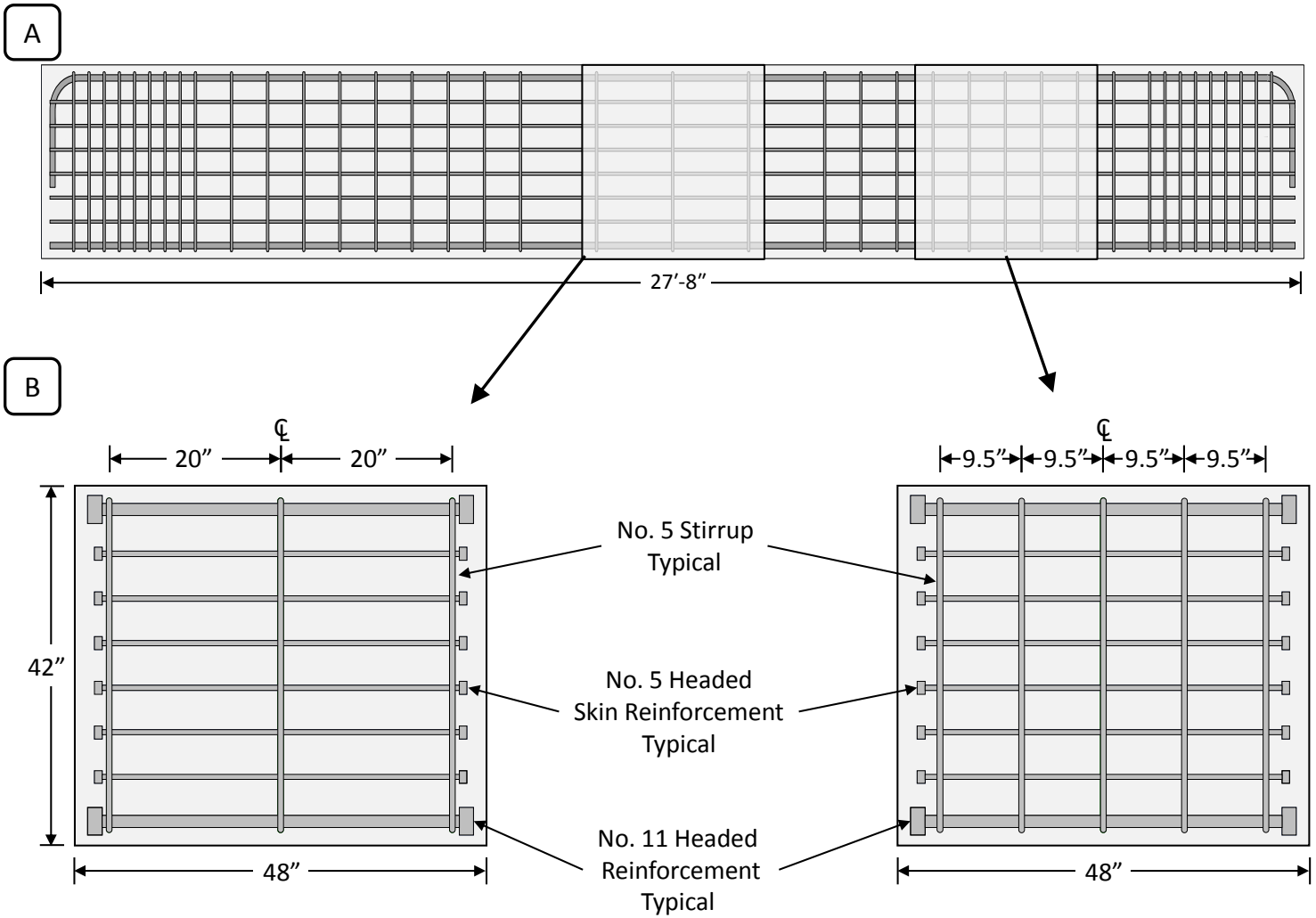

Figure 3-2: (A) Large Scale Flexural Test Specimen(s) (B) Related Beam Segments - Elevation

The design of the beam segments required the use of headed reinforcing bars in the longitudinal direction to satisfy the development requirements, while also minimizing the length of the specimens. ACI 318 (2008) code provisions conservatively require a development length (l_{dt}) for headed bars in tension according to Equation 3.1

$$l_{dt} = \left(\frac{0.016 \times \psi_e \times f_y}{\sqrt{f'_c}} \right) \times d_b \qquad (3.1)$$

where,

ψ_e = factor to account for epoxy-coated reinforcement

f_y = yield stress of reinforcement (psi)

f'_c = specified concrete strength (psi)

d_b = diameter of reinforcing bar (in)

and, l_{dt} is measured from the base of the head. Additionally, the Code allows for a reduction in the development length if excess reinforcement is provided or, in other words, if the expected stress within the bar is less than yield. Based on the expansion monitoring from Deschenes et al. (2009) and the monitoring of the large scale bent cap specimens of TxDOT project 0-6491 (see Kreitman 2011), the maximum strain within the longitudinal bars was expected to reach less than 0.1% or half of yield. Therefore, the development length calculated from Equation 3.1 for the No. 11 longitudinal bars within the beam segments could effectively be reduced by one half.

The minimum required length of the specimen was then calculated based on the confinement region for the maximum spacing of transverse reinforcement (twenty inches for Specimen 1). The use of headed anchorage effectively allowed for a twenty-inch fully developed region within the midspan of the beam segments with only a forty-eight-inch long specimen, as shown in Figure 3-3. Consequently, all monitoring of the specimens (Section 3.4) was to be performed through or across this region to be considered admissible and comparable to the larger bent cap specimens.

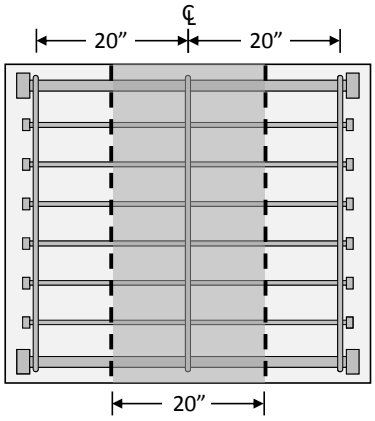

Figure 3-3: Fully Developed Monitoring Region

3.2.2 Concrete Mixture Designs

The selection of concrete mixture proportions was critical in the success of the experimental program to ensure the potential for the maximum possible distress within the limited time frame of the study. Three different concrete mixtures were used within the four beam segment specimens as indicated in Table 3-1. A list of the sources of all mixture components is included Table 3-2. Mixture proportions and a rationale for the selection of the mixture components are discussed in the following sections.

Table 3-2: Concrete Mixture Components and Sources

Material	Description	Source
Cement	Type III High-Alkali Cement	Lehigh Cement Company Allentown, PA
Fly Ash	Class F	Boral Material Technologies, Inc. Rockdale, TX
Water	Hot Tap Water (about 130°F)	Municipal Water Supply Austin, TX
Fine Aggregate	Jobe-Newman Sand	Cemex El Paso, TX
Coarse Aggregate	¾″ Crushed Limestone	Texas Crushed Stone Company Georgetown, TX
Sodium Hydroxide	50% NaOH Solution	Fisher Scientific Company Pittsburgh, PA

3.2.2.1 Reactive Concrete Mixture (Specimens 1 and 2)

The primary goal for the selection of reactive concrete mixture proportions and components was to maximize potential deleterious expansion. The proven effectiveness of the reactive concrete mixture for the construction of the large scale bent cap specimens (see Deschenes et al. 2009) warranted the use of an identical concrete mixture within the beam segments. Additionally, replication of the concrete mixture maintained compatibility with the previous studies, thus satisfying one of the original design objectives. The reactive concrete mixture proportions are included in Table 3-3.

Table 3-3: Concrete Mixture Design (Specimens 1 & 2)

	Reactive (Specimen 1 & 2)
Type III Cement	700 lb/yd^3
Water	385 lb/yd^3
Fine Aggregate	1155 lb/yd^3
Coarse Aggregate	1500 lb/yd^3
Water-to-Cement Ratio	0.55

An understanding of the chemical mechanism of alkali-silica reaction and delayed ettringite formation (see Chapter 2) allowed researchers to exploit the deterioration processes by careful selection of mixture components. A relatively large percentage of Type III cement was used to increase the alkali-content of the mixture. Jobe-Newman sand was selected because it is one of the most reactive aggregates within the state of Texas. Sodium hydroxide was added to the mixture to *boost* the alkali content to 1.25%, resulting in greater reactivity. Finally, hot mixing water was used in order to jumpstart the internal temperature of the concrete mixture to aid in the development of curing temperatures in excess of 158°F (70°C).

3.2.2.2 Concrete Mixtures Containing Fly Ash (Specimens 3 and 4)

Since 1995, TxDOT specifications have contained prescriptive options for concrete mixtures to prevent the development of ASR and DEF within new concrete

structures. One such option is the partial replacement of cement (twenty to thirty-five percent replacement) with Class F fly ash. Research suggests that the use of fly ash restricts the mobility of ions in the pore solution and limits the water permeability of the concrete; thereby, when used in sufficient dosages, is effective at controlling ASR/DEF expansions (Folliard et al. 2006).

The difficulty when applying this option for mixture designs is that fly ash also slows down the initial concrete strength gain and can have a significant impact during construction. Perhaps quite common in practice when strength gain becomes an issue, is the percentage of fly ash for cement replacement is *added* to the mixture proportions with no reduction in cement content. In effect, the ratio of fly ash to cement, or the total percent of cement replacement, is reduced, and it is possible that the effectiveness of the fly ash to control ASR/DEF expansions is then diminished.

The concrete mixtures for Specimens 3 and 4 are shown in Table 3-4. The reactive mix proportions served at the base mixture. Specimen 3 contained a 25% replacement of the cement with Class F fly ash while Specimen 4 contained a 25% addition. Chemical analysis of the fly ash, referred to as Rockdale ash, is included in Appendix A. Mixture proportions were kept as close to the reactive mixture as possible while also maintaining practicality. This required some additional trial batching and slight modifications to the percentages of water and aggregate. Similar to the reactive mixture, sodium hydroxide was added to *boost* the mix and hot water was used as mixing water; thus, the potential for a highly reactive concrete mix was established.

Table 3-4: Concrete Mixture Design (Specimens 3 & 4)

	25% Fly Ash Replacement (Specimen 3)	25% Fly Ash Addition (Specimen 4)
Type III Cement	525 lb/yd^3	700 lb/yd^3
Class F Fly Ash	175 lb/yd^3	175 lb/yd^3
Water	385 lb/yd^3	400 lb/yd^3
Fine Aggregate	1133 lb/yd^3	1052 lb/yd^3
Coarse Aggregate	1470 lb/yd^3	1375 lb/yd^3
Water-to-Cementitious Materials Ratio	0.55	0.57

3.3 SPECIMEN FABRICATION

The following section describes the processes, in chronological order, that resulted in the fabrication of the four beam segment specimens at FSEL.

3.3.1 Reinforcement Cage Fabrication

The reinforcement used in the beam segments was Grade 60 and conformed to the mechanical requirements of ASTM A615 (confirmed by mechanical testing to determine the yield point to be used with the expansion monitoring of Chapter 4). Longitudinal reinforcing bars were delivered pre-threaded, to receive the headed anchorage, in the specified length from a local supplier. The heads were screwed onto the bars and tightened to the manufacturer specified torque using a torque and pipe wrench. Instrumentation for expansion measurements (see Section 3.4.2.1) was pre-installed on the reinforcing bars before the reinforcement cage was tied at a staging area. Wooden block-outs were constructed and placed in the steel formwork (in order to facilitate construction of the beam segments within the same day) before the finished cages were moved to the soffit and enclosed within the side forms. An illustration of the fabrication procedure, before concrete placement, is shown in Figure 3-4.

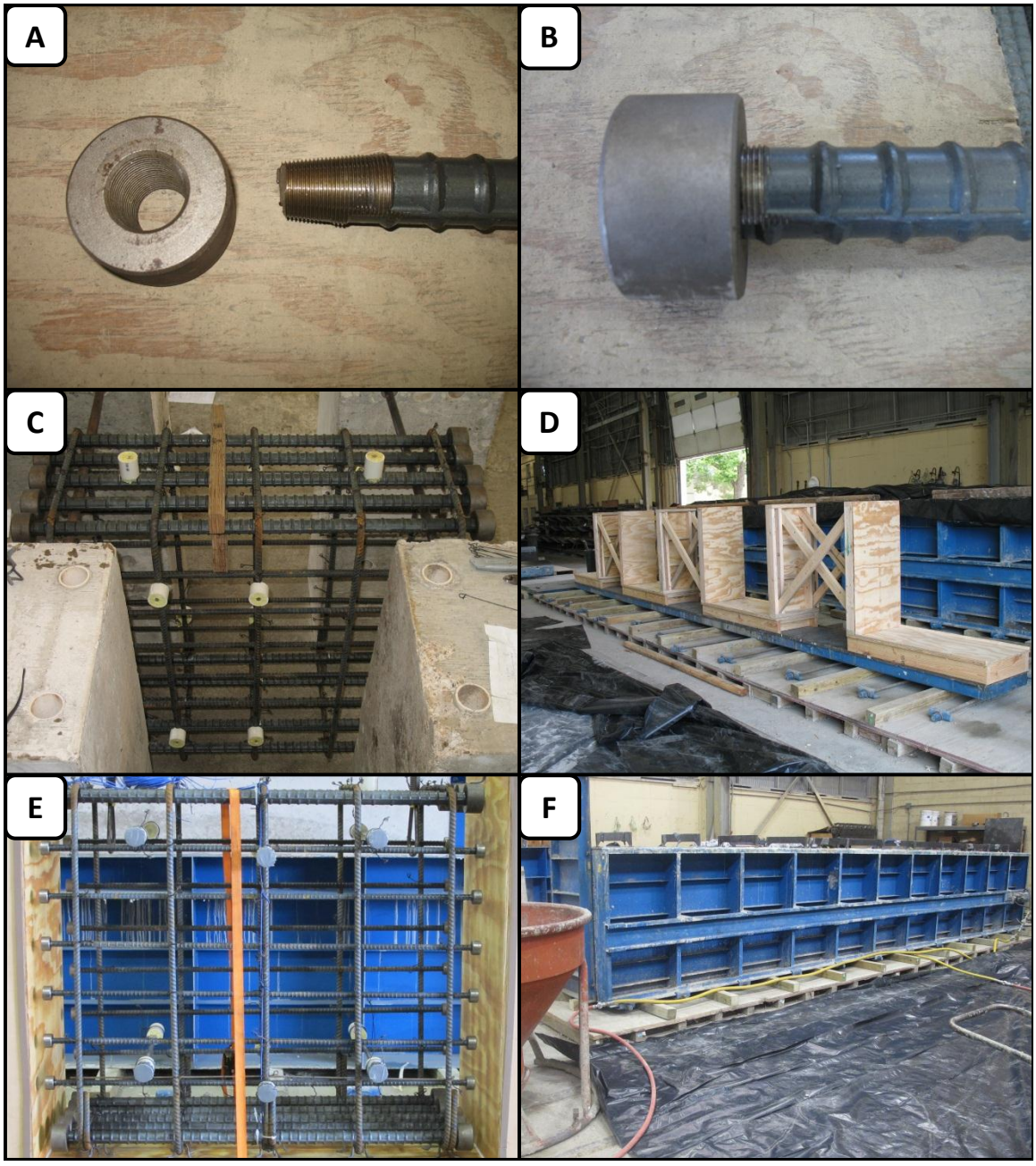

Figure 3-4: Specimen Fabrication before Concrete Batching
(A) Headed-Anchorage and Threaded Bar (B) Headed Reinforcing Bar
(C) Reinforcing Cage Being Fabricated (D) Wooden Formwork Block-Outs
(E) Instrumented Cage in Formwork (F) Steel Forms in Place

3.3.2 Concrete Batching & Placement

Proven methods from the production of the large scale bent cap specimens were employed for the concrete batching process. All three mixes were batched and placed within hours of one another, which required extensive planning and organization of materials beforehand. Prior to batching, the reactive Jobe-Newman sand was loaded in fifty-five gallon barrels and moved into the laboratory. The barrels were pre-weighed and sorted for the respective mixes using a load cell attached to the hook of the overhead crane. Forty sacks of Type III cement (delivered to the lab previously) were moved from an air conditioned room one day before casting in preparation for mixing. Finally, five gallon buckets were filled halfway with the sodium hydroxide solution for greater control and easier placement into the mixer.

Each mix was produced in an eleven cubic yard concrete mixer truck supplied by a local ready-mix company on the day of the cast. The timing of the trucks was such that as one mix was being placed, the next truck would be waiting ready outside the laboratory for batching of the next mix. Each truck was charged with the coarse aggregate at the ready-mix facility and the remainder of the materials were added into the mixer at the lab.

The pre-weighed barrels of sand were first loaded into a one cubic yard concrete bucket on the ground before the bucket was hoisted to the top of the mix truck with the overhead crane and the sand discharged into the mixer. The pre-batched sodium hydroxide was then added into the mixed aggregate. Approximately thirty-percent of the total mixing water (cold) was added to further dilute the sodium hydroxide before addition of the cement. A volumetric flow-meter plumbed into the water outlet was used for controlling the total amount of water. The Type III cement was discharged into the mixer in a similar manner as the sand via the concrete bucket and overhead crane. The remainder of the mix water (hot) was continuously supplied to the mixture as the cement was added to the mixer.

After all concrete materials were added, the mixer was turned at full speed for approximately five to ten minutes. A slump test was performed, according to ASTM C143, and additional cold water was added to the mixture, as necessary, to increase the workability of the mix. The final slump of the mixtures ranged from 6.5 inches to 9.25 inches. When the consistency of the mix was deemed acceptable, the fresh concrete was placed into the steel formwork. Concrete consolidation was achieved through the use of internal rod vibrators (stingers) and external side form vibrators. The concrete batching and placement process is illustrated in Figure 3-5. This process was repeated three times to accommodate the construction of all four beam segments within the same day. In total, 5.75 cubic yards of concrete was batched and placed within approximately three hours.

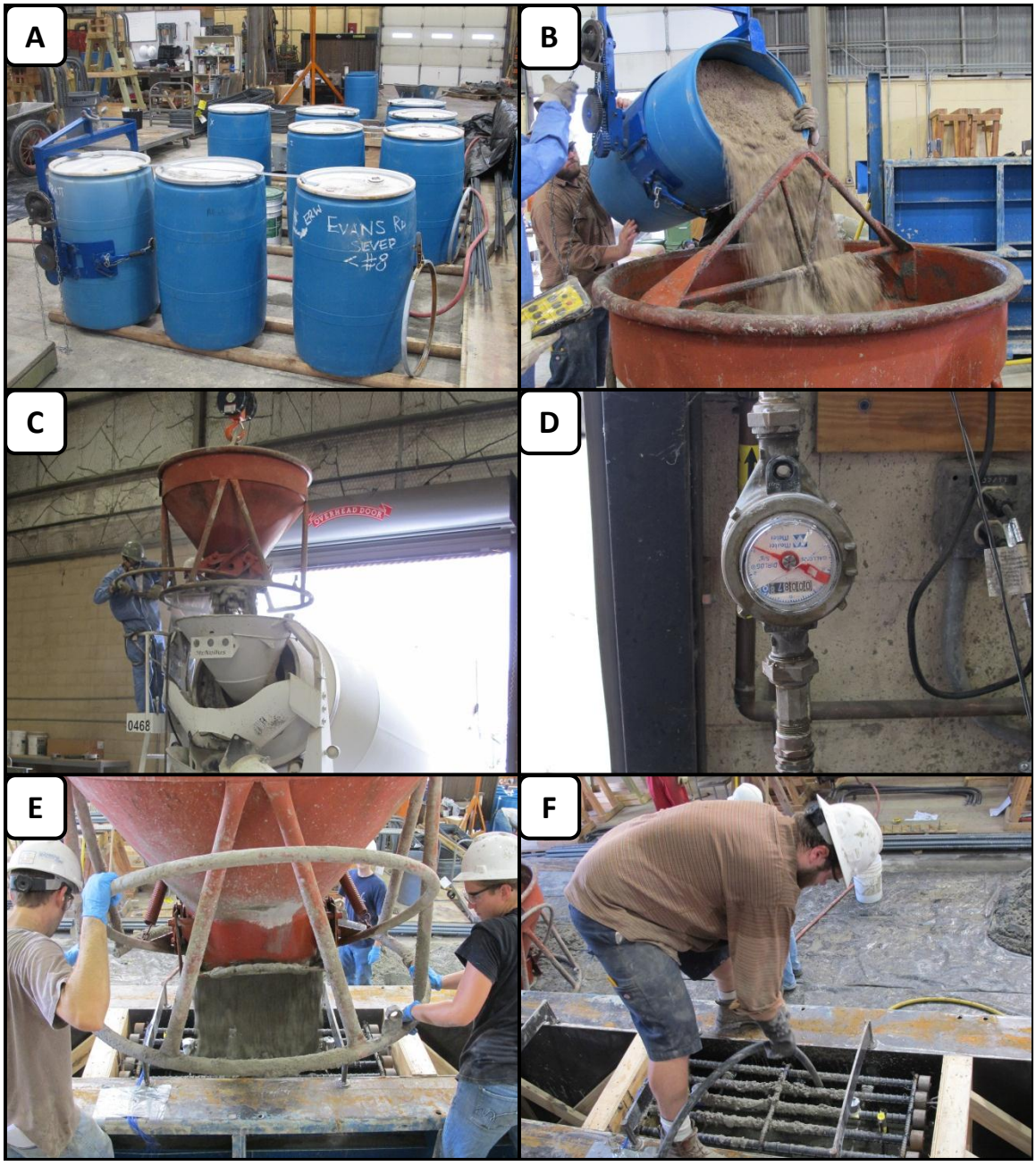

Figure 3-5: Concrete Batching & Placement

(A) Reactive Sand Pre-Weighed in Barrels (B) Sand Loaded in Bucket

(C) Cement Discharged in Mixer (D) Volumetric Flow Meter for Water Addition

(E) Concrete Placement in Formwork (F) Concrete Consolidation with Stinger

3.3.3 Curing

Fresh concrete temperatures ranged from 95°F to 102°F; however, the limited size of the specimens cast doubt on the ability of the curing temperature to reach and sustain the DEF threshold temperature of 158°F (70°C). Therefore, the beam segments were subject to a high temperature curing cycle to ensure the development of deleterious DEF. After concrete was placed and the top surfaces were trowelled smooth, wet burlap sacks were placed over the top of each specimen. A fire retardant tarp was then placed over the formwork to create a tent-like enclosure. Supplemental heat was applied within the enclosure via two portable kerosene heaters, positioned at opposite corners of the formwork (Figure 3-6). Heaters were operational approximately one hour after the last specimen was cast and the additional heat was maintained for approximately 17.5 hours.

Figure 3-6: High Temperature Curing Setup

The specimens were instrumented with thermocouples throughout the cross section for establishing the magnitude and variation of curing temperatures. The thermocouple layout is shown in Figure 3-7. The temperatures were continuously monitored for five days when the internal temperature of the concrete had reached ambient air temperature; at which point the steel side forms were removed.

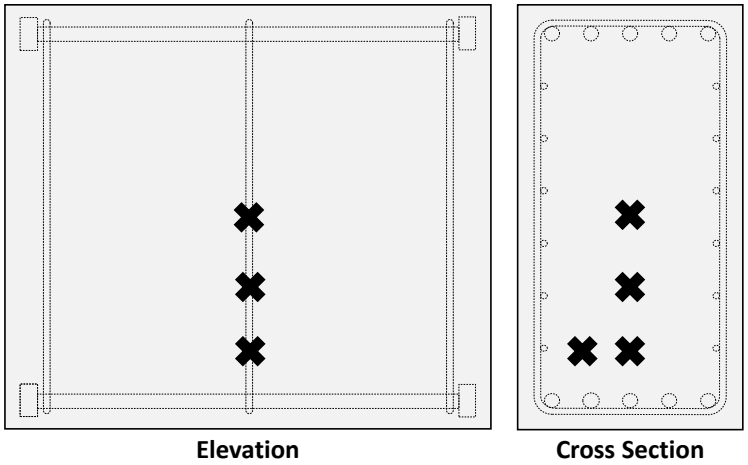

Figure 3-7: Typical Thermocouple Layout

Hydration curves from each beam segment can be found in Appendix A. The maximum variation of hydration temperature across the cross section was approximately 10°F; therefore, only the peak temperature hydration curves for the four beam segments are compared in Figure 3-8. With the exception of Specimen 3, the peak temperatures were achieved within about twelve hours after concrete was placed. For Specimen 3, hydration temperature leveled off at twelve hours before picking up again at approximately fifteen hours and peaking around twenty-four hours after initial hydration. The partial replacement of cement with fly ash resulted in the uniqueness of the curve for Specimen 3 and is likely a result of the delayed hydration of the fly ash after the initial hydration of the cement. Regardless, peak curing temperatures ranged from 168°F to 184°F and were sustained for a minimum of twenty-one hours. Consequently, the potential to develop deleterious DEF was established for all specimens.

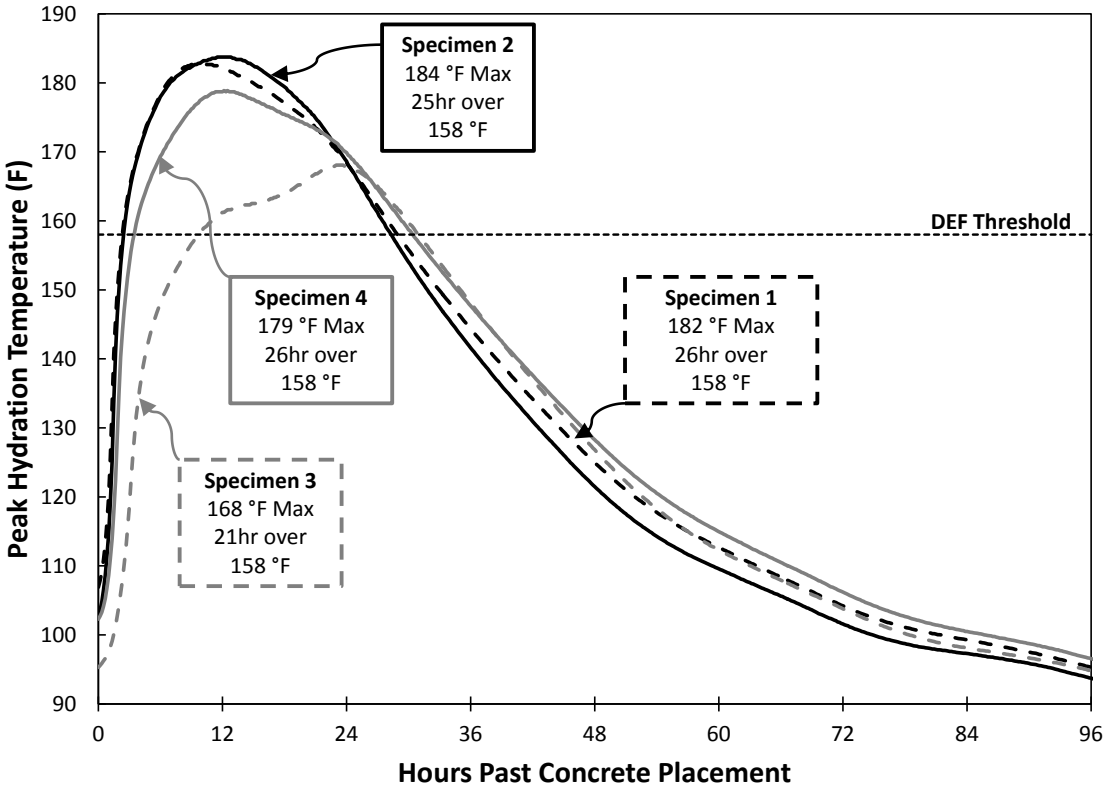

Figure 3-8: Peak Hydration Temperature Curves

3.4 CONDITIONING & MONITORING

The experimental program began within days following specimen fabrication. Within this section, details of all aspects of the expansion and NDT monitoring programs are preceded by a description of the storage conditions selected to accelerate premature concrete deterioration.

3.4.1 Storage Conditions

The storage conditions of the specimens were based on the need to maximize the potential for ASR/DEF-induced distress within the limited time frame of the study. The development rate of deleterious concrete expansion is dependent on a number of environmental factors, including the availability of moisture and temperature. Researchers will typically exploit these characteristics by way of various techniques of

supplying sufficient moisture and maintaining a high conditioning temperature (at or above 100°F) to accelerate the internal reaction. In the same way, the storage conditions of the beam segments were selected.

The beam segments were moved to a large concrete storage tank outside of the laboratory within two weeks of construction (Figure 3-9). Lifting inserts embedded into the concrete allowed for easy maneuverability and transport using a small forklift. Within the tank, the specimens were supported on eight inch tall concrete curbs over four to six inches of water. A black plastic tarp was placed over the beam segments to minimize water evaporation and keep the reactive concrete moist. Humidity was measured directly with a combination thermometer/hygrometer mounted inside the tank and was consistently maintained between 90 and 100 percent Additionally, a black, weather- resistant coated vinyl tarp was placed over the entire length of the tank to act as a solar heater during the daylight hours. The addition of the heavy tarp allowed for a ten to fifteen degree temperature increase inside the tank relative to the ambient air temperature.

Figure 3-9: Specimens in Concrete Storage Tank

A unique method of heating the water inside the tank was established during the winter months in order to sustain the rapid development of ASR/DEF deterioration when the outside air temperature in Austin began to decrease. Water inside the tank was circulated via a submersible pump through an 11kW electric spa heater mounted to the exterior of the tank (Figure 3-10). The addition of the heater increased the water temperature to a constant 100°F and the relative humidity within the tank to 100 percent; thereby, subjecting the specimens to the "worst case" conditions for accelerated deterioration.

Figure 3-10: Electric Water Heater for High Temperature Conditioning

3.4.2 Expansion Monitoring

3.4.2.1 Restrained Expansion Monitoring

The tank was periodically drained and the tarps removed for expansion monitoring and non-destructive testing (see Section 3.4.3 for NDT test procedures). A non-traditional implementation of mechanical strain measurements, developed by Deschenes et al. (2009), was used for expansion monitoring of the beam segments. The

measurements taken through the course of the study were used to quantify the level of physical ASR/DEF distress.

Instrumentation consisted of a grid of targets, spaced at twenty-four inches and centered on both faces of the beam segments, to directly measure the steel and concrete strains. The layout of the grid is shown in elevation and within the cross section in Figure 3-11. Both steel and concrete core measurements were taken longitudinally (horizontal) and transversely (vertical) on both faces of the specimens. In total, eleven individual strain/expansion measurements were recorded per beam segment.

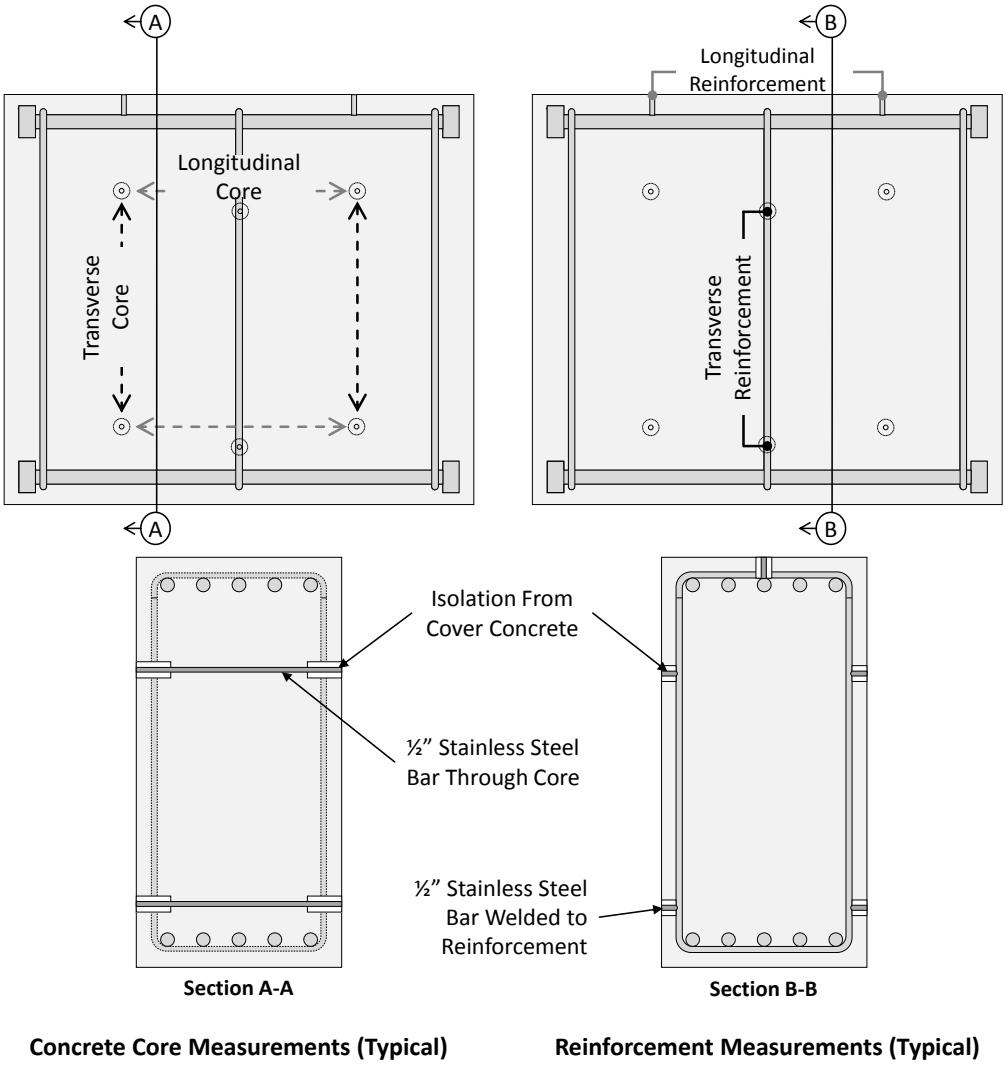

Figure 3-11: Typical Layout of Instrumentation for Expansion Measurements

The targets were fabricated from stock ½-inch diameter stainless steel rod (A303) and located within the beam segments before concrete placement. Concrete core targets were machined into the ends of a twenty-one inch long stainless steel rod. A 1½-inch diameter PVC pipe was centered on the rods, placed over both ends, and filled with compressible foam to segregate the rods from the cover concrete. The rods were suspended within the reinforcing cage at the correct location via wire ties to be embedded in the concrete. The reinforcement targets were produced in a similar way and welded to the longitudinal and transverse reinforcement. Extreme care was taken when placing the targets to maintain the desired twenty-four inch spacing. An illustration of the measurement target detail is shown in Figure 3-12.

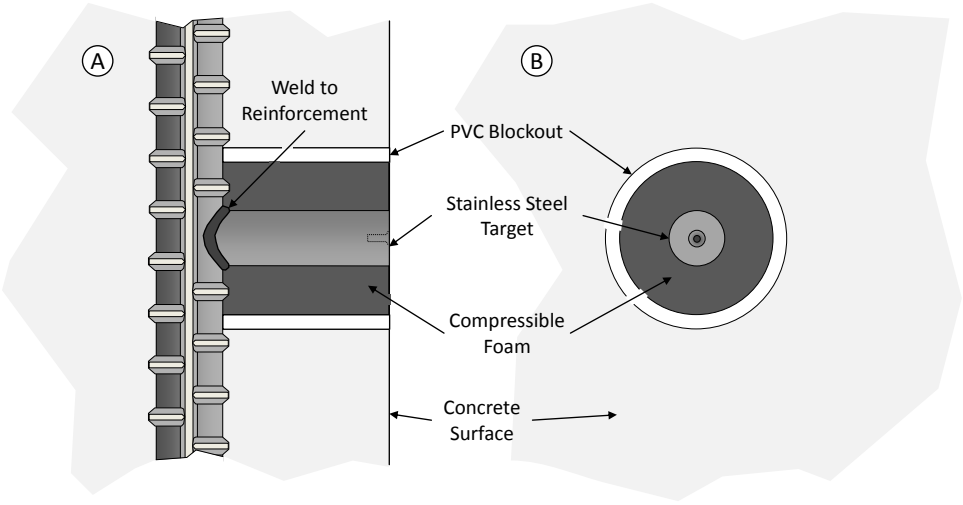

Figure 3-12: Measurement Target Detail (A) Section View (B) External View (Deschenes et al. 2009)

Expansion measurements were taken every one to four weeks using a modified long gauge length extensometer (Figure 3-13). The procedure for taking measurements was consistent throughout the course of the study. Water from the tank was drained the night before and the vinyl tarp and plastic sheathing was left on until the morning. Measurements were taken in the morning before the sun was in direct contact with the specimens. Additionally, the temperature within the tank was recorded and the expansion measurements were corrected for any large deviations from the baseline temperature of

70°F. As a result, consistency was maintained and the influence of environmental conditions to the expansion measurements was minimized. Results from the expansion monitoring are discussed in Chapter 4.

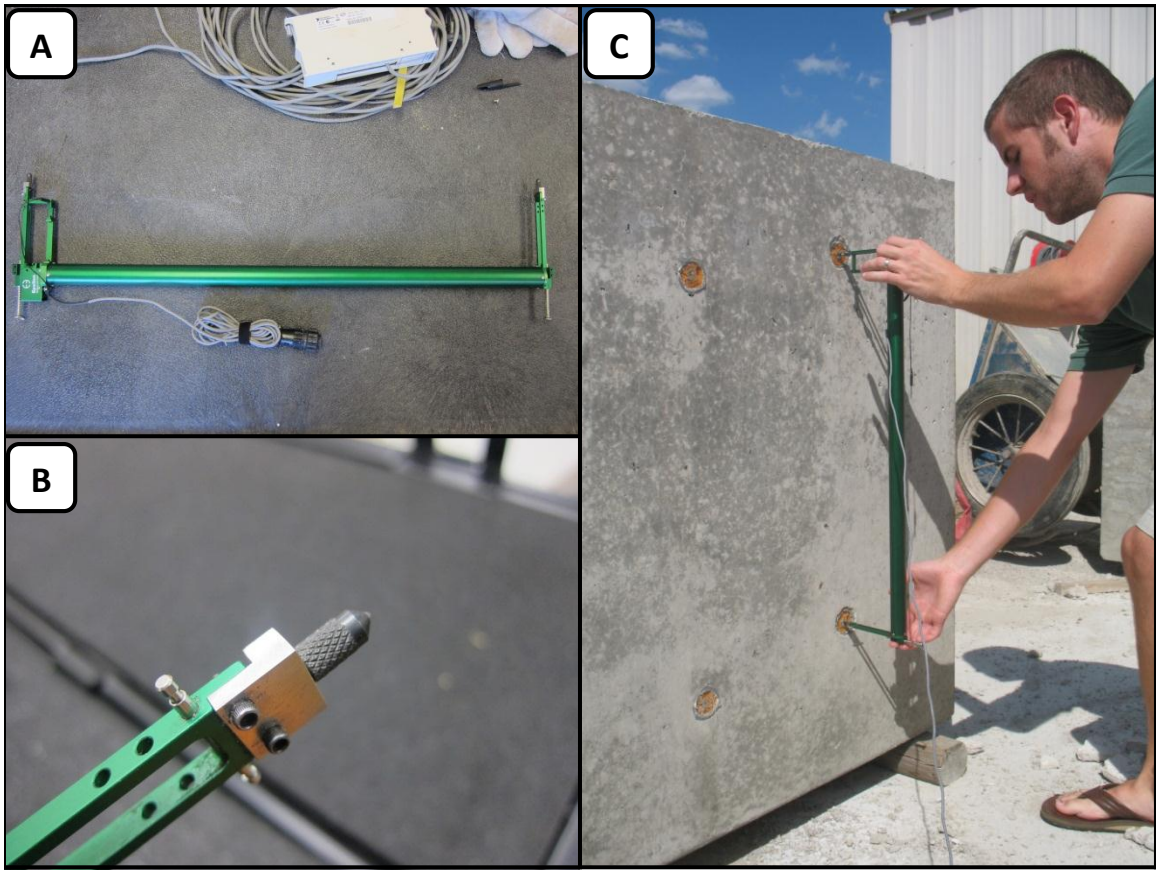

Figure 3-13: (A) Extensometer for Expansion Measurements (B) Modified Tip (C) Demonstration of Measurement

3.4.2.2 Prisms for Free Expansion Monitoring

A series of three plain concrete prisms from each concrete mixture were produced alongside the beam segments for free expansion measurements. The concrete samples were subjected to a similar curing regime and conditioning environment as the beam segments, and thus, a valid comparison between the samples and the specimens could be assessed. Prisms produced conformed to ASTM C157 (2008) and were tested according to ASTM C1293 (2008).

It should be noted that the curing regime for the concrete samples was unconventional to standard materials testing specifications; however, it was intended to give a more accurate representation of the deleterious concrete reactivity within the beam segments. Paired concrete samples were cast alongside the beam segments and then immediately placed within an oven (Figure 3-14A). The temperature within the oven was controlled in an attempt to match the hydration temperature of the reactive beam segments (see Section 3.3.3). This required manually adjusting the oven temperature periodically for approximately 18 hours while the kerosene heaters were kept on for curing the beam segments. After the 18 hour period, the oven was turned off and the prisms were kept inside to cool. Prisms were demolded approximately twenty-four hours after the samples were cast and stored in a moist room (fog room) for an additional day. The initial lengths were then measured using a comparator (Figure 3-14B). The samples were placed within a sealed storage container lined with felt and supported above water (Figure 3-14C) and then placed in an environmental chamber, with a constant temperature of 100°F, for storage.

Successive length change of each prism was measured over a period of one year. The frequency of measurements was based on ASTM C1293 materials protocol. The buckets were removed from the high temperature chamber and placed within a humidity controlled room the day before each subsequent measurement. Prism length and weight were recorded twelve to twenty hours after bucket removal and then placed back within the environmental chamber. Average expansion histories of the prisms are included in Appendix A.

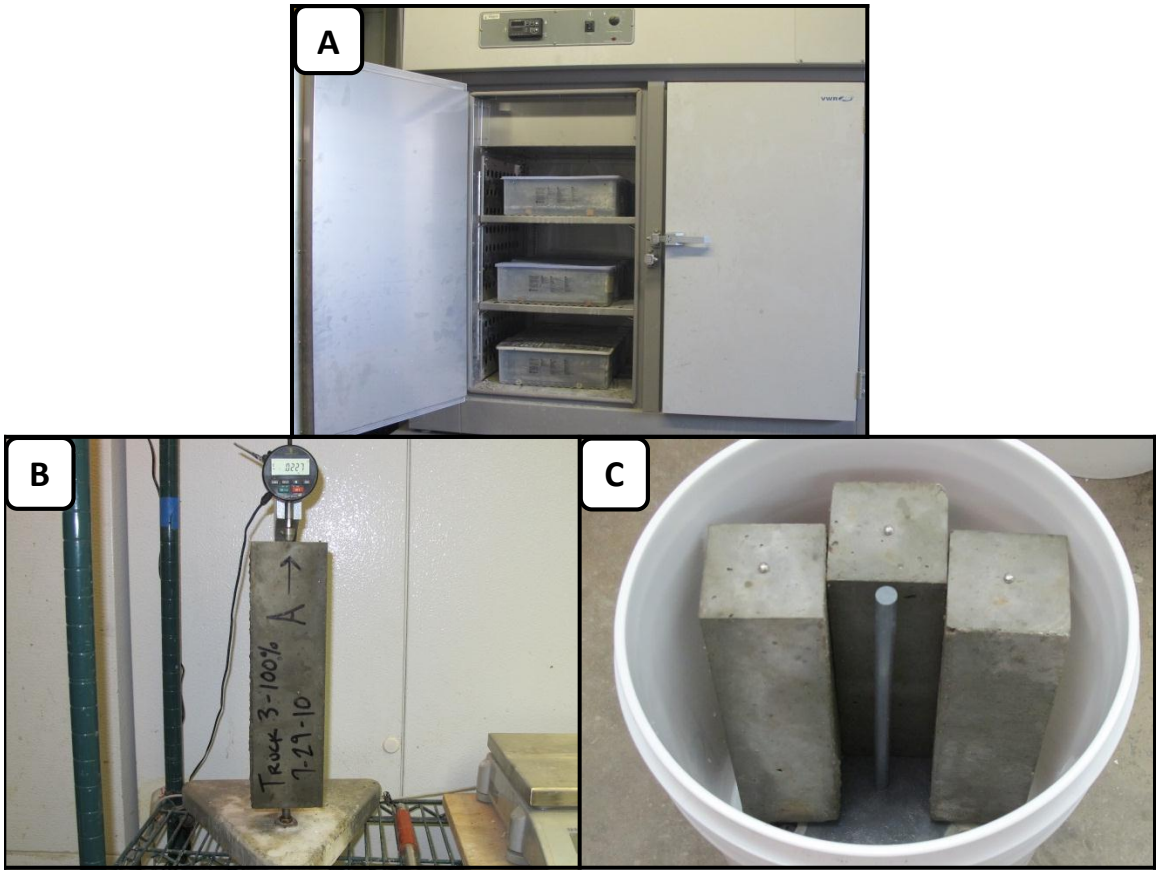

Figure 3-14: Prisms for Free Expansion Measurements

(A) Oven for High Temperature Match Curing (B) Digital Comparator for Length Change Measurements (C) Felt-Lined Bucket for Prism Storage

3.4.3 Non-Destructive Testing

Several non-destructive test (NDT) methods were repeated throughout the course of the study, on the reactive specimens, to monitor the progression of ASR/DEF deterioration. Ultimately, the results of the non-destructive testing were evaluated to assess their applicability to detect the loss in confinement through fracture of the transverse reinforcement (Section 3.5). A background of the parameters measured for each technique was included in Chapter 2. A summary of the test procedure is included in this section. A more detailed description of each test method can be found in additional theses from TxDOT Project 0-6491 (see Kreitman 2011).

3.4.3.1 Ultrasonic Pulse Velocity (UPV)

UPV testing was performed using the through-transmission technique following the procedures of ASTM C597 (2009). Travel times were measured via a PUNDIT 7 UPV test instrument. Figure 3-15A shows the grid layout for ultrasonic testing. Twelve individual velocities were computed for each beam segment both through the width of the cross section and across the diagonal of the top corners (Figure 3-15B). Testing required a minimum of two operators. Transducers were placed firmly against the concrete surface at the correct grid point, and the minimum travel time of the ultrasonic pulse was recorded. Frequent re-application of a water-based couplant was applied to the transducers to ensure a correct reading. Velocities were computed from the recorded travel time and known distance in a computer spreadsheet.

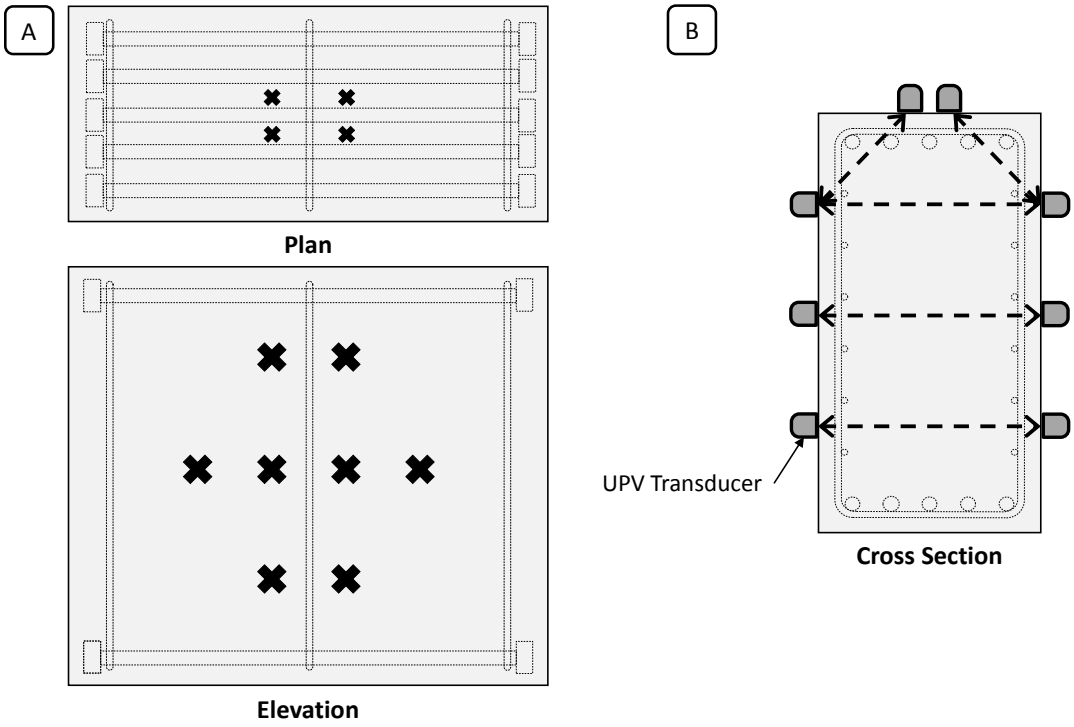

Figure 3-15: (A) UPV Testing Grid Layout (B) Associated Measurements

3.4.3.2 Impact Echo

Impact echo monitoring was performed following the procedures of ASTM C1383 (2004). As shown in Figure 3-16, twelve individual measurements, through the width and depth of the cross section, were recorded for each specimen at the same location of the UPV testing points (Figure 3-15A). Similarly, two operators were required for impact echo testing. A mechanically induced impact was imparted via a 10-mm diameter ball-pein hammer. Surface displacements were recorded via a Germann Instruments DOCter receiver connected to an 8-bit National Instruments (NI) digitizer and laptop computer. Data was later analyzed in a MATLAB program developed at UT Austin to compute the compression wave velocity.

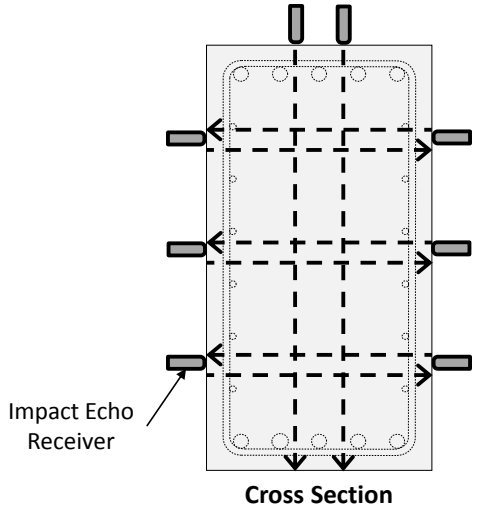

Figure 3-16: Impact Echo Measurements

3.4.3.3 Surface Wave Techniques (SASW & SWT)

Surface wave testing was performed using non-contact, air-coupled sensors (i.e. microphones) to detect the transmission of surface waves. The typical layout of testing points for surface wave measurements in both the longitudinal (horizontal) and transverse (vertical) directions is shown in Figure 3-17. Impact points were located on both sides of the sensors and the test procedure was performed on both faces of the specimen; thus, a total of forty data points were collected each time the test was performed. Three

operators were required for surface wave testing. The surface was impacted using a 13-mm steel ball. Changes in air-pressure caused by the surface motion of the concrete were recorded via two PCB microphones spaced twelve inches apart. The data was collected through a 3-channel PCB signal conditioner connected to an 8-bit NI digitizer and laptop computer. The same set of data was later analyzed for computation of the surface wave velocity (SASW method) and energy transmission (SWT method).

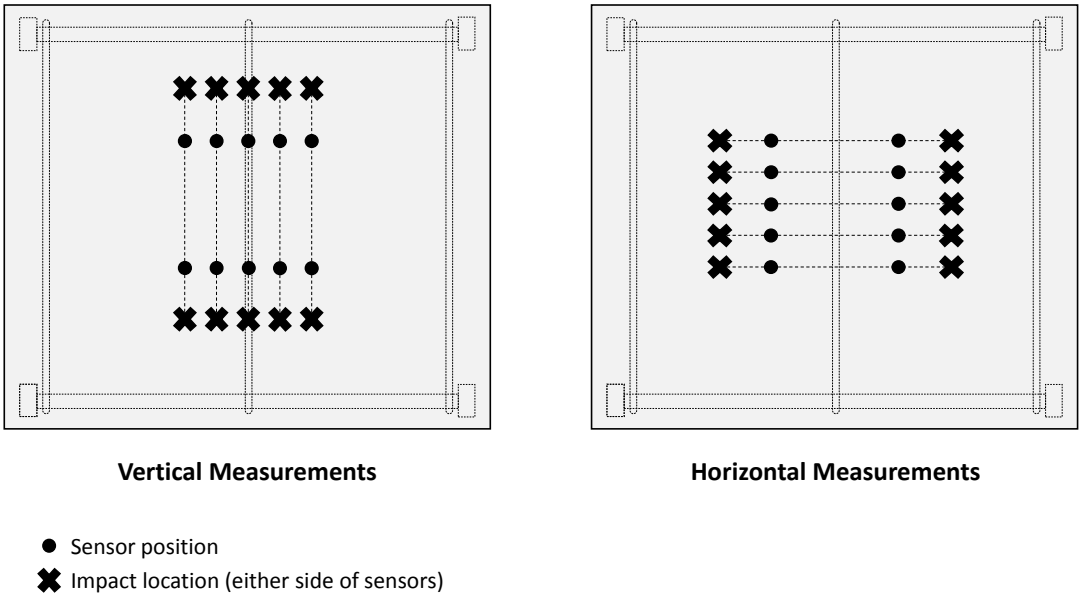

Figure 3-17: Surface Wave Testing Grid Layout

3.5 INDUCED STIRRUP FRACTURE

The primary objective of the *reactive* beam segments was to monitor the progression of ASR/DEF distress both before and after the development of reinforcing bar fracture. Results from NDT monitoring and observations of the surface crack patterns (discussed in Chapter 4) were expected to provide critical insight for the future assessment of existing deteriorated structures. Since the potential for PCD-induced reinforcing bar fracture was not likely within the timeframe of this study (recall that the discovery of fractures in Japan occurred after some twenty to thirty years of continuous expansion), a stirrup within one of the beam segments was intentionally severed approximately halfway through the testing program. Details of the processes for cutting

the bar will be discussed following a brief explanation of the rationale for the location and timing of the procedure.

Since the stirrup was going to be intentionally severed, it was desirable to cut the bar at the location where a fracture would most likely occur. A majority of the reported cases of bar fractures in Japan occurred at the stirrups in bent caps where the distribution of reinforcement was "low". In addition, fractures frequently occurred on the compression side of the beam and only at a designed bend. Therefore, the location of the cut was placed at the top corner of the center stirrup of Specimen 1 (recall spacing of transverse steel is twenty inches in Specimen 1). As stated earlier, the bar was severed approximately half way through the monitoring program. The reasoning for the timing of the cutting procedure was to allow for the expansion to progress beyond the yield strain of the steel reinforcing. Once the bars yielded, the maximum confining stresses were reached.

The procedure for cutting the stirrup is illustrated in Figure 3-18. First, the water within the concrete tank was drained. The cover concrete was chipped back with a hammer drill until the corner of the stirrup and underlying longitudinal bar was exposed. Only the concrete necessary to fit the cutting tool was removed, as feasible, to minimize the impact to the rest of the specimen. A pneumatic cut-off tool with a one-eighth inch thick cutting disc was used to sever the bar completely through. The final thickness of the cut was slightly over the thickness of the cutting disc; likely a result of user movement during the cutting operation and elastic rebound of the exposed section of bar. Expansion and non-destructive testing measurements were taken both before and immediately following the cutting operation.

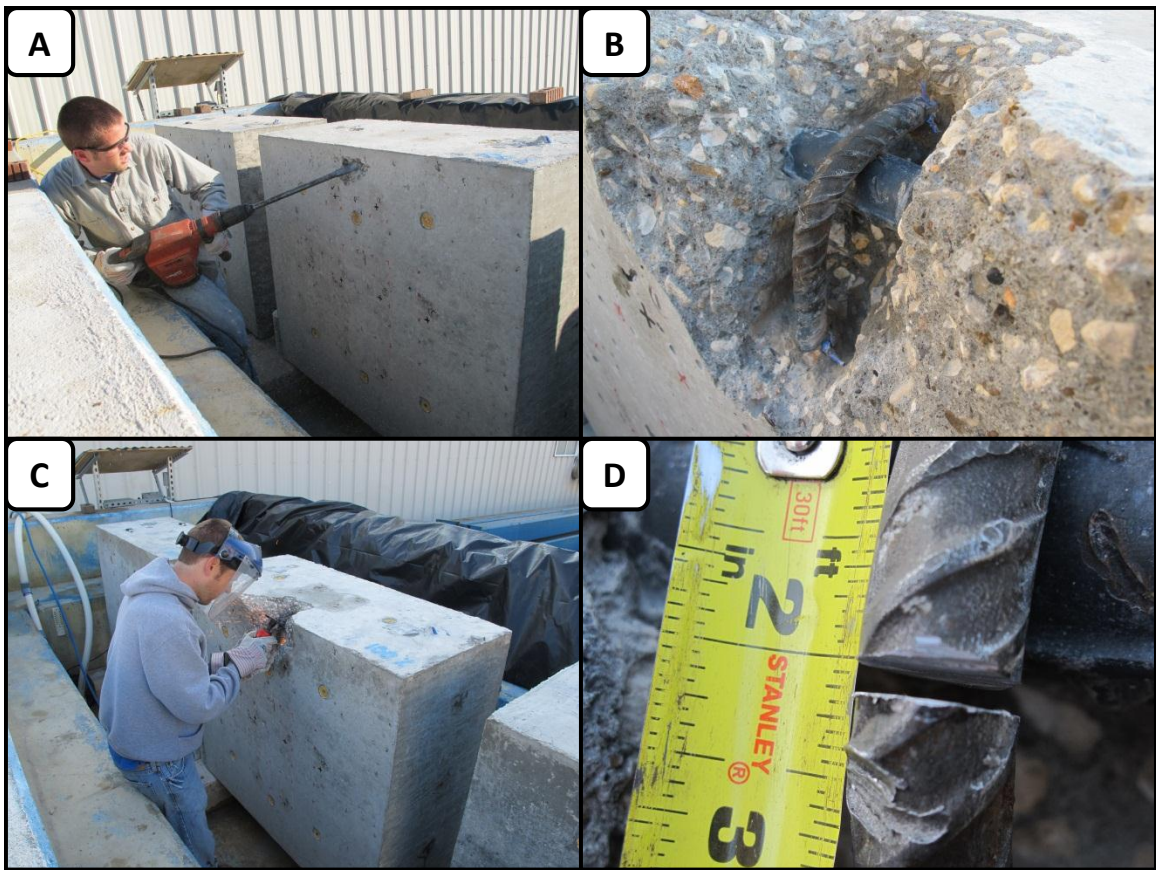

Figure 3-18: Induced Stirrup Fracture
(A) Concrete Cover Chipped Back (B) Stirrup Exposed
(C) Cutting Stirrup (D) Final Dimension of Cut

The chipped out concrete was patched following the cutting procedure. First, any loose concrete was chipped back using a welders' tomahawk style hammer and the area was flushed clean using a pneumatic blow gun and then moistened with a wet sponge. A sheet of plywood clamped to the face of the specimens served as formwork. A commercially available fast-setting repair mortar was mixed dry with sifted limestone gravel in a five-gallon bucket. Water was added to the dry repair mix until the desired consistency was achieved. The wet mix was then scooped into the chipped out area in approximately two inch layers. Each layer was consolidated with a standard cylinder rod. The top surface was feathered into the existing hardened concrete and finished with a concrete trowel. The repair was covered with a plastic sheet and cured for approximately

twenty-four hours. Photographs taken before and after the patch are shown in Figure 3-19. After the bar was severed and the patch cured, the tank was refilled and the specimens were covered for continued conditioning and monitoring.

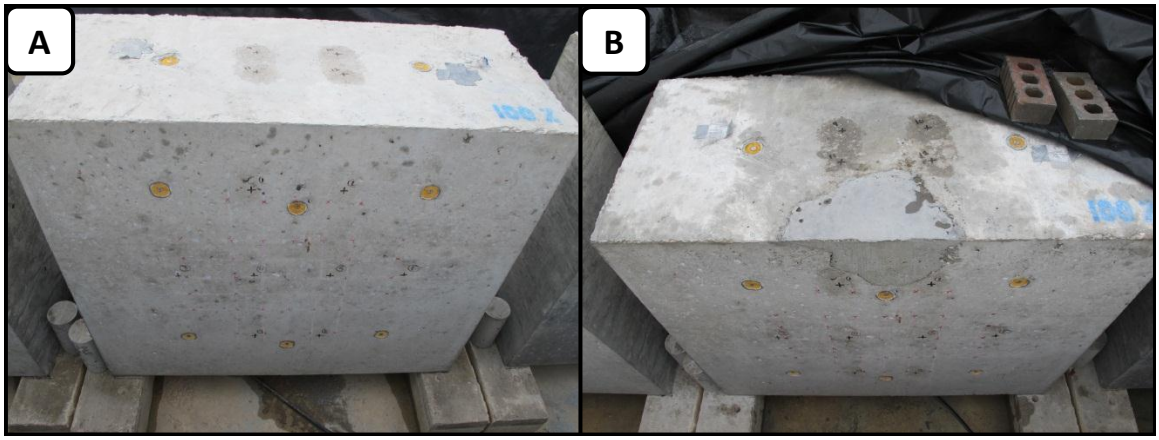

Figure 3-19: Specimen 1 (A) Before and (B) After Stirrup Severed

3.6 SUMMARY

In this chapter, details relating to the design and construction of the four beam segments were provided. Methods used in the experimental program for monitoring the specimens were explained. Special attention was paid to Specimen 1 and the procedure for intentionally severing the center stirrup. Observations made throughout the course of this study and results from continuous monitoring are examined in Chapter 4.

CHAPTER 4
Experimental Results: Beam Segments

4.1 OVERVIEW

Measurements and observations made over approximately three-hundred days of the experimental program are reviewed in this chapter. The development of premature concrete deterioration is explored first through an evaluation of the measured expansions and the observed cracking patterns. Results from the application of several non-destructive testing (NDT) techniques are examined in the context of their use in the evaluation of ASR/DEF-affected structures. Primarily, the influence of the intentionally severed stirrup on the behavior of the beam segments and the results of the various monitoring techniques is evaluated.

4.2 DEVELOPMENT OF ASR/DEF DETERIORATION

Expansion measurements made during the course of the study are presented in this section. In addition, details of the observed surface crack patterns are discussed. Emphasis is placed on the influence of the reinforcing configuration and the impact of the simulated bar fracture on the development of deterioration.

4.2.1 Measured Expansions

Expansion measurements presented herein served to quantify the level of physical ASR/DEF deterioration and were used for correlation with the NDT results discussed in Section 4.3. The expansion histories for the beam segments constructed of the reactive concrete mixture (Section 4.2.1.1) and those containing fly ash (Section 4.2.1.2) are presented separately to reflect the two independent objectives of the experimental program. Prior to presenting the data, a description of expansion calculations is given to aid in the interpretation of the results.

Expansion plots for each beam segment contain the history of both reinforcement strains and concrete core expansion in each direction (transverse and longitudinal). Each data point represents an average of all expansion measurements in the corresponding direction. For example, consider the illustration in Figure 4-1 at two different beam segment cross sections. The calculation of the reinforcement strains and concrete core expansion is an average of the measurements on each face of the specimen. Values across each cross section (see *Figure 3-11* for layout of targets in elevation) were then averaged to represent the total steel strain and core expansion in the transverse direction. Expansions in the longitudinal direction were computed using a similar approach. Using an average of the expansion measurements provided a reasonable representation of the individual measurements and was in agreement with the procedures used in the large scale bent cap specimens.

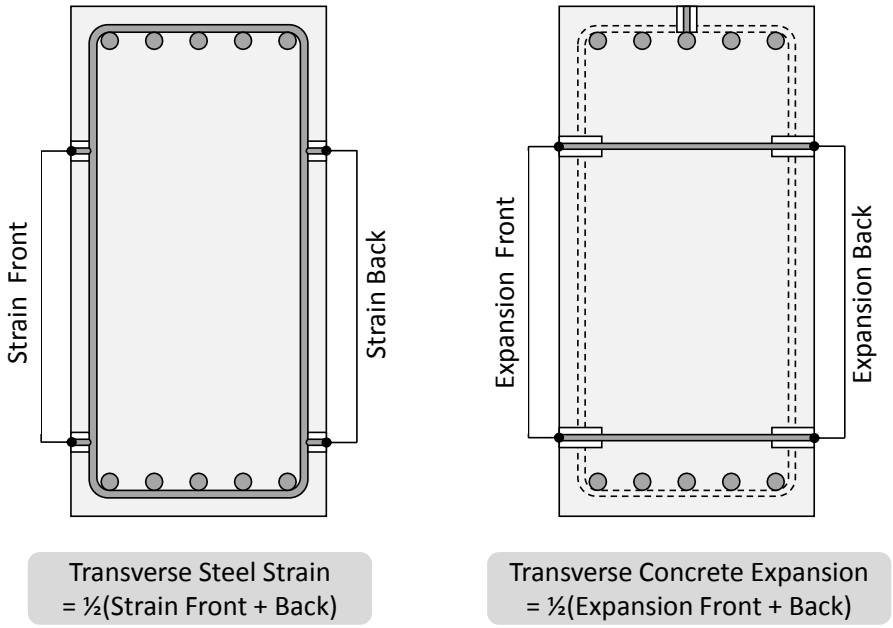

Figure 4-1: Calculation of Average Reinforcement Strains and Concrete Expansion (Adapted from Deschenes et al. 2009)

4.2.1.1 Specimens 1 & 2 (Reactive Concrete Mixture)

Expansion histories for the specimens constructed using the reactive concrete mixture are presented in Figure 4-2 and Figure 4-3. Reinforcement strains are presented as solid black lines, and corresponding concrete core expansions are shown using grey dashed lines. A small diagram in the upper left hand corner indicates the location of averaged measurements within each beam segment.

Specimen 1 began expanding immediately after construction. The expansion was primarily oriented in the less restrained transverse (vertical) direction. The addition of the water heater after ninety-eight days of storage seemed to slightly accelerate the rate of concrete expansion. Consequently, yielding of the transverse stirrup occurred within approximately one-hundred and ten days after fabrication. As predicted during design (based on results from the large scale specimens), the concrete expansion in the longitudinal direction failed to yield the longitudinal reinforcing steel, and the maximum strain in the steel was only 0.06 percent.

Initially, the core concrete expansion and the reinforcing strain in the transverse and longitudinal directions grew at the same rate. The two curves quickly deviated, however, and then "shadowed" each other in both directions. This is likely due to the arrangement of monitoring hardware within the beam segments, as the core and reinforcement measurements did not coincide at the same location on the beam segment, and minimal restraint was provided by the single transverse stirrup. After the stirrup was cut on the front face (see marker at 174 days on Figure 4-2), the transverse expansion in the core concrete and the strain in the reinforcement began to diverge from one another. Eventually, the strain in the stirrup began to level off as the cut stirrup was no longer able to confine the concrete. At the conclusion of the monitoring program, the maximum average strain within the transverse reinforcement was 0.67 percent.

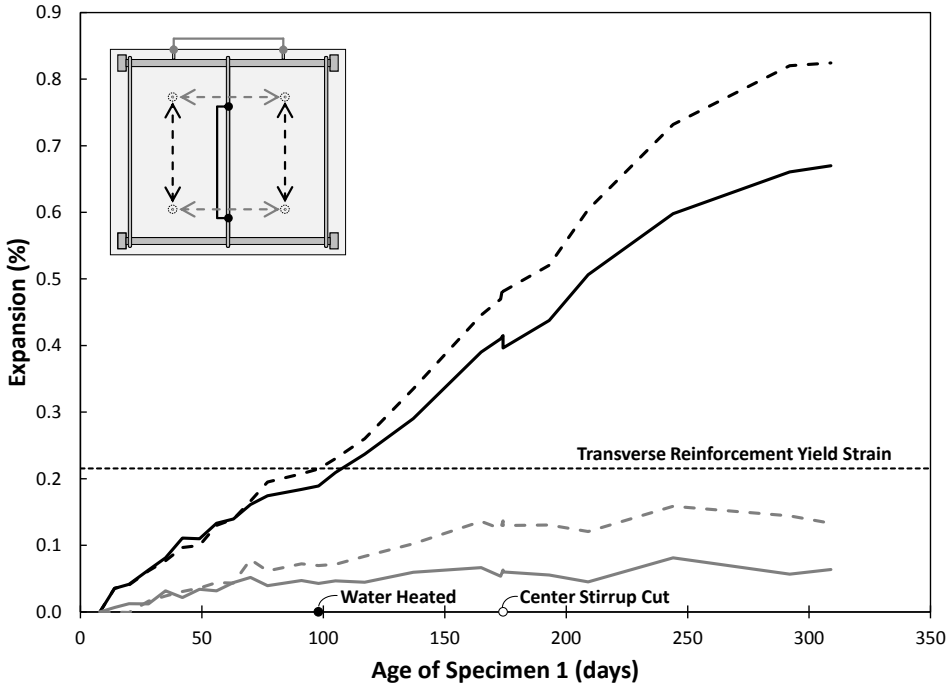

Figure 4-2: Specimen 1 Measured Expansions

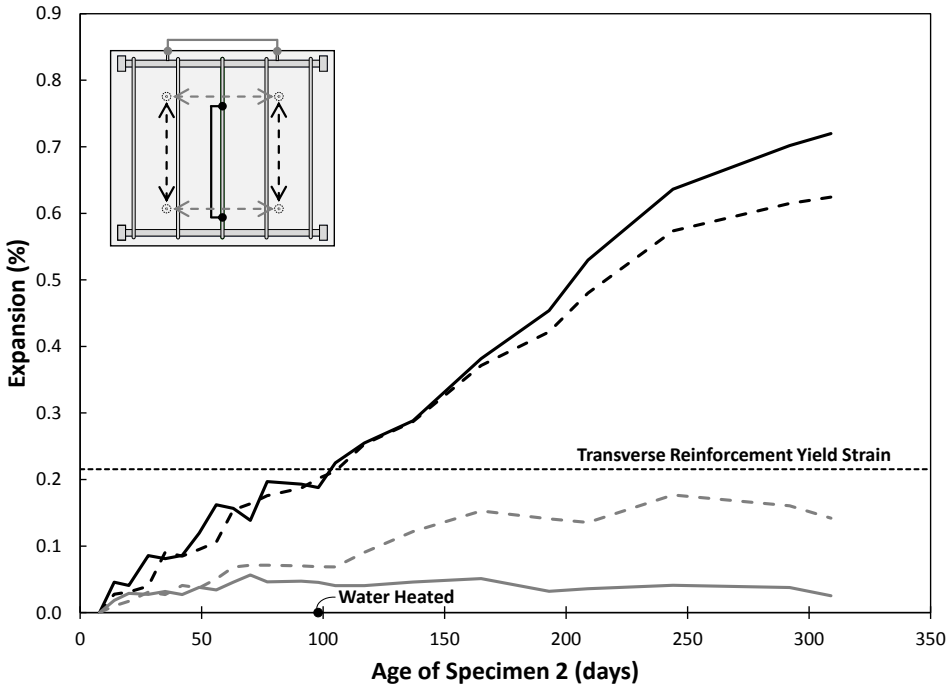

Figure 4-3: Specimen 2 Measured Expansions

The development of ASR/DEF deterioration in Specimen 2 was very similar to Specimen 1, and the expansion was primarily concentrated in the transverse direction. Slightly less deviation between the transverse core expansions and the steel strains were likely a result of the more closely spaced stirrups and a more even distribution of the expansion in the vertical direction. The maximum average strain in the transverse reinforcement was 0.72 percent. Moreover, the concrete expansions failed to significantly strain the longitudinal reinforcement. Therefore, the reduction in the development length calculation of the longitudinal bars during the design was justified for both reactive specimens.

4.2.1.2 Specimens 3 & 4 (Concrete Mixtures Containing Fly Ash)

The expansion histories for Specimen 3 (25% fly ash replacement) and Specimen 4 (25% fly ash addition) are shown in Figure 4-4 and Figure 4-5, respectively. The vertical scale is held the same as the reactive specimens so that a direct comparison can be made between the two. Initially, relatively low expansions were measured in both Specimens 3 and 4. Almost immediately, however, the expansion leveled off and continually fluctuated around the initial "spike". The largest average strain in the transverse steel was 0.08 percent in Specimen 3 and 0.06 percent in Specimen 4.

From the expansion histories, it appears that fly ash, as used within this study, is effective at arresting the development of deleterious concrete expansion. Although these results are promising, extreme caution should be exercised in their interpretation; as this study was limited in both time and breadth. It is possible that the internal reactions have only been delayed and that given time the effects (i.e. concrete expansion and surface cracking) will become noticeable. In addition, only a single type of fly ash was used in this study (Class F from Rockdale, Texas). This specific ash has proven to be quite effective in reducing ASR/DEF distress and another, less efficient, fly ash might require different proportioning to achieve the same results. In short, a more comprehensive materials testing program is necessary before conclusive recommendations can be made.

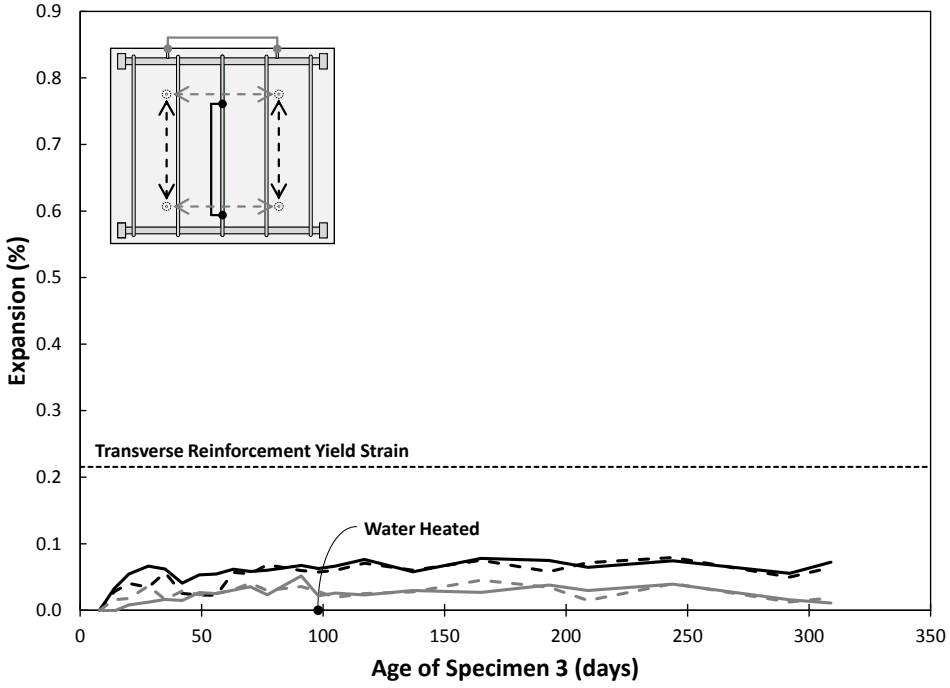

Figure 4-4: Specimen 3 Measured Expansions

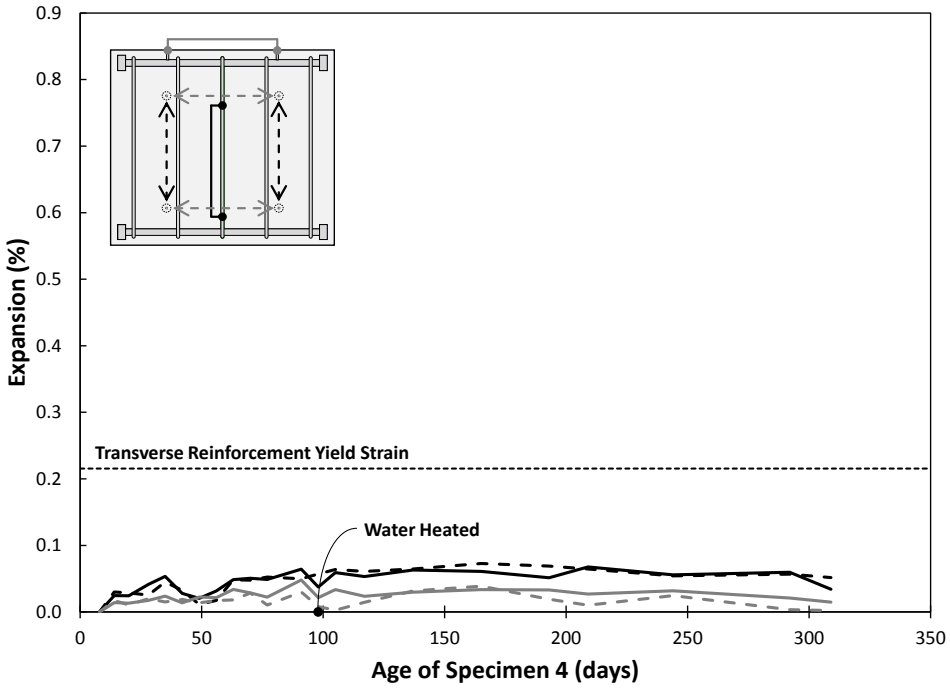

Figure 4-5: Specimen 4 Measured Expansions

4.2.2 Observed Cracking

The primary indication of ASR/DEF deterioration within structural elements is the development of surface cracking. Observed cracking of the reactive beam segments are discussed here through a review of photographs taken throughout the experimental program. Particular emphasis is placed on the influence of the reinforcement restraint and the effects of the simulated stirrup fracture on the cracking patterns. Note that Specimen 3 and Specimen 4 did not experience ASR/DEF- related expansion in the time frame of this study and, therefore, are excluded from this discussion.

4.2.2.1 General Observations

Visual signs of deterioration were first observed on Specimen 1 and Specimen 2 within weeks of construction. Vertical cracks first appeared on the ends of the beam segments and cracks oriented longitudinally (horizontal) on the faces at mid-depth. Eventually, a fine distribution of cracks manifested on all faces as the specimens continued to expand. Photographs of the front face of the reactive beam segments after approximately ten months are presented in Figure 4-6 and lead the discussion that follows.

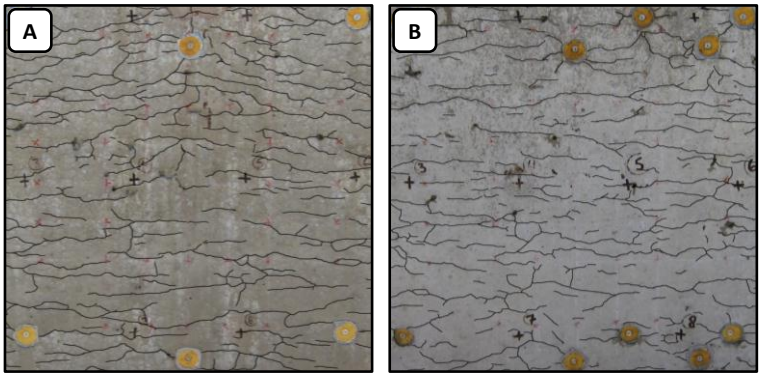

Figure 4-6: ASR/DEF Surface Cracking (A) Specimen 1 (B) Specimen 2

The distribution of surface cracks within the test regions of both specimens was a direct influence of the directionality of the ASR/DEF-induced expansion and the restraint imposed by the reinforcement. The cracks were primarily oriented in the longitudinal

direction (i.e. running the length of the specimens) due to the dominating transverse expansion. The average spacing between longitudinal cracks was approximately one to two inches. Crack widths were typically limited to 0.003 inches in width. The largest cracks were located at approximately 1/3 and 2/3 of the total height and measured 0.012 inches in width on Specimen 1 and 0.008 inches on Specimen 2. Consideration of the maximum crack widths showed that the distribution of transverse reinforcing (20-inch stirrup spacing for Specimen 1 as opposed to 9.5-inch stirrup spacing for Specimen 2) directly influenced the development of surface cracking. Furthermore, the cracking in the transverse direction (i.e. vertical) was an effect of the greater percentage of reinforcing in the longitudinal direction. Crack widths in the transverse direction were much smaller and fewer were observed. Transverse cracks were typically spaced four to six inches apart and were only as long as the spacing of the longitudinal cracks.

Particularly severe vertical cracks were observed on the ends of each reactive beam segment as shown in Figure 4-7. The vertical cracks originated at mid-depth and then terminated as a diagonal crack at each corner. The maximum crack width measured approximately one-eighth of an inch. In addition, the ends of the specimens distorted substantially as the core concrete expanded (Figure 4-8). Recall from the layout of reinforcing steel (see Chapter 3) that no reinforcement was provided across the beam segment ends to control horizontal expansion and limit the growth of surface cracks. The observed damaged demonstrates that the directionality and severity of ASR/DEF expansion is directly influenced by the restraint imposed by the reinforcement.

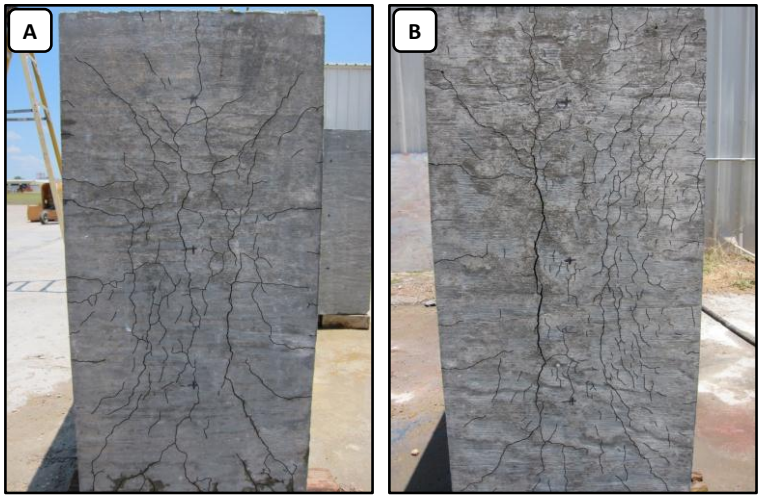

Figure 4-7: Cracking at Beam Segment Ends (A) Specimen 1 (B) Specimen 2

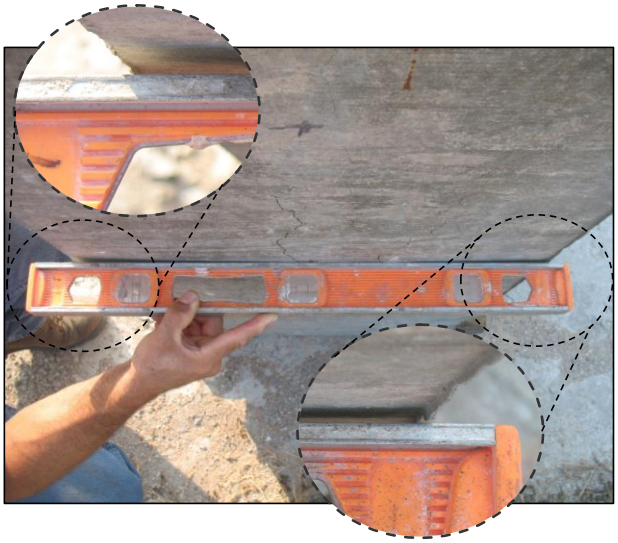

Figure 4-8: Distortion of Beam Segment Ends

4.2.2.2 Influence of Fractured Stirrup

Specimen 1 was used to explore the influence of a fractured bar on the observed crack patterns. As discussed in Chapter 3, approximately midway through the monitoring program the center stirrup was intentionally cut and the concrete repaired. Consequently, future monitoring of the surface cracking in the vicinity of the patch provided insight into the development of ASR/DEF distress after the loss of reinforcement restraint.

As reviewed in the previous section, the surface cracking within the test region of Specimen 1 was virtually indistinguishable from cracking observed on Specimen 2; however, the crack pattern was remarkably different at the location of the fractured stirrup. A crack had developed across the front face of the specimen at the level of the longitudinal reinforcing within weeks after cutting the stirrup and patching the chipped out concrete. As shown in Figure 4-9, as the specimen continued to expand the width of the crack continuously grew until, when the surface cracking was last documented within Specimen 1, the crack width was 0.08 inches. Additionally, a narrower vertical crack with a maximum width of 0.008 inches had developed in-line with the stirrup.

Figure 4-9: Surface Cracking at Location of Fractured Stirrup

It should be noted that the pattern of cracking observed on Specimen 1 was not observed on Specimen 2 and was consistent with the reinforcing bar fracture investigations conducted in Japan (see Chapter 2). The development of a large crack was easily attributed to the loss in restraint caused by the fractured stirrup. As shown in Figure 4-10, a final inspection of the fractured bar revealed that the stirrup had opened up to five-sixteenths of an inch as the specimen continued to expand. In effect, cutting the stirrup resulted in a loss of confinement and allowed for typical narrow ASR/DEF-induced surface cracks to grow almost freely.

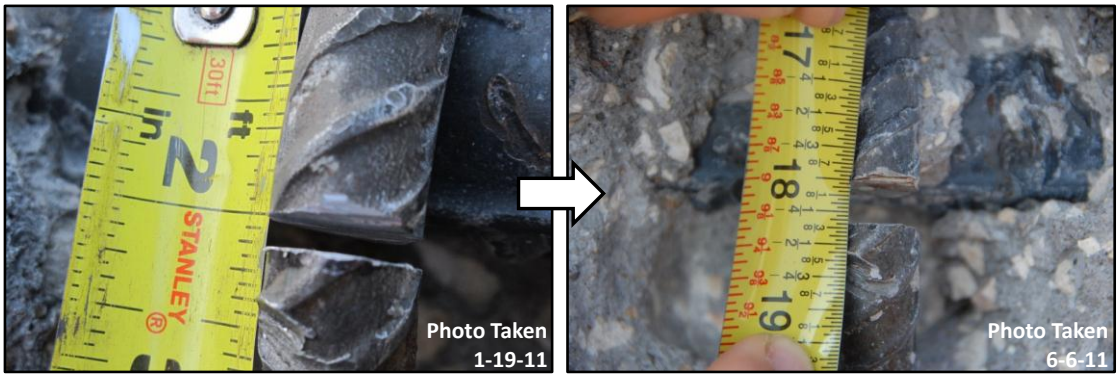

Figure 4-10: Growth of Cut in Stirrup due to Concrete Expansion

Practically speaking, monitoring of the surface cracking can be used quite effectively during an inspection of a structural element, as cracking in the vicinity of the bend in a stirrup may indicate the development of bar fracture. As was the case for Specimen 1, a large surface crack atypical of the essentially uniform cracking elsewhere on the specimen revealed the existence of the fractured bar.

4.3 NON-DESTRUCTIVE TEST RESULTS

Results from the four NDT techniques evaluated during the monitoring program are contained in this section. Although the reactive beam segments were monitored continuously throughout the experimental study, emphasis is placed on the applicability of the test methods to detect a reinforcing bar fracture. A detailed description of the procedures for analyzing the test measurements and computing the response parameters, as well as further evaluation of each method's use in assessing the extent of ASR/DEF deterioration in field structures, are contained in additional work from TxDOT Project 0-6491 (see Kreitman 2011).

The results are provided as a plot of the NDT parameter on the ordinate and the average transverse expansion on the abscissa. Generally, the primary y-axis (left side) is of the actual NDT parameter and the corresponding secondary y-axis (right side) is of the percent change in measurements computed from the initial value. Expansion measurements were used on the x-axis rather than time to "normalize" the level of deterioration so that results from both reactive specimens (i.e. Specimen 1 and Specimen 2) could be plotted and compared on the same graph. A small diagram of the cross section on each plot indicates the direction of NDT measurements. Each data point is representative of an average of the NDT measurements in each direction across the entire test region on a particular day of recording data. In this manner the presentation of results is consistent with the NDT testing conducted on the large scale bent cap specimens. In addition, a marker on the x-axis points to the timing when the stirrup was cut on Specimen 1.

4.3.1 Ultrasonic Pulse Velocity (UPV)

UPV testing was one method used for computing the compression wave velocity through the deteriorated specimens. In general, a decrease in the velocity is indicative of damage, and it was originally conceived that the loss of confinement due to fracture of the transverse stirrups would result in almost free expansion of the concrete core and, consequently, a drop in the compression wave velocity.

Results from UPV testing horizontally through the width of the cross section are shown in Figure 4-11A. The change in compression wave velocity was almost identical for the two specimens. A drop in the average compression wave velocity of approximately thirteen-percent initially occurred at low levels of expansion (up to 0.1 percent). As deterioration progressed, the rate of loss in velocity began to slow and eventually leveled off. After the stirrup was cut in Specimen 1 and the beam segment continued to expand, a loss in velocity of only one and a half percent was observed.

Similarly, results for measurements taken diagonally across the top corners (Figure 4-11B) revealed a similar trend, although the data was much more scattered. The inconstancies in the results are likely due to coupling issues encountered during testing as the top surface of the specimens was only trowel finished and very rough as opposed to the smooth side surfaces that were cast against the steel formwork. Regardless, it was believed that as the surface crack at the location of the fractured bar was able to penetrate into the concrete core, the compression wave velocity would decrease as it took longer to travel through or around the crack. After the stirrup was cut in Specimen 1, the loss in average velocity measured across the diagonals began to decrease, and a drop of approximately twelve percent was measured. At first glance these results seem promising; however, at equivalent levels of expansion a sudden drop in the velocity for Specimen 2 of approximately eight percent was also observed.

Practically speaking, the use of UPV testing as indication of the presence of a fractured bar is not warranted. Primarily, the compression wave velocity measured through UPV is a very local test. Results can vary greatly throughout a structural element where ASR/DEF deterioration is also non-uniform or other forms of defects (i.e. poor consolidation, delamination, mechanical distress) exist. A change in velocity from one section of a structure to another could easily exceed the virtually insignificant changes observed within this study after the stirrup was fractured in Specimen 1. Furthermore, it is not likely that an inspection would be initiated until surface cracking indicative of concrete deterioration had already progressed to the point where very little change in velocity was observed.

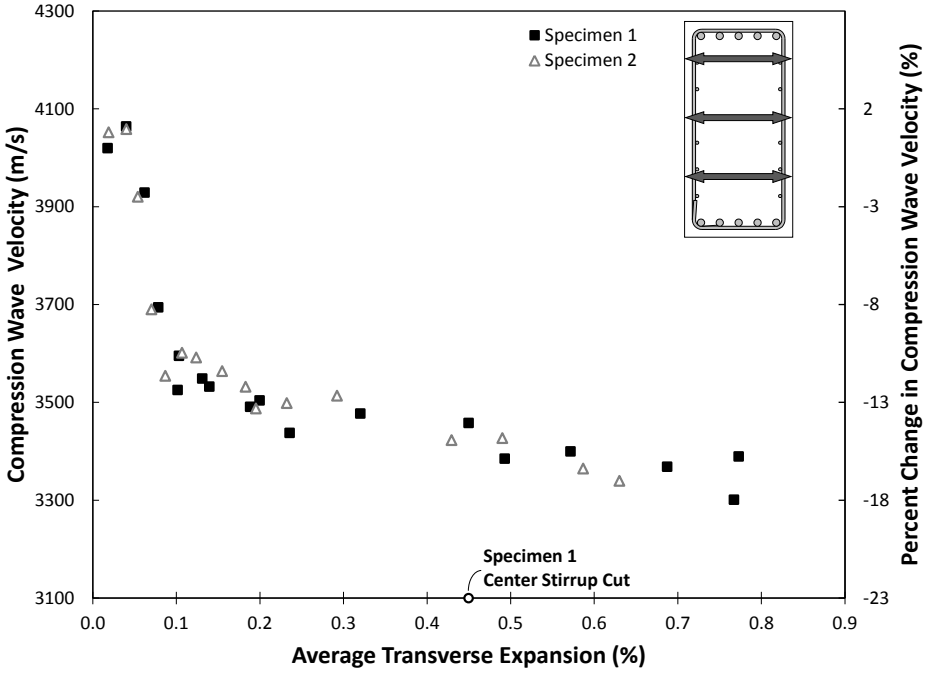

(A)

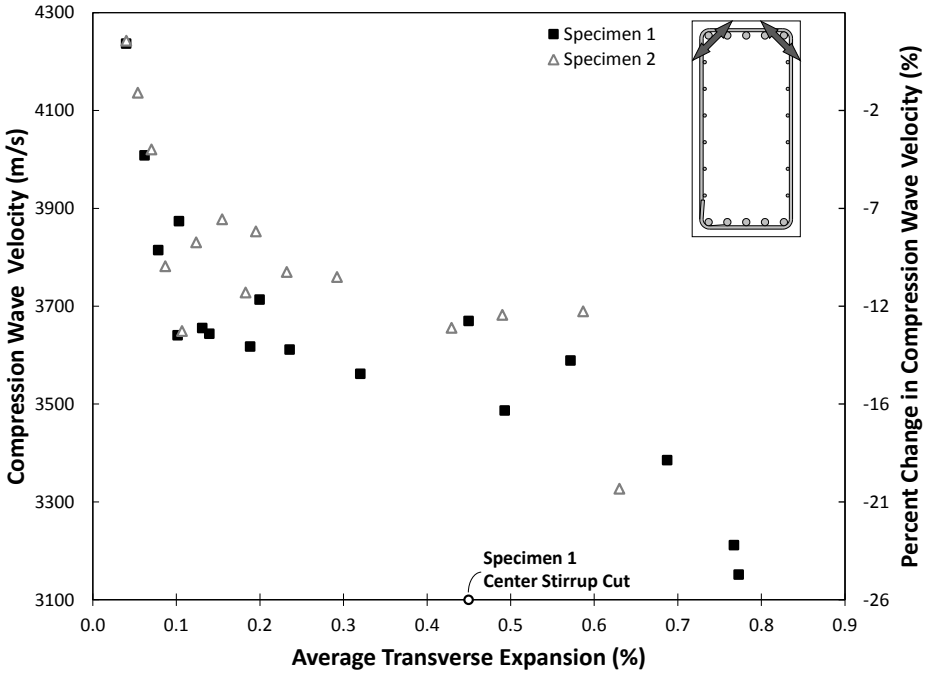

(B)

Figure 4-11: UPV Test Results

4.3.2 Impact Echo

The compression wave velocity, computed from an analysis of the surface displacement signals recorded via impact echo testing, was also used for quantifying the level of ASR/DEF distress. Similar to UPV testing, a loss in the compression wave velocity is indicative of an increase in deterioration. Results from impact echo testing are presented in Figure 4-12. The scale of the primary y-axis is consistent with the results from UPV testing so that a direct comparison can be made between the two methods.

Impact echo testing results through the width of the cross section are shown in Figure 4-12A. The impact echo method was developed for plate-like elements; therefore, the data shown is only an average of the points on the testing grid that were located at mid-depth on each side. The trends and actual values of the compression wave velocity from impact echo testing are very similar to those observed from the UPV test method. A sharp decrease in the velocity at early levels of expansion was followed by a gradual decline as deterioration progressed. A downward spike was observed in the velocity from testing through the width of Specimen 1 near the end of the monitoring program that appears to indicate further deterioration. However, when the last measurement was recorded the velocity rebounded and only a two percent decrease in velocity was observed after the stirrup was cut.

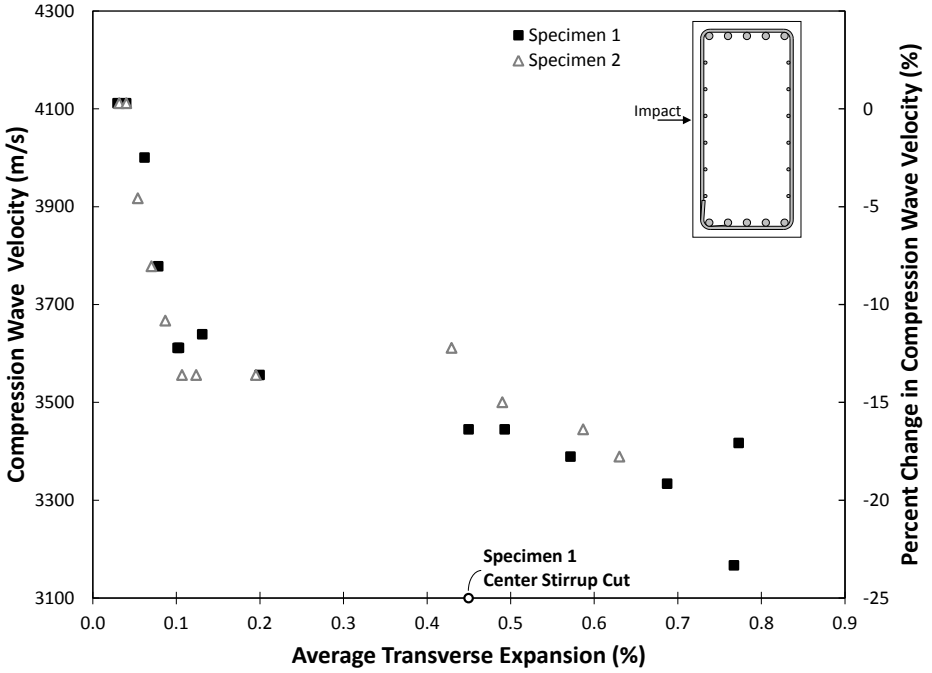

(A)

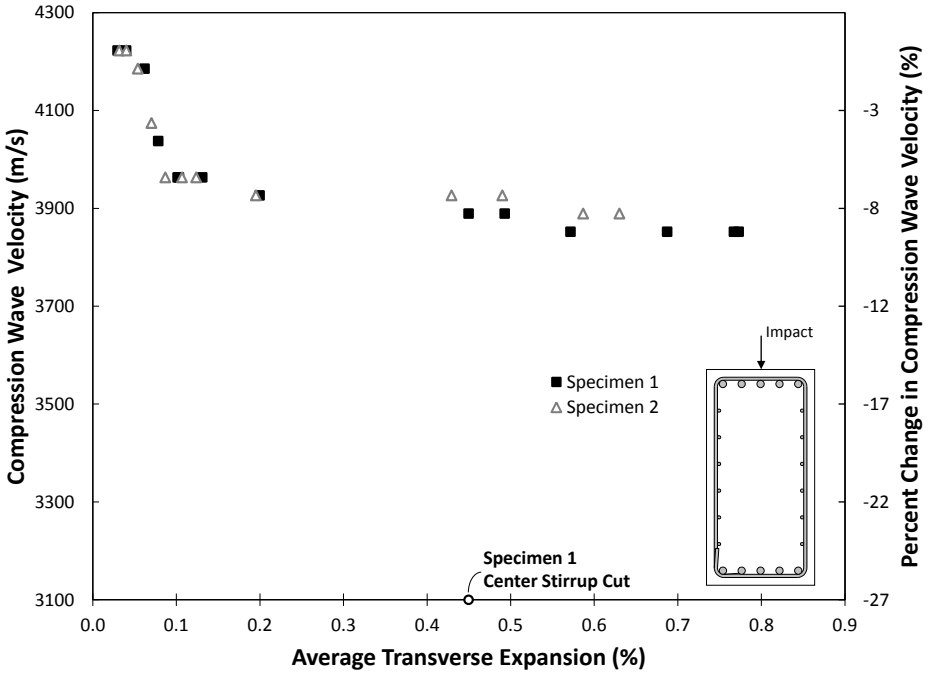

(B)

Figure 4-12: Impact Echo Test Results

Variations in the compression wave velocity, computed from impact echo testing, through the depth of the cross section are shown in Figure 4-12B. Again, the trends are similar from testing through the side of the member; however, the magnitude of the compression wave velocity is slightly different. The velocity in the transverse direction started at approximately 4200 m/s and then initially decreased by approximately seven percent. After the center stirrup was cut in Specimen 1, the velocity only decreased by an additional one percent. Furthermore, only slight differences between the compression wave velocity through Specimen 1 and the velocity measured through Specimen 2 were observed.

The considerably smaller decrease in the velocity observed between testing in the vertical direction versus testing through the cross section is possibly an effect of the geometry of the specimen that results in reflections of the compression wave off the side boundaries. These reflections are more prominent in the received signals than reflections that indicate damage and can skew the results. Recall that the width of the beam segments is only one-half of the total height and, therefore, measurements through the side of the specimens were better suited for the impact echo technique.

Like the UPV test method, the impact echo technique is not intended for the purpose of characterizing ASR/DEF-related deterioration. As observed in the results from the monitoring of Specimen 1, irrespective of direction, the compression wave velocity both before and after the stirrup was cut was virtually indistinguishable. Therefore, the use of impact echo testing for detecting the loss in confinement through the fracture of a bar is not recommended.

4.3.3 Surface Wave Methods

4.3.3.1 Spectral Analysis of Surface Waves (SASW)

The velocity of a mechanically induced wave travelling through the concrete surface was calculated using the SASW method. As with the compression wave techniques, a decrease in velocity as the wave travels through or around defects is an indicator of damage. Results from SASW testing in both the transverse and longitudinal direction are shown in Figure 4-13. As discussed in Chapter 3, each data point is representative of an average of all measurements within the test region.

Results from the SASW testing are widely scattered. An initial drop in the surface wave velocity of approximately eight percent in both directions is followed by an unclear trend as deterioration progresses. Little to no impact on the surface wave velocity was observed after the stirrup was severed in the beam segment. In fact, a rebound in the velocity (indicating less deterioration) was observed in the longitudinal direction at larger levels of expansion. A discussion of the usefulness of the SASW method for quantifying ASR/DEF deterioration and detecting a reinforcing bar fracture follows a presentation of the results from surface wave transmission test method.

4.3.3.2 Surface Wave Transmission (SWT)

The loss in energy between the two receivers, rather than velocity, of a mechanically induced surface wave is computed using the SWT method to characterize damage. The energy loss is presented as a transmission coefficient which is the ratio of energy present at the second receiver to that at the first. The transmission coefficient is plotted against the average transverse expansion for SWT testing in both the transverse and longitudinal directions in Figure 4-14. The ideal transmission coefficient, representing the expected energy loss in undamaged concrete due solely to the spacing of the receivers, is represented on the graph as a horizontal dashed line.

The loss in energy transmission was similar to what was observed in the surface wave velocity measurements. Any loss in the transmission coefficient at early levels of

deterioration either leveled out or rebounded as the expansion continued. Moreover, the results of the SWT test do not indicate a loss of confinement through the fracture of the transverse reinforcement.

It is clear from the results of both the SASW and SWT methods that the use of surface wave testing for characterizing ASR/DEF deterioration, or detecting induced stirrup fracture, is not justified. Although the distribution and severity of cracking on the concrete surface continuously grew as the specimens expanded, the results from the surface wave testing indicated little to no additional damage beyond the initial drop. It is believed that this is likely a result of reflections from the cracks affecting the signal, making signal analysis more difficult. Thus, the surface wave techniques are not suited for the fine distribution of cracking associated with ASR/DEF distress. More importantly, as discussed in Chapter 2, the structural integrity of a deteriorated reinforced concrete elements is maintained by the confinement of the concrete core. The network of finely distributed surface cracking typical of ASR/DEF distress gives little indication of the condition of the confined core and, therefore, testing of these cracks on the damaged surface via surface wave techniques is of no value.

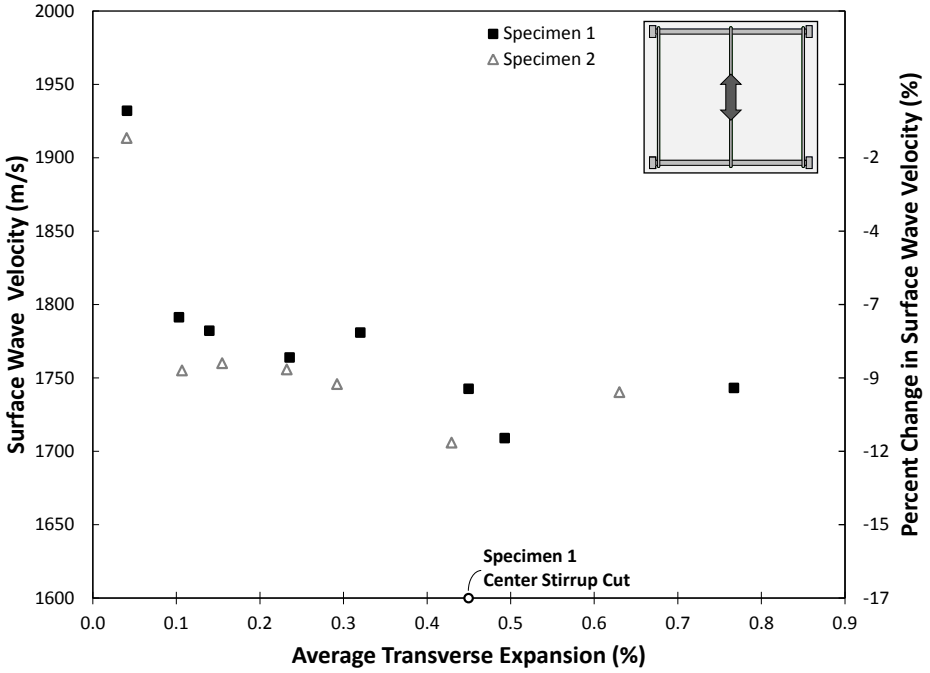

(A)

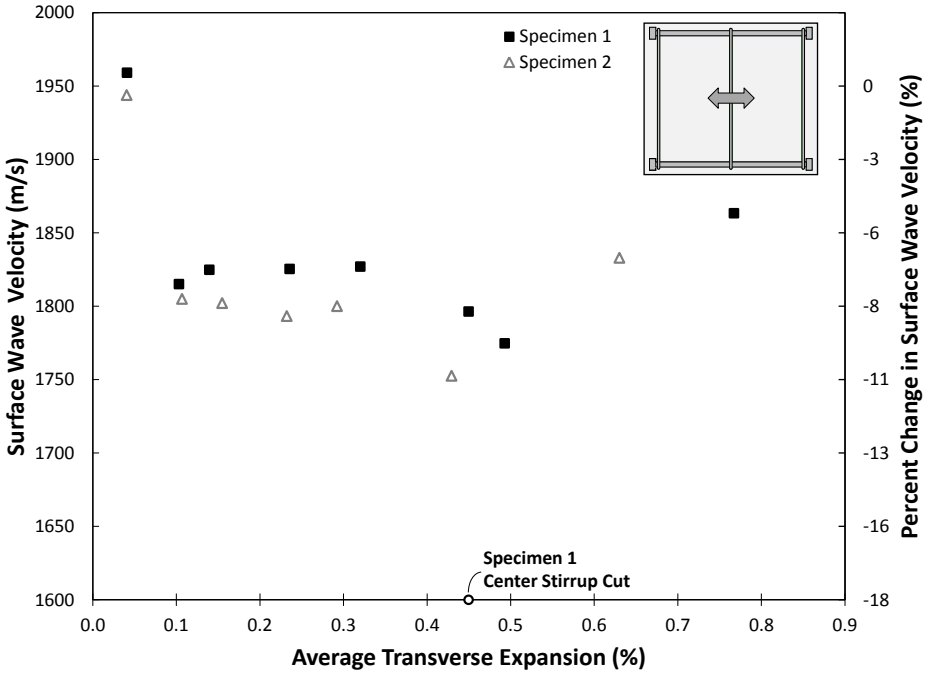

(B)

Figure 4-13: SASW Test Results

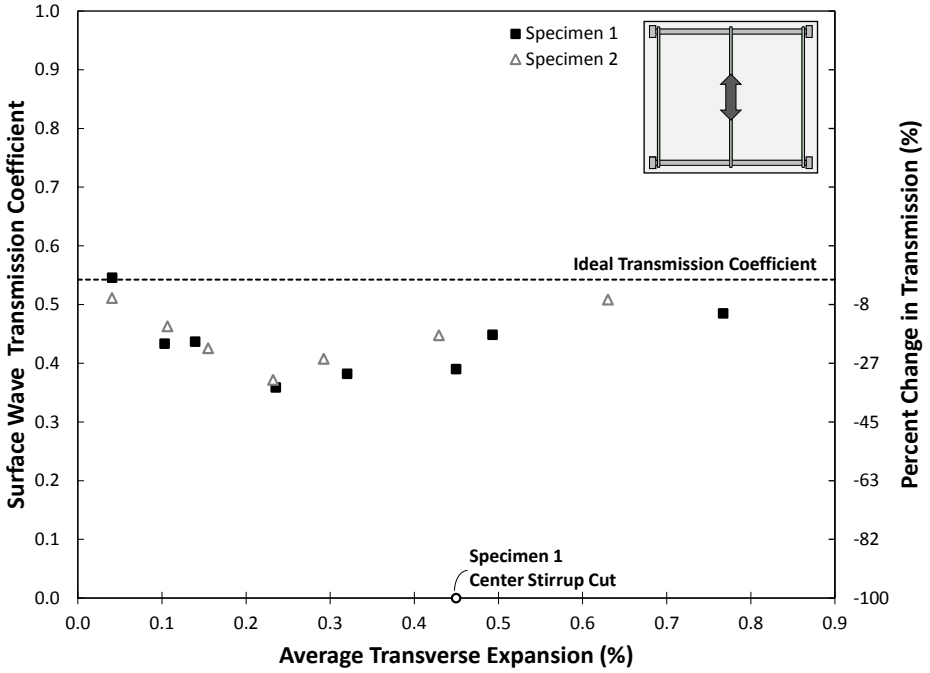

(A)

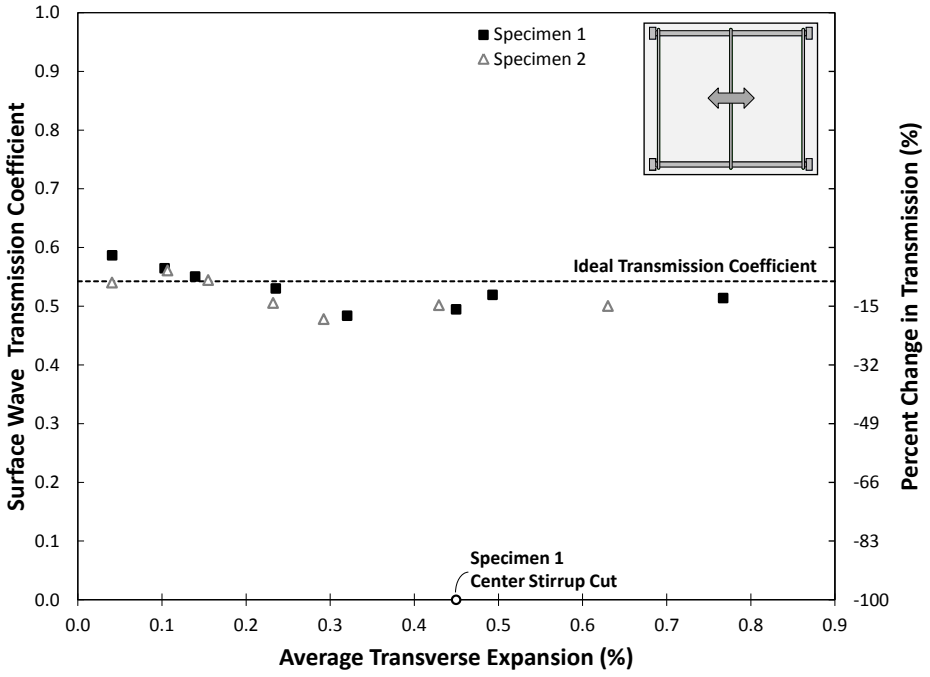

(B)

Figure 4-14: SWT Test Results

4.4 SUMMARY

In Chapter 4, experimental results for the monitoring of the concrete beam segment specimens were discussed. An emphasis was placed on Specimen 1, in which the influence of a fractured reinforcing bar was explored by cutting the center stirrup partway into the experimental program and monitoring the specimen after further deterioration. The development of ASR/DEF distress was characterized by a detailed description of the measured expansions and the observed cracking patterns. While Specimen 1 and Specimen 2 started expanding almost immediately after construction and continued throughout the testing program, expansions in Specimen 3 and Specimen 4 were limited to very low values. In general, expansions of the reactive beam segments were primarily concentrated in the transverse direction due to the behavior of ASR/DEF distress and the layout of reinforcing.

As a result of the anisotropic expansion, the surface cracking in the testing region was very similar between the two reactive specimens. Cracks running the length of the specimens (longitudinally) were much wider and more frequent than cracks running in the transverse direction. The intentional fracturing of the stirrup in Specimen 1 had little influence on the crack patterns within the test region; however, at the location of the severed bar, a crack developed across the surface almost immediately and continued to open up as the specimen expanded. A final inspection of the stirrup revealed that the bar had opened up from the initial cut by an additional three-sixteenths of an inch which resulted in a 0.08 inch wide penetrating surface crack. It was concluded that monitoring of surface cracks on deteriorated structures could give an indication of an ASR/DEF-induced bar fracture.

Lastly, monitoring of the specimens included the application of several NDT techniques. UPV, impact echo, and two surface wave methods (SASW and SWT) were evaluated to determine their use in characterizing ASR/DEF deterioration and for detecting the loss of confinement of the concrete core through fracture of the transverse stirrup. Almost no change in any of the test results was observed at higher levels of

expansion, regardless of the condition of the stirrups. Furthermore, it was noted that each of these test methods evaluates local conditions of the concrete material and they lack any structural context (i.e. confinement provided by reinforcement) necessary for implementation in field structures.

The reader is advised to note that the remainder of this thesis, Chapter 5 and Chapter 6, is dedicated to an independent, yet related, study. A summary of all the experimental work and the primary conclusions drawn from the beam segments are reported in Chapter 7.

CHAPTER 5
Experimental Program: Reinforcing Bar Bend Tests

5.1 OVERVIEW

The discovery of reinforcing bar fracture in Japan as a result of ASR-induced concrete expansions was discussed in detail within Chapter 2. Fortunately, no cases of reinforcing bar fracture have been reported within the Texas (or the United States) inventory of ASR/DEF-affected structures and, thus far, the discovery of such fractures has been limited to Japan. However, in recognition of the implications of reinforcing bar fracture as a serious compromise of structural safety, it is of interest to investigate the potential for bar fracture within Texas and the United States. An experimental program was developed at The University of Texas at Austin to address the shortcomings identified in Chapter 2 regarding the mechanisms of reinforcing bar fracture and the difficulties in accurately comparing Japanese steel with the U.S. counterpart.

Experimental research conducted in Japan (see summary of research in Chapter 2) classified the process of reinforcing bar fracture into two categories: (1) initial cracks formed during construction (bending) and (2) the development of cracks that occur due to ASR induced expansion (Kawashima et al. 2008). A total of twenty-seven reinforcing bar bend test specimens (classified as Series I and Series II) were considered to investigate (I) the existence of cracks formed during bending and (II) the development of cracks after application of an expansive force.

The organization of this chapter is as follows: Reinforcing bars used for the bend test specimens are examined first. Details of the bend test program, more specifically the selection of test variables and the testing procedure for both the Series I and Series II Bend Tests, are then revealed. Finally, a discussion of the techniques used for detecting potential cracks is followed by a description of the nomenclature used for identifying the bend test specimens.

5.2 REINFORCING BAR DETAILS

The selection of reinforcing steel bar samples for bend testing was based on three criteria. First, the samples were chosen so that a variety of commonly produced deformation patterns available in the United States would be represented. Japanese investigations revealed that the development of cracks at the interior of the bend was highly dependent on the rib geometry, and so it was desirable to test a number of bars with different rib shapes. In general, the deformation patterns on a reinforcing bar are specific to the mill where the bars are manufactured. Thus, for the purposes of this study, samples of bar were ordered from three different manufactures.

Secondly, the selection of bar size to maximize the ratio of bar diameter to the Code specified minimum bend diameter was essential to investigate the worst case for bar fracture. For a fixed bend diameter, an increase in bar size will enhance the likelihood of larger stress concentrations, and possible compression cracking, at the base of the transverse ribs. Likewise, if the bar size is held constant, a decrease in bend diameter will increase the probability of cracking on the interior radius of the bend (Erasmus 1981). As such, for the purposes of this study, the size of bars to be tested should be indicative of the worst case for producing a crack at the interior of a bent bar.

Finally, to control all aspects of the bending operation, all samples were to be bent cold at Ferguson Structural Engineering Laboratory (FSEL) rather than delivered from the materials supplier pre-bent. The practicality of bending bars without the aid of hydraulic powered reinforcing bar bending machinery limited the size of bars for test specimens to No. 5 and smaller.

In order to satisfy the above mentioned criteria, No. 5 reinforcing bar was selected for the bend tests. Samples of bar were delivered to Ferguson Laboratory from three different manufacturers, identified as A, B, and C. Prior to bend testing, a representative sample from each bar manufacturer was selected for materials testing. A comparison of the deformation geometry, mechanical properties, and chemical composition, of the three

sets of bar are included in this section to aid in identifying the key parameters when interpreting the results of the bend tests.

5.2.1 Deformation (Rib) Geometry

Deformation patterns from the three suppliers are shown in Figure 5-1. The angle of deformations with the axis of the bar is 90° for Manufacturer A, 60° with a reversal in direction on each side of the bar for B, and 60° alternating with a reversal for C. The transverse deformations on the bars from Manufacturer A and Manufacturer C taper slightly before intersecting the longitudinal rib. The deformations on the bars from Manufacturer B extend to the longitudinal rib with no taper.

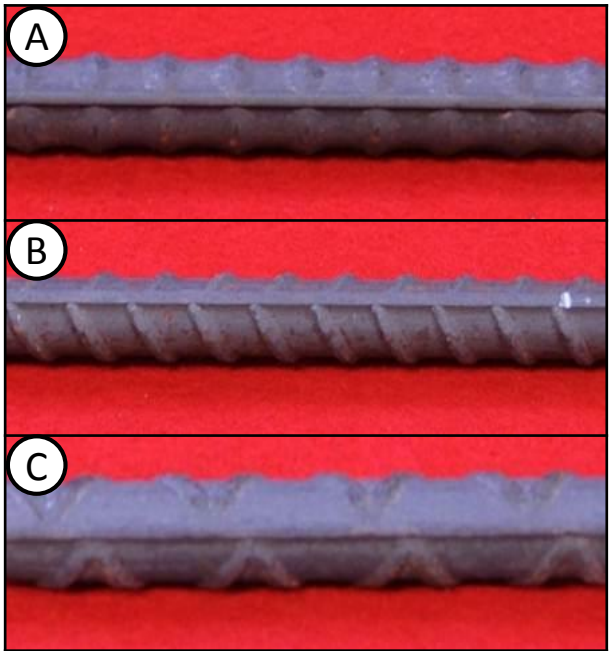

Figure 5-1: Deformation Patterns of Reinforcing Bars by Manufacturer

Geometric properties of the ribs that were measured for this study are shown in Table 5-1. A depth gauge was used to measure the height of the deformations. The reported value for each bar is the average of six height measurements taken at the quarter, middle and three-quarter points of two ribs. The spacing of the ribs was computed by measuring the distance of ten consecutive deformations. Additionally, the "steepness" of

the ribs and the "sharpness" at the base of the rib were evaluated; as they are reported to affect the stress concentrations at the base of a rib during bending (see Chapter 2). The "steepness" of the ribs was considered by measuring the rib flank angle. The radius at the rib base was used to quantify the "sharpness". The quantity is similar to the knot shape defined by Japanese researchers and is "evaluated as the [radius] of a circle defined by the arc formed between the linear portion of the rib and the linear portion of the reinforcing bar" (Kawashima et al. 2008). Both the rib flank angle and the radius at the base of the rib were measured by cutting a bar in half along the longitudinal axis and measuring the geometry at 45X magnification (Figure 5-2). The reported value is the average measurement of three ribs.

Table 5-1: Measured Deformation Geometry

Manufacturer I.D.	**Measured Parameter**			
	Average Spacing, S	Average Height, H	Flank Angle, θ	Radius at Rib Base, R
A	0.419 in	0.038 in	69°	0.159 in
B	0.419 in	0.041 in	54°	0.058 in
C	0.422 in	0.036 in	51°	0.033 in
ASTM A615 Limit	≤ 0.437 in	≥ 0.028 in	—	—

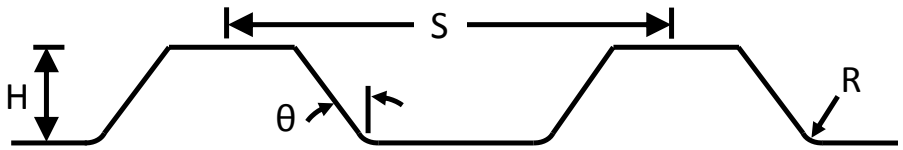

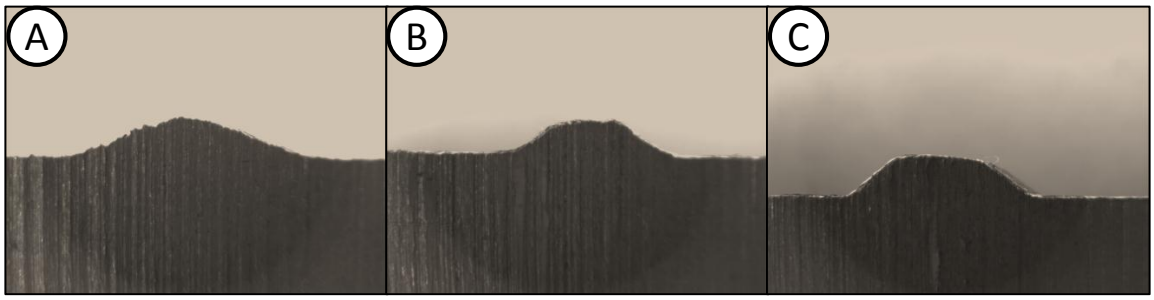

Figure 5-2: Rib Geometry of Reinforcing Bar by Manufacturer

5.2.2 Mechanical Testing

One sample from each manufacturer was tested in tension using a 60-kip universal testing machine at FSEL to determine the mechanical properties. Testing machine load cells and an axial extensometer with a 9-inch gauge length were used for recording the steel stress-strain response and capturing the yield strength of each sample. Testing was halted at the onset of strain hardening for extensometer removal and testing was then continued to failure. The ultimate load and elongation, computed by measuring the distance between marks filed into the longitudinal rib, were recorded at failure. Results from the tensile testing are included in Table 5-2 and plots of the recorded stress-strain response are included in Appendix B.

Table 5-2: Mechanical Properties of Bend Test Specimens

Manufacturer I.D.	Measured Property		
	Yield Strength	Tensile Strength	Elongation
A	62.0 ksi	101.0 ksi	12.0 %
B	63.5 ksi	102.5 ksi	13.5 %
C	62.0 ksi	104.0 ksi	15.5 %
ASTM A615 Limit	≥ 60 ksi	≥ 90 ksi	≥ 9 %

5.2.3 Chemical Composition

The chemical analysis of the test specimens was obtained from mill test reports provided by the suppliers and reproduced in Table 5-3. No attempt was made in producing a more detailed chemical analysis for the purposes of this study.

Table 5-3: Chemical Composition of Bend Test Specimens

Manufacturer I.D.	Chemical Properties (% Mass)												
	C	Mn	P	S	Si	Cu	Cr	Ni	Mo	V	Cb	Sn	Al
A	0.39	1.10	0.011	0.038	0.23	0.30	0.16	0.18	0.06	0.002	.001	0.01	.002
B	0.40	1.01	0.020	0.043	0.15	0.44	0.15	0.14	0.03	0.004	.001	NR	NR
C	0.43	1.03	0.010	0.020	0.20	0.28	0.11	0.08	0.02	0.000	NR	0.02	NR
ASTM A615 Limit			≤0.06										

NR Not reported on mill certificates

5.3 SERIES I BEND TESTS

The objective of the first series of bend tests was to investigate the existence of cracking on the inner radius of reinforcing bar samples bent cold using a reinforcing bar bender at FSEL. A discussion of the *Test Variables* (Section 5.3.1) is followed by a description of the *Test*ing *Procedure* (Section 5.3.2). Methods and procedures for identifying cracks are identified in Section 5.5.

5.3.1 Test Variables

The primary variables for the first series of bend tests are given in Table 5-4 and include the angle of bending, the finished bend diameter, and the axis of bending. The matrix of test variables was applied to samples from all three manufactures; therefore, a total of twenty-one specimens were produced for the Series I Bend Tests.

Table 5-4: Series I Bend Test Variables

Degree of Bend	Pin Diameter	Axis of Bend
90°	1 $^1/_2$ in	Weak
	2 $^1/_4$ in	Weak
135°	1 $^1/_2$ in	Weak
	2 $^1/_4$ in	Weak
		Strong
180°	2 $^3/_{16}$ in	Weak
		Strong

Note: Test variables for specimens from manufacturers A, B, and C

A summary of ACI 318 code provisions for detailing bends in reinforcement and ASTM A615 material specifications was reviewed in Chapter 2 and served as the basis for the selection of bend test variables. Samples bent to both 90° and 135°, per ACI provisions, and 180°, per ASTM bend test guidelines, were evaluated to investigate the effects of the degree of bending on the severity of cracking at the interior radii.

Similarly, samples were bent to various bend diameters. ACI 318-08 requires a minimum bend diameter of four times the bar diameter (2.5-inches) for No. 5 bar used as stirrups and ties. Bar fabricators will typically use a pin that is slightly smaller than the finished bend diameter to account for springback (Kudder and Gustafson 1983); therefore, a 2 ¼-inch diameter pin was used to achieve the Code specified minimum bend diameter. In addition, a 1 ½-inch diameter pin was also used for the bend testing because it was desirable to investigate bend diameters much smaller than the current code minimum. The 1 ½-inch diameter pin is the smallest pin that could be used with the bar bender in the laboratory and for a No. 5 reinforcing bar, results in a finished bend diameter approximately 2.5-3.0 times the bar diameter.

In addition, ASTM standards require a 180-degree bend around a pin of a diameter 3.5 times the diameter of the bar for bend tests. A 2 $^3/_{16}$-inch diameter pin was machined for the purposes of the bend test program, and samples were bent to ASTM specifications to ensure that no cracking was observed on the outside, as well as the

inside, of the bent bar. Although such extreme bending is not permitted per ACI provisions, it is important to recognize that cracking on the interior of the bend is not a cause for rejection by ASTM standards, and it is necessary to investigate the existence of cracks forming on the inner radius of a bent bar that might pass a standard bend test.

Finally, although standard reinforcing steel bend tests require that the steel be bent around the weak axis, it is not uncommon to have bar that is bent around the strong axis delivered from a supplier and used in reinforced concrete construction. Therefore, the investigation of bars bent around both the weak and strong axis was also included as part of the first series of bend tests (Figure 5-3).

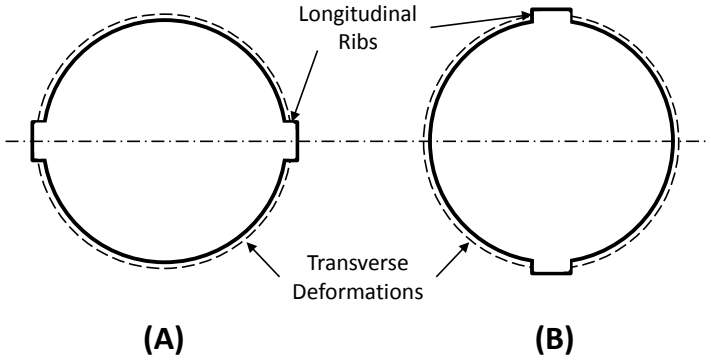

Figure 5-3: Axis of Bending (A) Weak (B) Strong

5.3.2 Test Procedure

Reinforcing bar samples were delivered to FSEL in straight four-foot lengths from three separate manufacturers. A number of the bars were cut by the supplier from standard lengths using a torch; therefore, both ends were cut off using a chop saw to remove any flame cut ends and ensure that any heating as a result of the torch cutting would not affect the results of the bend tests. A single bar from each manufacturer was used to measure the deformation geometry and for mechanical testing (Section 5.2).

The specimens were bent in the laboratory using the reinforcing bar bender shown in Figure 5-4. The temperature inside the lab when bending was approximately 65-70 °F. A single bar was positioned on the bender with the longitudinal rib in the correct orientation for weak axis or strong axis bending. Care was taken so that the

manufacturer's identification marks were not located within the bend. The bar was held parallel to the floor and firmly against the desired bending pin at a 90° angle until the backup ram was locked against the bar and the drive roller was seated against the free end of the bar. Approximately nine inches of free end, measured from the centerline of the bending pin, was left before the bend was made so that an excess remained after bending. A steel tube was placed over the drive roller arm to increase the lever arm for bending. A smooth, continuous motion was applied, as was feasible, to bend the samples. Experimentation with some scrap bar proved that the bars needed to be bent slightly past the desired degree of bending to account for springback. The largest deviation from the target bend angle was -3° and +6°.

Figure 5-4: Reinforcing Bar Bender Used for Bend Tests

After the samples were bent the bars were visually inspected for cracks on the interior and exterior of the bend. A detailed analysis of the procedures used for detecting and measuring cracks after bending is included in Section 5.5 following a description of the second series of bend tests.

5.4 SERIES II BEND TESTS

A second series of bend tests were performed to investigate the development of cracks on the inner radius of a reinforcing bar that were "straightened" through the application of an opening force (see Chapter 2 for a discussion of the effects of ASR/DEF induced concrete expansion). A discussion of the *Test Variables* unique to the Series II Bend Tests (Section 5.4.1) is followed by an overview of the *Test Procedure* (Section 5.4.2), including a method developed to simulate an ASR-induced opening force at the corner of a bent reinforcing bar.

5.4.1 Test Variables

Six specimens were produced for the Series II Bend Tests. All specimens were initially bent to 90° about the weak axis, and then the bend was opened 1.5-degrees to investigate the development of cracking with application of an expansive straightening force. Both a 1 ½-inch and 2 ¼-inch bending pin were used as was done in the first series of testing. The test matrix is detailed in Table 5-5.

Table 5-5: Series II Bend Test Variables

Degree of Bend	Pin Diameter	Axis of Bend	Extent of Re-bending
90°	$1\,{}^{1}/_{2}$ in	Weak	Bend opened 1.5 degree
	$2\,{}^{1}/_{4}$ in		

Note: Test variables for specimens from manufacturers A, B, and C

The geometry and reinforcing layout of the concrete specimens (Chapters 3 & 4) served as the basis for the selection of a 1.5-degree angle for opening a bent bar. To review, from Chapter 2, the effects of ASR/DEF-induced concrete expansion on the transverse steel of a reinforced concrete member, consider the illustration in Figure 5-5. As the core concrete expands, the member cross section "bulges" outward. The greatest expansion occurs at the center of the cross section where the transverse stirrups are least restrained and the stirrup is forced "open". If the assumption is made that the expansion

occurs only in the vertical and horizontal direction, that the bent corner of the stirrup does not displace, and that the expansion is concentrated at the lines of symmetry of the stirrup, then the angle that the stirrup corner is "opened" can be computed. Based on the geometry of the concrete cross section and assuming that the expansion reaches a value equal to 1% (commonly assumed strain at the onset of hardening for Grade 60 reinforcing steel), the total angle that the stirrup will open is equal to 1.5-degree.

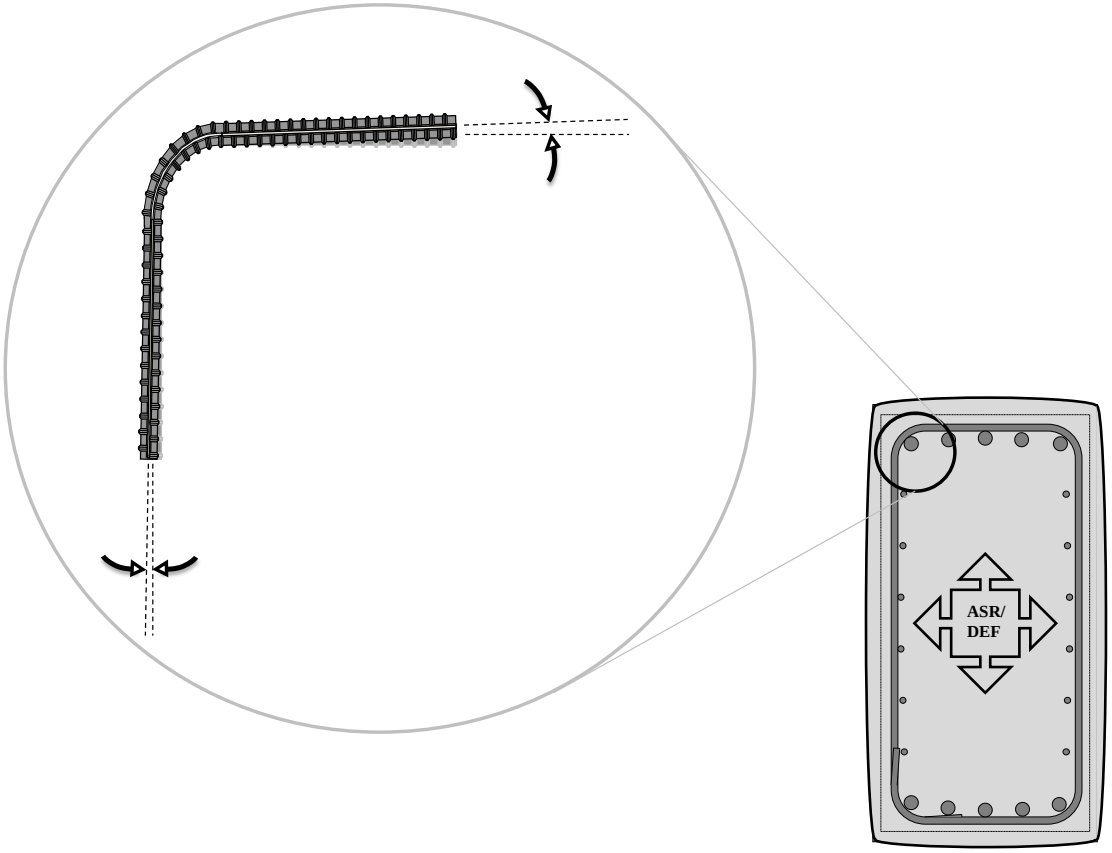

Figure 5-5: Effects of ASR/DEF Induced Expansion

It is important to recognize the number of assumptions that were included in the previous discussion and the limitations of this approach. First, the directionality of ASR/DEF induced expansion is largely influenced by a number of factors and in general occurs in all dimensions at varying rates. Additionally, the selection of 1% expansion is thought to be quiet high in an actual structure with deleterious concrete expansion and expansions this large could take decades to reach, if possible. Finally, the result of

decades of ASR/DEF-induced expansion is a tensile force at the corner of the highly stressed stirrup. Although the time dependent altering of the mechanical properties of the steel (i.e. strain aging) can be simulated with the use of accelerated heat treatments, the resultant tensile force at the corner of the bent bar is not captured in an experiment by simply "straightening" the bar and not pulling on it at the same time. Regardless, the experimentally simulated "straightening" force is intended only to give an indication of the development of cracking on the interior of a bent reinforcing bar and the potential for brittle fracture as a result of an extreme case of ASR/DEF-induced expansion.

5.4.2 Test Procedure

Reinforcing bar specimens were initially bent cold following the procedures of Section 5.3.2 and then placed in an oven to accelerate strain aging (Figure 5-6). The bent bars were kept at an elevated temperature of 100 °C (212 °F) for 4 hours, equivalent to one year of ageing at room temperature (Hundy 1954). The oven was turned off after 4 hours and the bars were kept inside and allowed to cool before they were re-bent.

Figure 5-6: Bent Specimens in Oven for Artificial Strain Ageing

A jig was machined at FSEL for the purposes of consistently opening a specimen 1.5-degree. The jig consisted of two, ¾-inch steel plates with an undersized hole drilled

at one end that, when clamped in a vise, would secure one leg of a bent specimen. A notch was cut into the top of the jig to receive a 1.5-degree steel shim for opening the other leg of the bent bar. This process was repeated for each specimen so that each bar placed in the jig would consistently be straightened 1.5-degrees. An example of the test procedure is shown in Figure 5-7. As with the first series of bend tests, the "straightened" bars were then inspected for cracks.

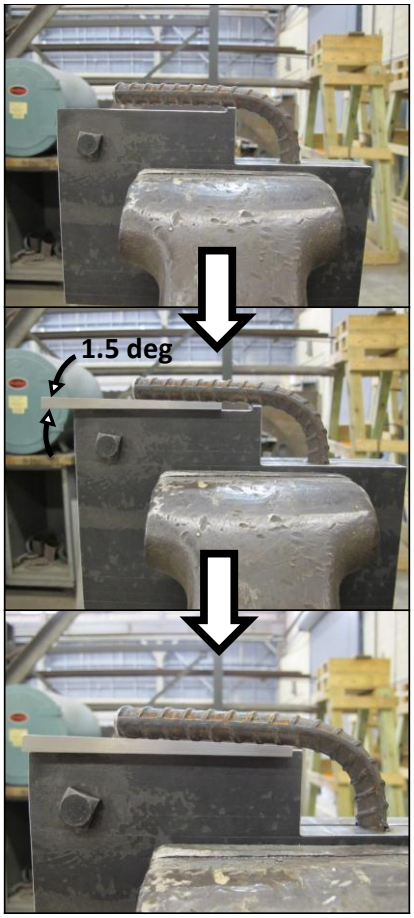

Figure 5-7: Test Procedure to Simulate ASR-Induced Expansive Force

5.5 CRACK DETECTION & MEASUREMENTS

Immediately after the samples were bent the excess was cut off on a chop saw so that only the bent portion remained. The bent portions of the bars were then visually inspected for cracks on the inside and outside of the bend. Care was taken to distinguish between an actual crack versus a surface irregularity or a break in the mill scale due to bending. Where a crack seemed likely from a visual inspection, a sample was cleaned with a hand wire brush followed by an inspection with a liquid dye penetrant. The Liquid Penetrant Inspection (LPI) (Figure 5-8) consisted of three parts: (1) a cleaner/degreaser, (2) a red dye penetrant, and (3) a developer. First, the surface of the bar was cleaned with a degreaser to remove any surface dirt and grease. Then, a red dye penetrant was sprayed on the surface and allowed to set for 15-30 minutes. Excess penetrant was removed with a cloth sprayed with additional cleaner. Finally, a developer was sprayed on the surface and allowed to set for 15-30 minutes. The specimen I.D. and the location of possible cracks were noted for inspection using an optical microscope.

Figure 5-8: Liquid Penetrant Inspection

The bent bars were prepared for microscopy by cutting the bars in half longitudinally on a vertical band saw. The bars were inserted between two steel angles

that were bolted together and clamped between the band saw vise (Figure 5-9). After cutting, the samples were wiped clean to remove coolant from the cutting operation and the burrs were removed from the edges with a piece of fine emery cloth.

Figure 5-9: Cutting Bent Specimen on Band Saw

The longitudinally half-cut bent specimens were viewed under an optical microscope at a magnification of 45-90X. Crack depths were measured from photographs taken using a digital high-resolution camera installed in one of the microscope eyepieces. A picture of the equipment used for microscopic analysis is shown in Figure 5-10.

Figure 5-10: Microscope and Camera for Inspecting Specimens

5.6 NOMENCLATURE & LIST OF BEND TEST SPECIMENS

A simple nomenclature was developed for identifying the specimens from both series of bend tests. An example of the nomenclature and description of the terms is included in Table 5-6. Table 5-7 lists all twenty-seven specimens of the bend test program.

Table 5-6: Nomenclature of Bend Test Identifiers

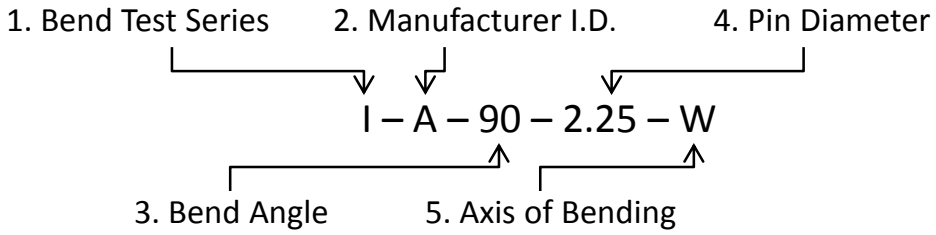

Term	Description	Choices
1.	**Bend Test Series** – designates the bend test series	I …….Series I II……. Series II
2.	**Manufacturer I.D.**	A, B, or C
3.	**Bend Angle** – the target degree of bending	90, 135, or 180
4.	**Pin Diameter** – given in inches Note: final bend diameter larger than pin diameter after springback	1.5……..1 ½” 2.25……2 ¼” 2.188....2 $^{3}/_{16}$”
5.	**Axis of Bending** – the orientation of the longitudinal axis of the bar for bending	W……..Weak S …….Strong

Table 5-7: List of All Bend Test Specimens

Specimen I.D.
I – A – 90 – 1.5 – W
I – B – 90 – 1.5 – W
I – C – 90 – 1.5 – W
I – A – 90 – 2.25 – W
I – B – 90 – 2.25 – W
I – C – 90 – 2.25 – W
I – A – 135 – 1.5 – W
I – B – 135 – 1.5 – W
I – C – 135 – 1.5 – W
I – A – 135 – 2.25 – W
I – A – 135 – 2.25 – S
I – B – 135 – 2.25 – W
I – B – 135 – 2.25 – S
I – C – 135 – 2.25 – W
I – C – 135 – 2.25 – S
I – A – 180 – 2.188 – W
I – A – 180 – 2.188 – S
I – B – 180 – 2.188 – W
I – B – 180 – 2.188 – S
I – C – 180 – 2.188 – W
I – C – 180 – 2.188 – S
II – A – 90 – 1.5 – W
II – B – 90 – 1.5 – W
II – C – 90 – 1.5 – W
II – A – 90 – 2.25 – W
II – B – 90 – 2.25 – W
II – C – 90 – 2.25 – W

CHAPTER 6
Experimental Results: Reinforcing Bar Bend Tests

6.1 OVERVIEW

Measurements and observations from analyses of the reinforcement bend test specimens are reviewed in this chapter. Results from the Series I Bend Tests constitute a majority of the testing and are presented first. The influences of the test variables on the formation of cracks during bending are evaluated. The development of cracking after application of an expansive opening force is explored from the results of the Series II Bend Tests. Conclusions drawn from the bend tests are presented in Chapter 7.

6.2 SERIES I BEND TEST RESULTS

Observations made from an analysis of the first series of bend test specimens are presented here. Specifically, cracking observed at the base of the ribs after bending is explored through photographs and crack depth measurements. Table 6-1 provides a summary of all specimens from the Series I Bend Tests and indicates if cracking was identified. Analyses of the bend test results are included in Section 6.3

Table 6-1: Summary of Results from Series I Bend Tests

Specimen I.D.	Crack(s) Identified
I – A – 90 – 1.5 – W	No
I – B – 90 – 1.5 – W	No
I – C – 90 – 1.5 – W	**Yes**
I – A – 90 – 2.25 – W	No
I – B – 90 – 2.25 – W	No
I – C – 90 – 2.25 – W	No
I – A – 135 – 1.5 – W	No
I – B – 135 – 1.5 – W	No
I – C – 135 – 1.5 – W	**Yes**
I – A – 135 – 2.25 – W	No
I – A – 135 – 2.25 – S	No
I – B – 135 – 2.25 – W	No
I – B – 135 – 2.25 – S	No
I – C – 135 – 2.25 – W	**Yes**
I – C – 135 – 2.25 – S	No
I – A – 180 – 2.188 – W	No
I – A – 180 – 2.188 – S	No
I – B – 180 – 2.188 – W	No
I – B – 180 – 2.188 – S	No
I – C – 180 – 2.188 – W	**Yes**
I – C – 180 – 2.188 – S	No

Cracking on the interior of the bent reinforcing bars at the base of the ribs was identified on four of the twenty-one specimens. No cracking on the *exterior* of the bend was observed on any of the test specimens. Cracking only occurred on reinforcing bar from Manufacturer C and only when the bars were bent about the weak axis.

Figure 6-1 to Figure 6-4 show the location and magnified images of the cracks identified on the first series of bend test specimens. The original and unaltered images are included in Appendix B. Two images at the same location, such as images A and B for Specimen I-C-135-1.5-W, is indicative of images from each half of the longitudinally cut specimen. Cracking occurred at only one location for Specimen I-C-135-2.25-W, at

two locations for Specimens I-C-90-1.5-W and I-C-135-1.5-W, and at three locations for Specimen I-C-180-2.188-W. In all cases where cracks were identified, the crack originated at the base of a transverse rib. Additionally, cracking occurred only at the ribs located at the midpoint, or one deformation away from the midpoint, along the length of the bend.

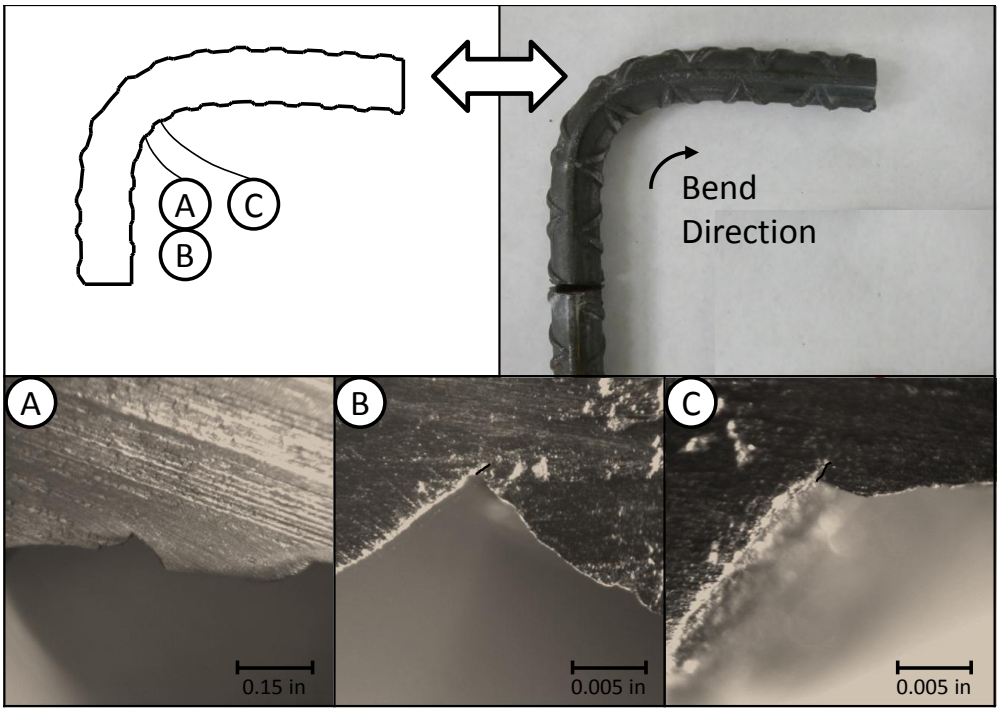

Figure 6-1: Cracks Identified After Bending for Specimen I-C-90-1.5-W

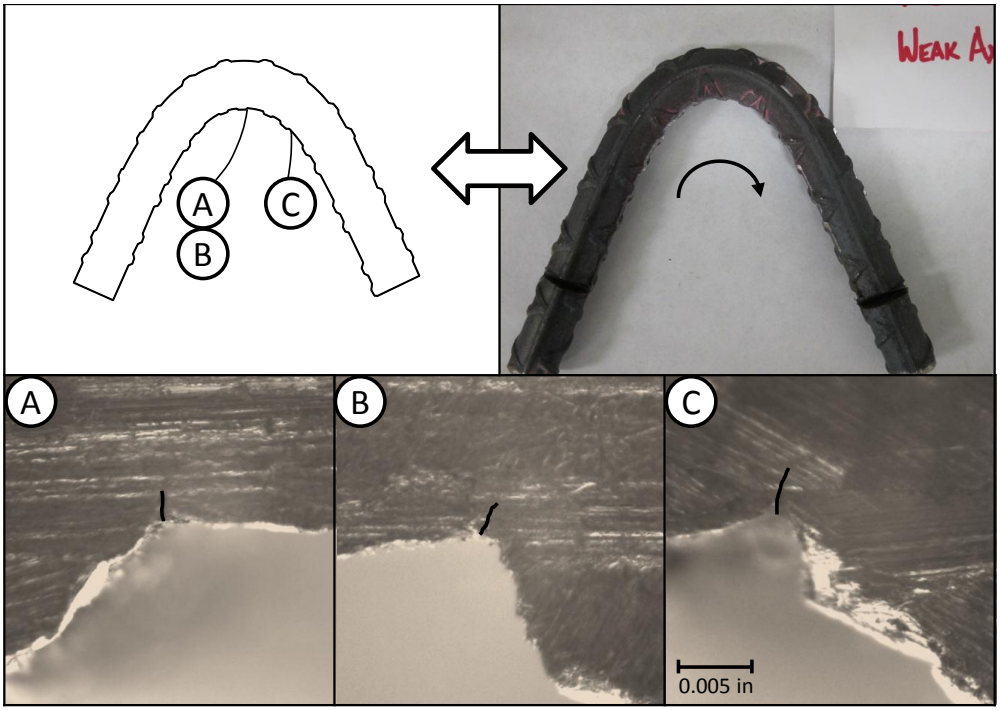

Figure 6-2: Cracks Identified After Bending for Specimen I-C-135-1.5-W

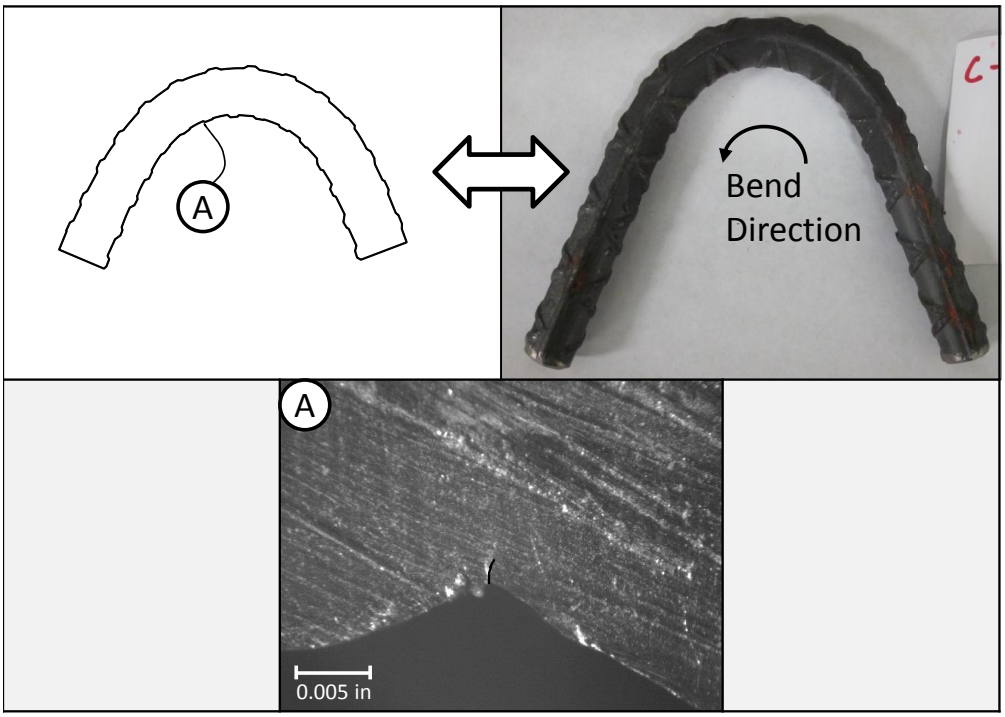

Figure 6-3: Cracks Identified After Bending for Specimen I-C-135-2.25-W

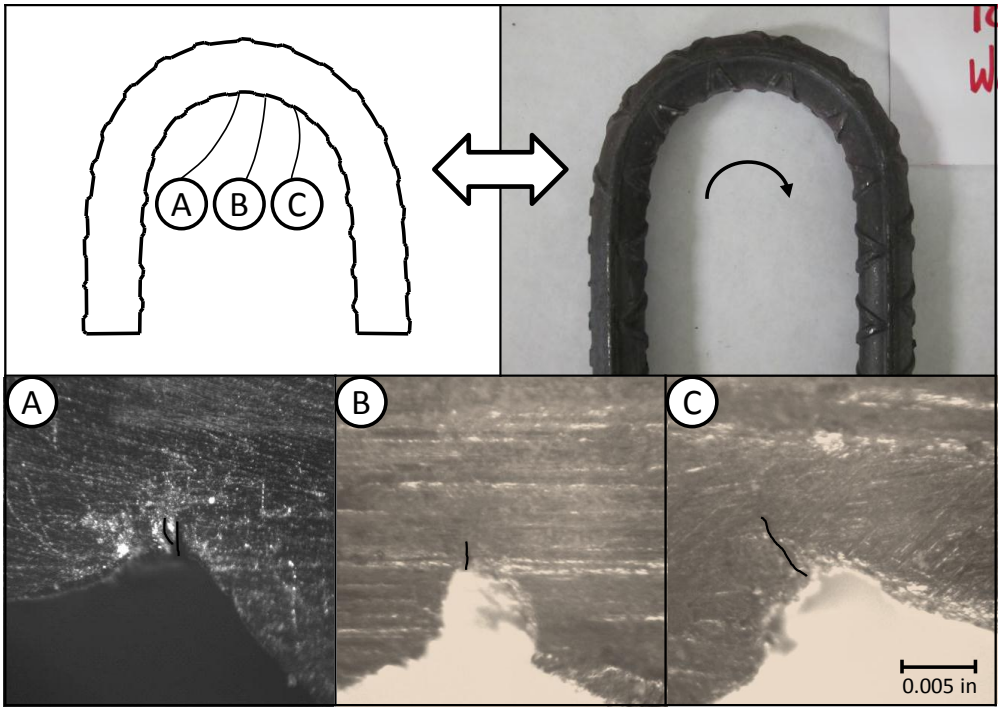

Figure 6-4: Cracks Identified After Bending for Specimen I-C-180-2.188-W

Maximum crack depth measurements are shown in Table 6-2. The location of the maximum crack depth corresponds to image C for all specimens expect Specimen I-C-135-2.25-W, which only has one crack identified in image A (see Figure 6-1 - Figure 6-4). As the severity of bending increased (i.e. decreased bend diameter, increased bend angle), so did the severity of cracking (measured by the quantity of cracks and the maximum crack depths) on the inner radius of the Series I test specimens.

Table 6-2: Maximum Crack Depth from Series I Bend Test Specimens

Specimen I.D.	Max. Crack Depth
I – C – 90 – 1.5 – W	0.002 inch
I – C – 135 – 1.5 – W	0.003 inch
I – C – 135 – 2.25 – W	0.003 inch
I – C – 180 – 2.188 – W	0.006 inch

6.3 ANALYSIS OF SERIES I BEND TEST RESULTS

The effects of the test variables on the potential for the development of cracks during bending are investigated by comparing the material properties of the specimens, photographs of the observed cracking, and the measured crack depths.

6.3.1 Effects of Bar Manufacturer

The most significant factor that affected the formation of cracks on the interior of the bent reinforcing bars was the bar manufacturer, marked by the fact that the specimens that cracked during bending were from Manufacturer C. A review of material properties presented in Chapter 5 provides a discussion for the possible explanation for the consistent cracking in bars from Manufacturer C.

The mechanical and chemical properties of the specimens were presented in Table 5-2 and Table 5-3, respectively. There are slight differences in the chemical properties and there is little difference in the mechanical properties between the three manufacturers. Additionally, all specimens satisfy the minimum standards of ASTM A615. Surprisingly, the elongation (a measure of the deformability) of the sample from Manufacturer C was the greatest, yet only bars from this manufacturer cracked during bending.

Two geometric properties of the ribs governed by ASTM A615 standards, rib height and spacing, were similar for all three samples. The rib flank angle and the radius at the base of a rib, quantities relating to the "steepness" and "sharpness" of the rib geometry, were considerably lower for the samples obtained from Manufacturer C. It should be noted that this observation may not be typical for all bars from Manufacturer C; only a limited sample size was obtained for this study. Nonetheless, since these two quantities were small, the possibility of cracking at the base of the ribs to develop during bending was considerably higher for bars from Manufacturer C than the bars from Manufacturers A or B, evident in the results of the bend tests.

6.3.2 Effects of Bend Diameter & Degree of Bending

The effects of the bend diameter are pronounced when comparing the quantity of cracks and the maximum crack depth measurement for Specimen I-C-135-1.5-W with Specimen I-C-135-2.25-W. The maximum crack depth measured was 0.003 inches for both; however, cracks at two locations developed for the specimen bent around a pin with a diameter of 1.5-inches as opposed to cracking at only one location for the specimen bent to a final diameter equal to 4 times the bar diameter.

A comparison of the results for Specimen I-C-90-1.5-W with Specimen I-C-135-1.5-W highlights the effects of the degree of bending. Although the quantity of cracks identified was identical, the maximum crack depth increased from 0.002 inches to 0.003 inches as the final bend diameter increased from 90° to 135°.

6.3.3 Effects of Axis of Bending

The generation of cracks during bending was only identified on specimens bent about the weak axis. When bending bars about the strong axis only the longitudinal ribs running the length of the bar are in contact with the bending pin. In effect strong axis bending eliminates the stress concentrations generated at the root of the ribs during bending that resulted in compression cracks observed for specimens bent about the weak axis.

6.4 SERIES II BEND TEST RESULTS

Observations of the second series of bend test specimens are reviewed here. A collection of photographs from microscopic analysis is used to investigate the development of cracks in a bent reinforcing bar specimen after the bend has been opened using the procedures described in Chapter 5. A summary of the Series II Bend Tests results is included in Table 6-3.

Table 6-3: Summary of Results from Series II Bend Tests

Specimen I.D.	Crack(s) Identified
II – A – 90 – 1.5 – W	No
II – B – 90 – 1.5 – W	No
II – C – 90 – 1.5 – W	**Yes**
II – A – 90 – 2.25 – W	No
II – B – 90 – 2.25 – W	No
II – C – 90 – 2.25 – W	No

Figure 6-5 identifies the location of the cracking observed on Specimen II-C-90-1.5-W. No cracks were observed on the *exterior* of any specimens. Cracks were initiated at the base of two ribs, approximately located at the center of the bent portion. The maximum crack depth was 0.005 inches. The location of the maximum crack depth for Specimen II-C-90-1.5-W is located at image A in Figure 6-5.

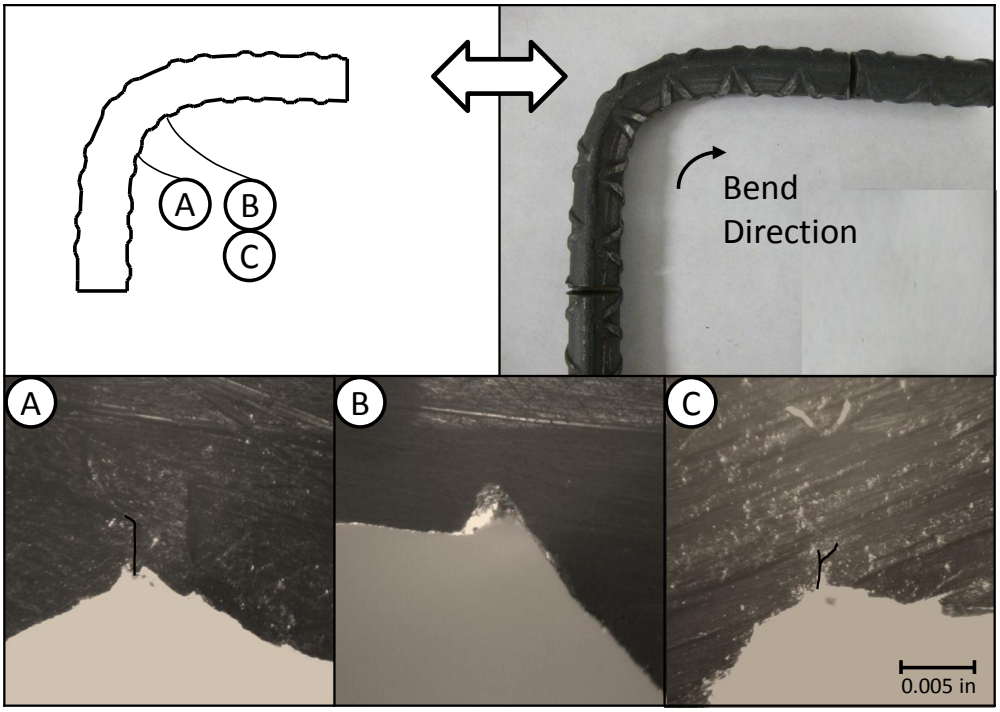

Figure 6-5: Cracks Identified on Specimen II-C-90-1.5-W

6.5 ANALYSIS OF SERIES II BEND TEST RESULTS

6.5.1 Effects of Re-Bending

The development of cracks after the application of an opening force, to simulate the effects of deleterious concrete expansion, is investigated by comparing the crack depths from the second series of bend tests with the companion specimen from the first series of bend tests. Recall from Section 6.4 that cracks were only identified on Specimen II-C-90-1.5-W, and the maximum crack depth was 0.005 inches. The maximum crack depth from Specimen I-C-90-1.5-W was 0.002 inches (see Table 6-2).

Two observations can be made from the comparison of the re-opened specimens and the companion specimens from the first series of bend testing. First, only the companion specimens that cracked from the first series of bend tests (Specimen I-C-90-1.5-W) cracked in the second series of bend tests after the bent bar was opened 1.5-degrees (Specimen II-C-90-1.5-W). Thus, the potential for a crack to develop after application of an expansive opening force is dependent on the formation of an initial crack during bending.

Second, an increase of the maximum crack depth of 150% between the specimen that was only bent and the specimen that was bent and then re-opened was observed. It was not possible to determine the progression of crack growth for Specimen II-C-90-1.5-W because the cracks formed during bending could not be measured without cutting the bar before re-bending. However, based on the maximum crack depth measurements, it is feasible that an initial crack formed during bending can propagate after application of an opening force.

6.6 SUMMARY (POTENTIAL FOR REINFORCING BAR FRACTURE)

The potential for reinforcing bar fracture within Texas and the United States was assessed in the experimental research program in two parts. First, the possibility of crack formation during bending was investigated from the results of the Series I Bend Tests.

Second, the development of cracks after application of an opening force to simulate ASR/DEF-induced expansion was evaluated from the results of the Series II Bend Tests.

Descriptions such as crack depth measurements and the quantity of cracks proved useful for characterizing the cracks formed during bending. However, the simple fact that cracks developed as a possible nucleation point for reinforcing bar fracture is perhaps just as useful for a structural engineer who is assessing the potential for bar fracture. Although three of the four specimens were bent to much smaller radius and/or to greater degrees than allowed by current Code provisions, Specimen I-C-135-2.25-W developed a crack at the base of one rib. Additionally, the "extreme" bending of Specimen I-C-90-1.5-W and I-C-135-1.5-W was not considered extreme by Code provisions in our recent history (see Chapter 2), and it is possible that bars with much smaller minimum bend diameters than the current Code requires are within serviceable structures today.

Observations from the second series of bend tests revealed that the development of cracks was possible only if the specimen was prone to the formation of an initial crack. Although it is feasible that the cracking observed on Specimen II-C-90-1.5 propagated from an initial crack formed during bending, it is not possible to quantitatively access the development of cracking because the depth of an "initial" crack could not be measured.

Additionally, although cracking was observed, no specimens from the second series of bend tests actually fractured; however, in an assessment of the bend test results it is important to note the limitations of the simulated opening force discussed in Chapter 5 (i.e. the lack of a tension when opening up the bent bars) and the limited sample size of the study. In conclusion, a definitive assessment of the development of initial cracks formed during bending and resulting in a brittle bar fracture is inconclusive.

In the following chapter, the work conducted will be summarized and the primary conclusions reported.

CHAPTER 7
Summary, Conclusions, and Recommendations

7.1 SUMMARY OF EXPERIMENTAL RESEARCH

A number of experimental studies aimed at investigating the effects of alkali-silica reaction and/or delayed ettringite formation on the structural performance of affected reinforced concrete members have indicated little to no loss in capacity. Primarily, these results are attributed to the confinement provided by the highly stressed reinforcing steel. However, the potential loss of confinement through fracture of the reinforcement, as experienced in Japan, calls into question the structural integrity of severely deteriorated members. A two-part experimental program was conducted at Ferguson Structural Engineering Laboratory at The University of Texas at Austin, and reported in this thesis, to (1) evaluate the use of various non-destructive testing (NDT) methods to detect reinforcing bar fracture in concrete members, and (2) address the potential for reinforcing bar fracture within affected infrastructure in Texas through a bar testing study.

In agreement with the research objectives of TxDOT Project 0-6491, four concrete specimens, representative of a segment from the large scale bent cap specimens, were constructed at FSEL and continuously monitored throughout the experimental study. Specimens 1 and 2 were made using a proven reactive concrete mixture; while, Specimens 3 and 4 both contained various proportions of fly ash. Consideration and selection of concrete materials, high temperature curing, and storage conditions made certain that the most severe circumstances of rapid ASR/DEF deterioration were produced. A single stirrup within Specimen 1 was intentionally severed after significant expansion had developed in the reactive beam segments. Subsequent monitoring allowed for an evaluation of the various monitoring techniques and their ability to identify the loss in confinement through the fracture of the transverse reinforcement.

A total of twenty-seven reinforcing bar specimens were produced for the reinforcement bend tests. Testing variables included bar size, bar deformation geometry, bending angle, bend diameter, axis of bending, and the application of an opening force to simulate the effects of ASR/DEF-induced expansion. Specimens from the Series I Bend Tests were first bent cold in the laboratory and later analyzed under a microscope to identify cracks formed on the inner radius of the bent portion of the bar. Similarly, specimens from the Series II Bend Test were initially bent cold in the laboratory; after which, a simulated opening force was applied to each bar. Series II test specimens were then analyzed, and the development of cracks after application of simulated expansion was evaluated. Conclusions relating to the effects of each test variable on the formation and development of cracks were independently identified.

7.2 RESEARCH FINDINGS & CONCLUSIONS

Observations made and conclusions drawn from the two independent, yet related, experimental studies detailed in this thesis are summarized below.

7.2.1 Experimental Program: Beam Segments

1. Several non-destructive testing (NDT) techniques evaluated throughout the course of this study failed to detect the loss of confinement through the simulated fracture of the transverse reinforcement in ASR/DEF-affected specimens. Furthermore, their future use as a tool for evaluating the level of PCD related distress within deteriorated in-service concrete structures is questionable. Although an initial loss in compression wave velocity, measured via UPV or impact echo testing, and the surface wave velocity, measured via the SASW method, were observed at low levels of expansion, the changes in velocity at higher levels of deterioration were minimal. Considering that an inspection of in-service structures is generally initiated after the manifestation of surface cracking (presumably after significant expansion has occurred) and that reinforcing bar fracture, as experienced in Japan, is only possible at high levels of expansion, the monitoring of in-situ damage using the NDT methods is of little value.

2. Monitoring the effects of ASR/DEF-related structural core expansions (i.e. surface cracking) provided the most practical means of indicating the presence of a fractured reinforcing bar. Whereas the distribution of surface cracking was typical of ASR/DEF-induced damage elsewhere on the faces of the beam segments, the development of a single wide crack at the location of the intentionally severed stirrup was observed as deterioration progressed in Specimen 1.
3. The use of Class F fly ash in concrete mixture designs proved to be effective in arresting the development of ASR and/or DEF in the proportions used in Specimens 3 and 4 and in the time frame of this study. However, similar results from other types of fly ash as well as in different proportions would be necessary to validate these findings.

7.2.2 Experimental Program: Reinforcing Bar Bend Tests

1. Cracking at the base of the *interior* ribs, a potential nucleation point for the development of brittle reinforcing bar fracture, was identified on four of the twenty-one Series I Bend Test specimens after cold bending in the laboratory, despite the fact that the bars complied with the specifications of ASTM A615 (2009). Furthermore, no cracks were observed on the *exterior* of the bent portion of the bars that would initiate a cause for rejection during manufacturing.
2. Cracking was only identified on specimens from Manufacturer C and only when the reinforcing bars were bent about the weak axis. Primarily, this was attributed to the geometry of the deformations; in particular, the sharp radius at the base of the deformations and the steepness of the angle between the deformation and the bar.
3. The severity of cracking, characterized by the number of cracks and the maximum crack depths, increased as the bending diameter decreased and when bending to a more severe angle. Three of the four specimens with cracking on the interior portion of the bend were considered "extreme" cases of bending (i.e. less than the code specified minimum). However, a crack was identified on one specimen that was bent 135° to finished diameter equal to the code minimum.

4. Based on the limited sample size examined as part of this experimental program, the potential for ASR/DEF-induced reinforcing bar fracture is possible only if an initial crack is formed during the bending operation. As explored in the Series II Bend Tests, cracking was observed on a single specimen, wherein cracks were also identified on the companion specimen from the first series of bend tests, after the application of a simulated opening force. Accordingly, investigating the development of an initial crack to form during bending is critical in the assessment of the future potential for reinforcing bar fracture within the United States.

7.3 RECOMMENDED FUTURE WORK

As motivation for the current study, the potential for ASR/DEF-induced reinforcing bar fracture is of paramount concern for the maintenance of structural safety. Although the experimental work contained in this thesis has provided critical insight into the mechanisms of reinforcing bar fracture, a number of questions are left unanswered. It is hoped that this limited study has laid the groundwork for a more comprehensive research effort aimed at assessing the possibility for bar fracture within affected infrastructure in Texas and the United States.

First and foremost, the reinforcing bend tests were very limited in scope. Only one bar size from three different manufactures was tested as part of this study. No attempt was made to evaluate the effects of roller wear during manufacturing on the shape of the deformations. In addition, bars were bent in the laboratory under very controlled conditions. It is recommended that future testing include multiple bar sizes from a number of different bar manufactures. The age of the rollers and the effects that roller wear has on the geometry of the deformations would be of interest. Furthermore, bars bent using commercial bending machines produce much more severe bends that could potentially increase the likelihood of cracking at the base of the deformations.

Additionally, although it is not likely that manufacturing practices and material specifications have changed that drastically over the years, it is recommended that bars of the same time period and of the same type as those that are contained in existing

structures be examined. Also, it would be of interest to extract bars from affected structural elements and analyze them for cracks at the interior of the bent portion of the bar. With knowledge of the condition of bars that are contained in existing and/or damaged structures, a more definite assessment on the potential for reinforcing bar fracture could be established.

APPENDIX A

Supplementary Material - Beam Segment Specimens

Appendix A includes the following supplementary material that was referenced in Chapter 3, but not reported.

- Table A-1: Chemical Analysis of Rockdale Fly Ash
- Table A-2: Match-Cured Concrete Cylinder Compressive Strength Test Results
- Figures A-1 thru A-3: Hydration Temperature Curves
- Figures A-4 thru A-6: Expansion Results from ASTM C1293 Prisms

Table A-1: Chemical Analysis of Rockdale Fly Ash (Drimalas 2010)

Compound	% by Mass
Silicon Dioxide (SiO_2)	52.04
Aluminum Oxide (Al_2O_3)	23.75
Iron Oxide (Fe_2O_3)	4.59
Calcium Oxide (CaO)	12.63
Magnesium Oxide (MgO)	2.01
Sulfur Trioxide (SO_3)	0.79
Sodium Oxide (Na_2O)	0.28
Potassium Oxide (K_2O)	0.81
Total Alkalies (as Na_2O)	0.81

Table A-2: Match-Cured Concrete Cylinder Compressive Strength

Concrete Mixture	Average* Cylinder Compressive Strength		
	7 Day	28 Day	90 Day
Reactive	4520 psi	4790 psi	---
25% Fly Ash Replacement	5000 psi	5590 psi	5480 psi**
25% Fly Ash Addition	5860 psi	6570 psi	6770

*Average of Two 4" x 8" Cylinders
**Only One Cylinder Available for Test

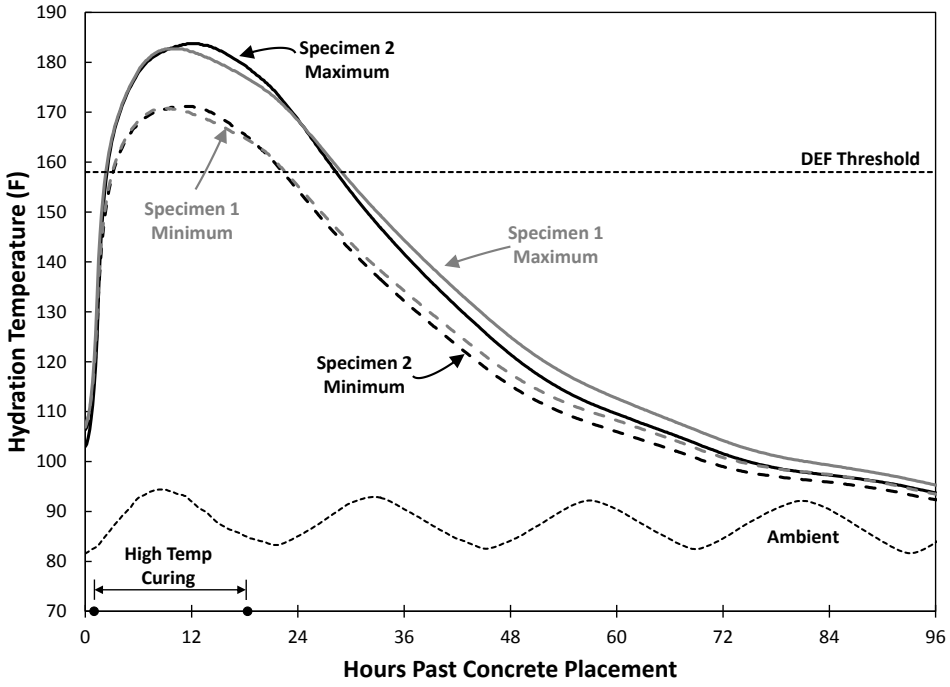

Figure A-1: Hydration Temperature Curve - Specimens 1 and 2

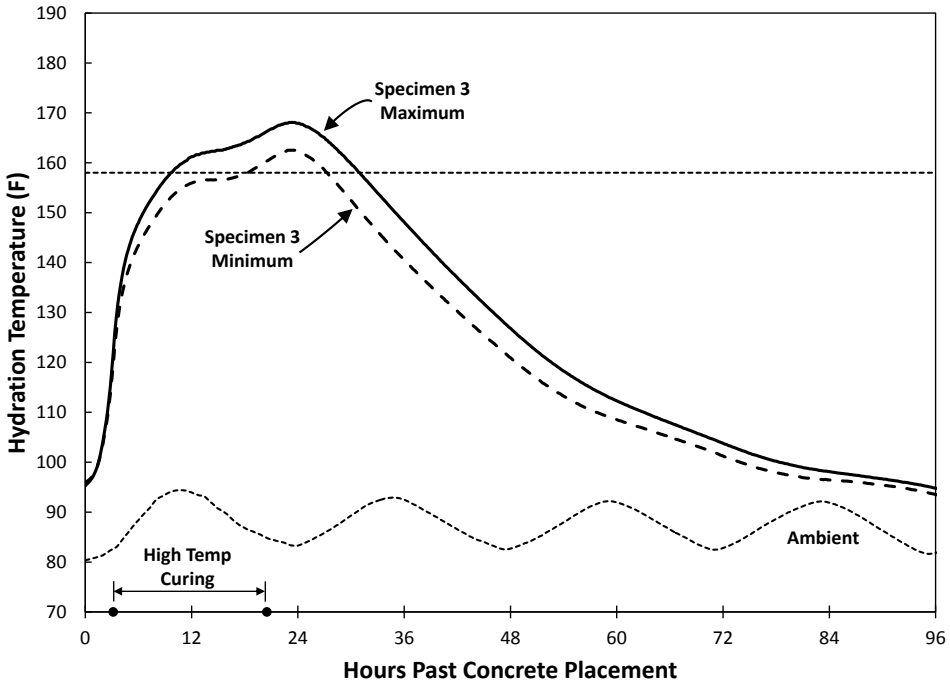

Figure A-2: Hydration Temperature Curve - Specimen 3

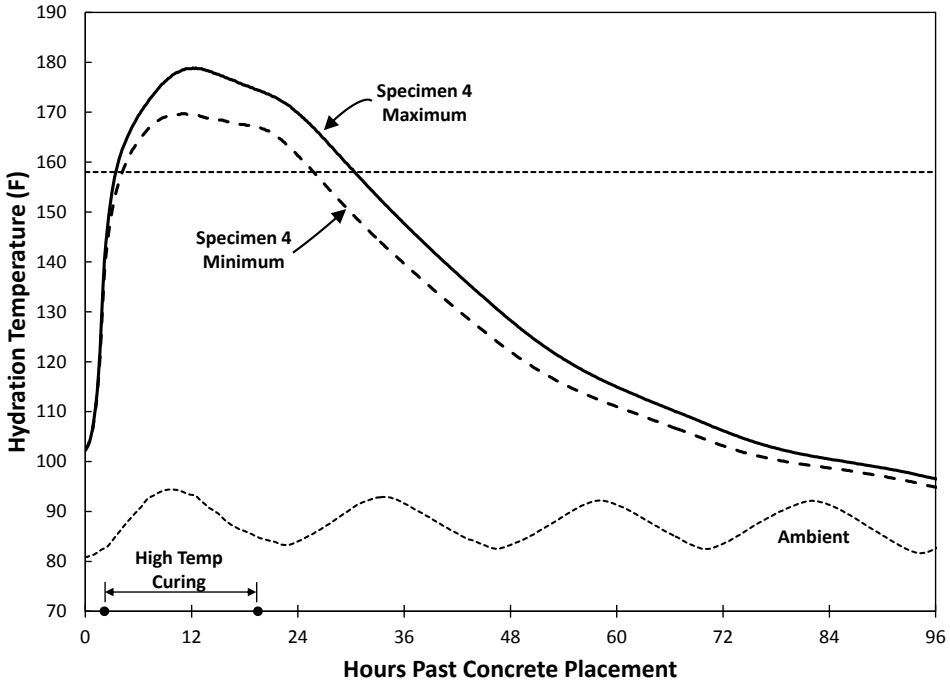

Figure A-3: Hydration Temperature Curve - Specimen 4

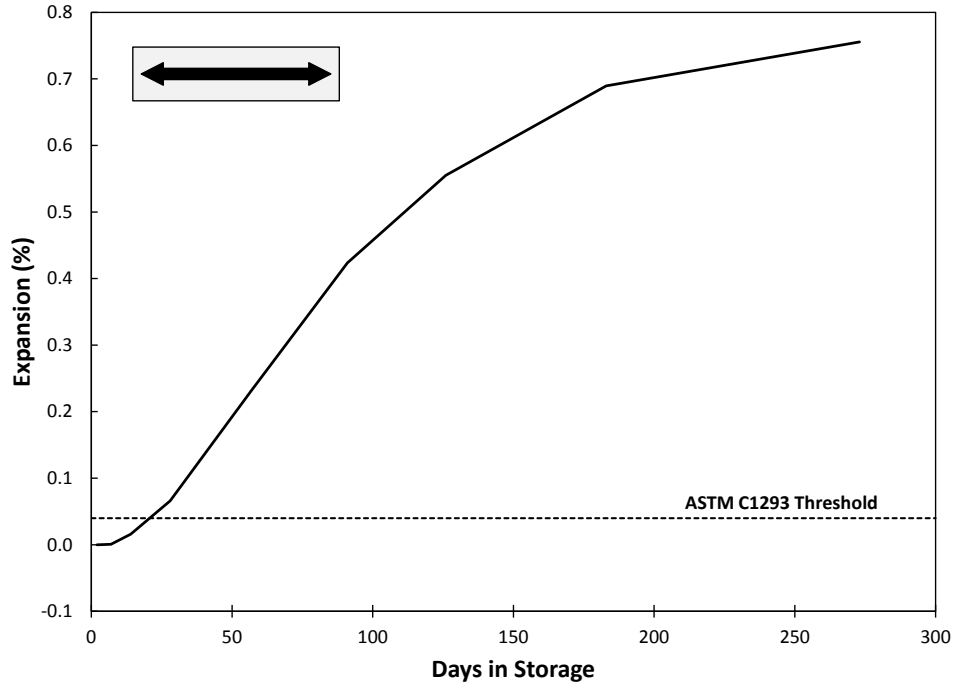

Figure A-4: Free Expansion of ASTM C1293 Prisms – Specimens 1 and 2

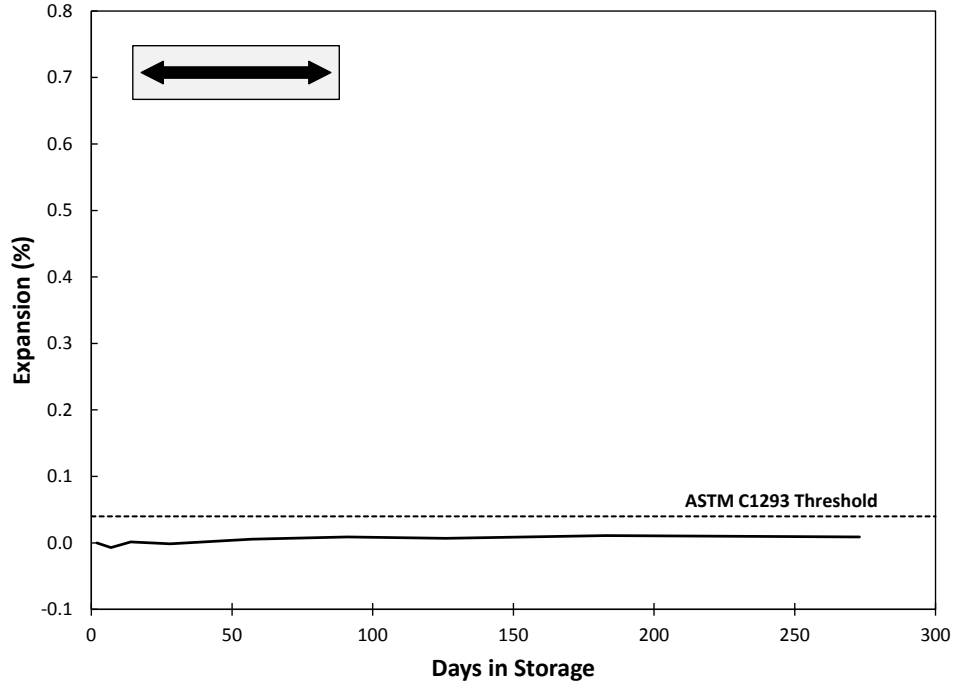

Figure A-5: Free Expansion of ASTM C1293 Prisms – Specimen 3

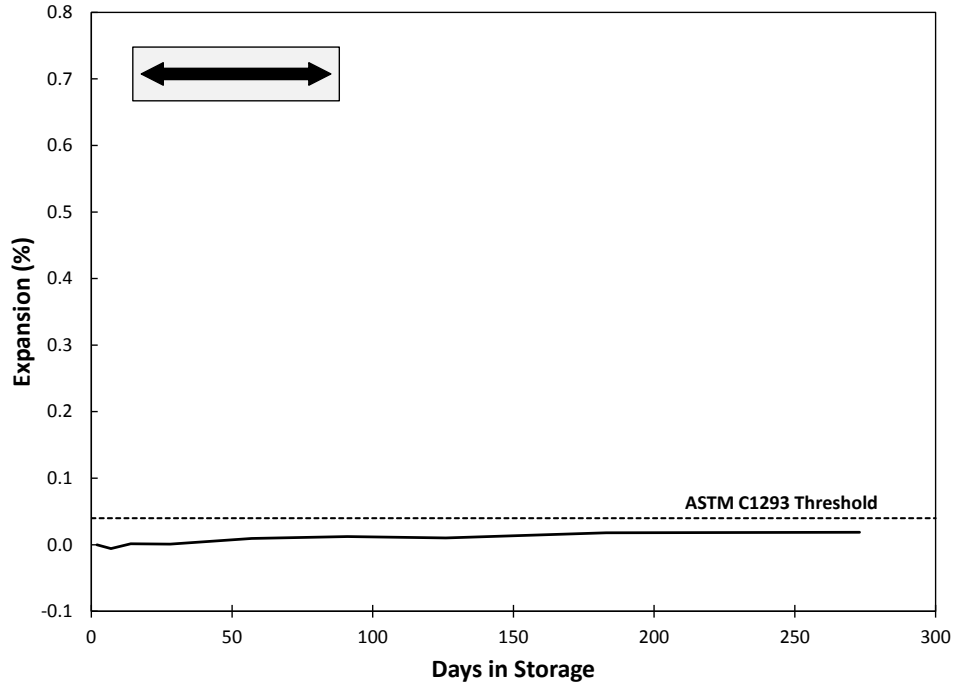

Figure A-6: Free Expansion of ASTM C1293 Prisms – Specimen 4

APPENDIX B

Supplementary Material – Reinforcing Bar Bend Tests

Appendix B includes the stress-strain curves from the mechanical testing of reinforcing bar samples used for the reinforcement bend tests in Chapters 5 and 6. In addition, the original and unaltered photographs from the bend test results contained in Chapter 6 are provided.

- Figures B-1 thru B-3: Stress-Strain Response of Bar by Manufacturer
- Figures B-4 thru B-8: Original Photographs of Bend Test Specimens

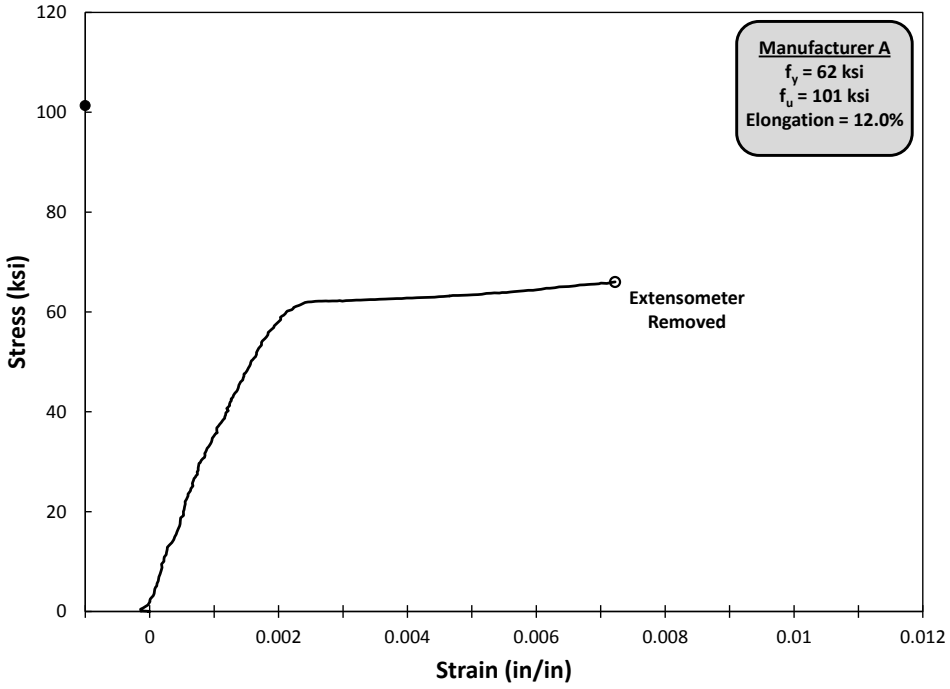

Figure B-1: Stress-Strain Response of Bar Sample – Manufacturer A

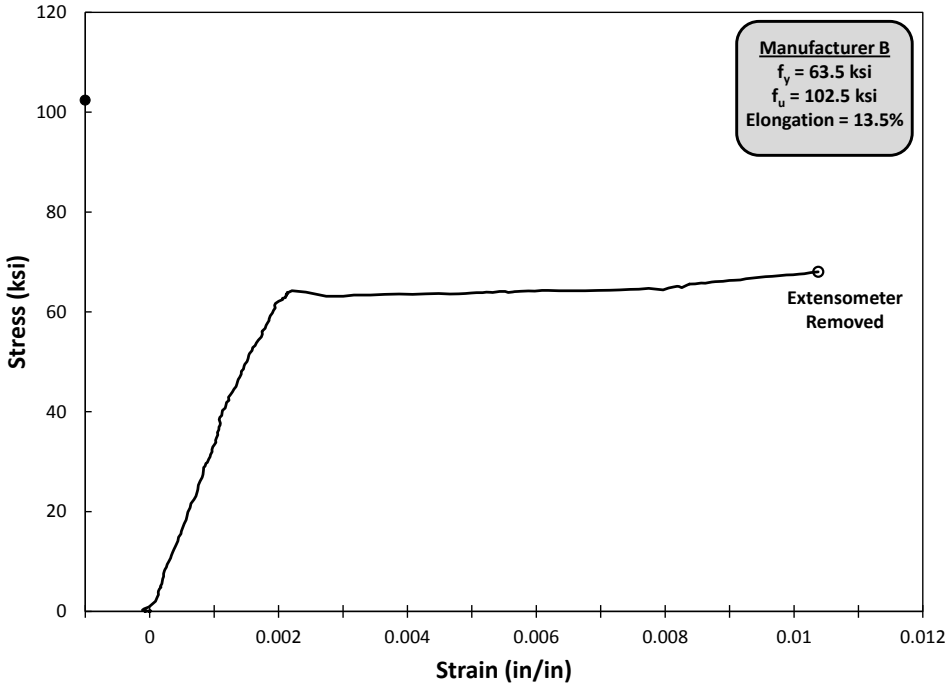

Figure B-2: Stress-Strain Response of Bar Sample – Manufacturer B

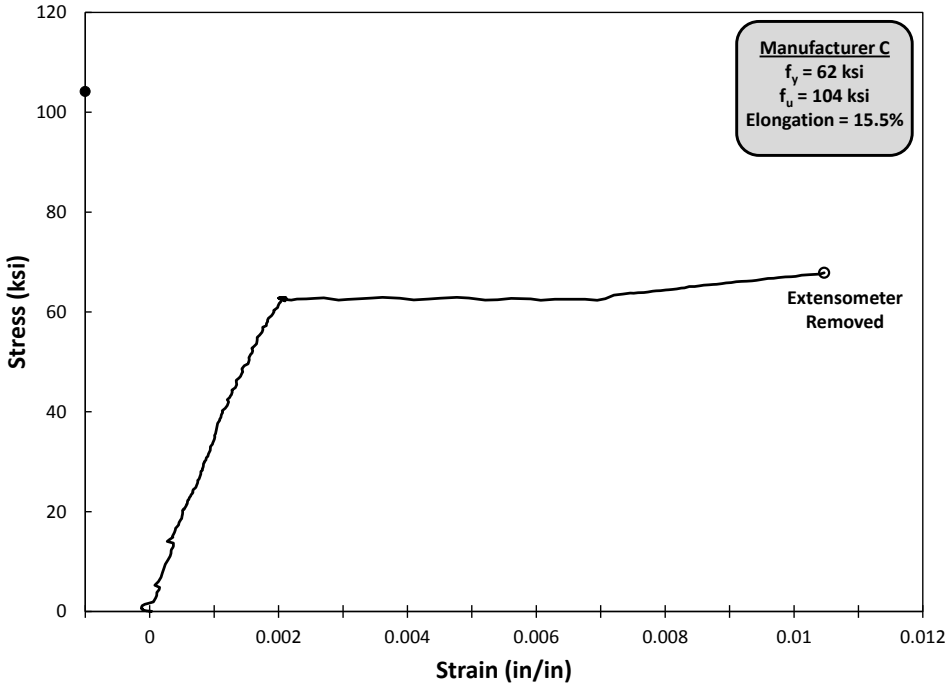

Figure B-3: Stress-Strain Response of Bar Sample – Manufacturer C

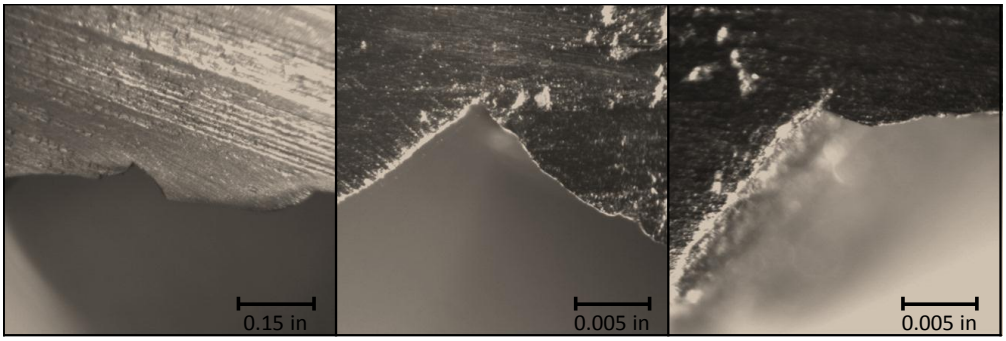

Figure B-4: Specimen I-C-90-1.5-W

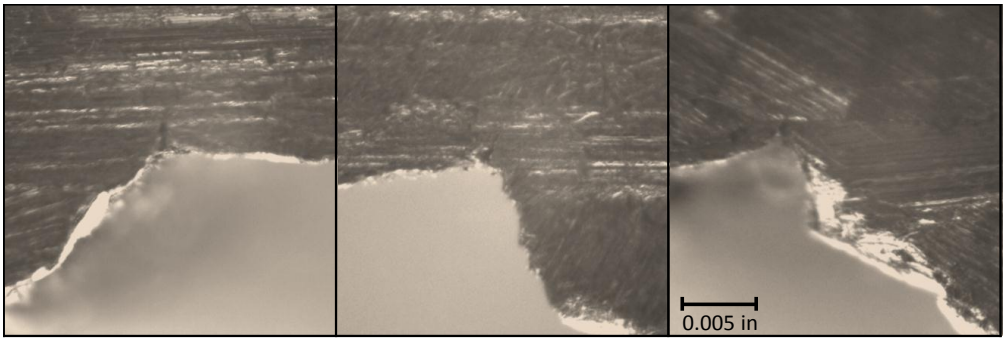

Figure B-5: Specimen I-C-135-1.5-W

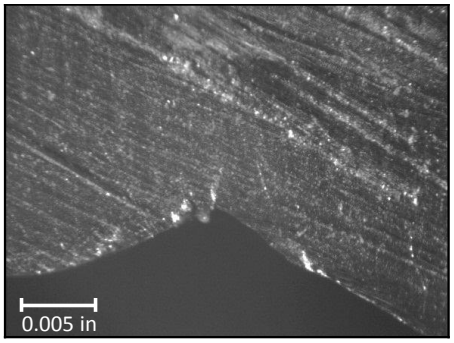

Figure B-6: Specimen I-C-135-2.25-W

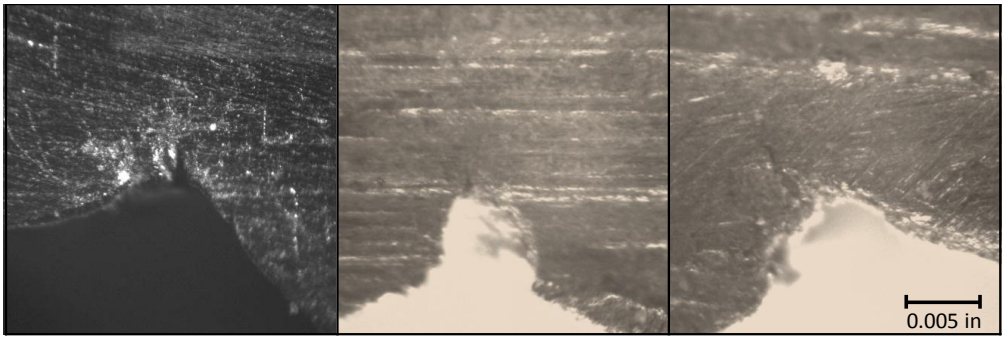

Figure B-7: Specimen I-C-180-2.188-W

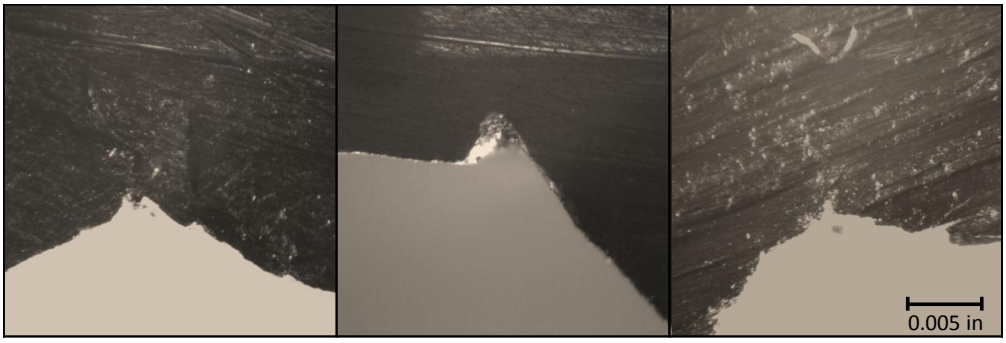

Figure B-8: Specimen II-C-90-1.5-W

References

1. *AASHTO Standard Specifications for Highway Bridges, Twelfth Edition*. Washington, D.C.: American Association of State Highway and Transportation Officials, 1977.

2. ACI. *ACI Standards 1963*. Detroit: American Concrete Institute, 1963.

3. ACI Committee 318-1971. *Building Code Requirements for Reinforced Concrete (ACI 318-71)*. Detroit: American Concrete Institute, 1971.

4. ACI Committee 318-2008. *Building Code Requirements for Reinforced Concrete (ACI 318-08)*. Farmington Hills: American Concrete Institute, 2008.

5. *ASTM A370 Standard Test Methods and Definitions for Mechanical Testing of Steel Products*. West Conshohocken: American Society for Testing and Materials, 2008.

6. *ASTM A615/A615M Standard Specification for Deformed and Plain Carbon-Steel Bars for Concrete Reinforcement*. West Conshohocken: American Society for Testing and Materials, 2009.

7. *ASTM A706/A706M Standard Specification for Low-Alloy Steel Deformed and Plain Bars for Concrete Reinforcement*. West Conshohocken: American Society for Testing and Materials, 2009.

8. *ASTM C157/C157M Standard Test Method for Length Change of Hardened Hydraulic-Cement Mortar and Concrete*. West Conshohocken: American Society for Testing and Materials, 2008.

9. *ASTM C597 Standard Test Method for Pulse Velocity Through Concrete*. West Conshohocken: American Society for Testing and Materials, 2009.

10. *ASTM C1293 Standard Test Method for Determination of Length Change of Concrete due to Alkali-Silica Reaction*. West Conshohocken: American Society for Testing and Materials, 2008.

11. *ASTM C1383 Standard Test Method for measuring the P-Wave Speed and the Thickness of Concrete Plates Using the Impact-Echo Method*. West Conshohocken: American Society for Testing and Materials, 2004.

12. Clark, L.A. *Critical Review of the Structural Implications of the Alkali-Silica Reaction in Concrete*. Crowthorne: Transport and Road Research Laboratory, Department of Transport, 1989. Contractor Report 169.

13. Daidai, T. and Torii, K. "A Proposal for Rehabilitation of ASR-Affected Bridge Piers with Fractured Steel Bars." *Proceedings of the Thirteenth International Conference on Alkali-Aggregate Recation in Concrete*. Trondheim. 2008.

14. Deschenes, D.J.; Bayrak, O. and Folliard, K.J. *ASR/DEF-Damaged Bent Caps: Shear Tests and Field Implications.* Austin: The University of Texas at Austin, 2009. TxDOT Report 12-8XXIA006.

15. Drimalas, T. "rockdale ash" Message to Zach Webb. 19 Nov. 2010. E-mail.

16. Erasmus, L.A. "Cold Straightening of Partially Embedded Reinforcing Bars – A Different View." *Concrete International* Vol. 3 No. 6 (1981): 47-52.

17. Folliard, K.J.; Barborak, R.; Drimalas, T.; Du, L.; Garber, S.; Ideker, J.; Ley, T.; Williams, S.; Juenger, M.; Fournier, B. and Thomas, M.D.A. *Preventing ASR/DEF in New Concrete: Final Report*. Austin: Center for Transportation Research, University of Texas at Austin, 2006. TxDOT Report 0-4085-5.

18. Hundy, B.B. "Accelerated Strain Ageing of Mild Steel." *Journal of the Iron and Steel Institute* Vol. 178 (1954): 34-38.

19. *JIS G 3112 Steel Bars for Concrete Reinforcement*. Tokyo: Japanese Industrial Standards, 2004.

20. JSCE. *Standard Specifications for Concrete Structures – Structural Performance Verification*. Tokyo: Japanese Society of Civil Engineers, 2002.

21. Kawashima, Y.; Kosa, K.; Goda, H. and Koroki, N. "Experimental Simulation of Reinforcing Bar Fracture by ASR." *Proceedings of the Thirteenth International Conference on Alkali-Aggregate Recation in Concrete*. Trondheim. 2008.

22. Kreitman, K. “Nondestructive Evaluation of Reinforced Concrete Structures Affected by Alkali-Silica Reaction and Delayed Ettringite Formation.” MS Thesis. University of Texas at Austin, 2011.

23. Kubo, Y.; Iketomi, O.; Nakashima, T. and Torii, K. “Experimental Study of Fracture of Reinforced Steel Bar in Concrete Structures Due to Alkali-Silica Reaction.” *Proceedings of Sixth CANMET/ACI International Conference on Durability of Concrete*. Thessaloniki. 2003. 637-652.

24. Kudder, R.J. and Gustafson, D.P. “Bend Tests of Grade 60 Reinforcing Bars.” *ACI Journal Proceedings* Vol. 80 No. 3 (1983): 202-209.

25. Miyagawa, T.; Seto, K.; Sasaki, K.; Mikata, Y.; Kuzume, K. and Minami, T. “Fracture of Reinforcing Steels in Concrete Structures Damaged by Alkali-Silica Reaction - Field Survey, Mechanism, and Maintenance.” *Journal of Advanced Concrete Technology* Vol. 4 No. 3 (2006): 339-355.

26. Nakamura, E. “RE: Japanese Standards” Message to Zach Webb. 20 July 2011. E-mail.

27. Nomura, N.; Kakio, T. and Matsuda, Y. “Investigation and Repair Process of Fractured Reinforcements Due to ASR.” *Proceedings of the Twelfth International Conference on Alkali-Aggregate Recation in Concrete*. Beijing. 2004. 1271-1276.

28. Stecich, J.P.; Hanson, J.M. and Rice, P.F. “Bending and Straightening of Grade 60 Reinforcing Bars.” *Concrete International* Vol. 6 No. 8 (1984): 14-23.

29. Torii, K.; Wasada, S.; Sasatani, T. and Minato, T. “A Survey of ASR-Affected Bridge Piers with Fracture of Steel Bars on Noto Expressway.” *Proceedings of the Thirteenth International Conference on Alkali-Aggregate Recation in Concrete*. Trondheim. 2008. 1017-1022.

30. Torii, K.; Yamato, H.; Andrade, O. and Tarui, T. “Mechanisms of Fracture of Steel Bars in ASR-Affected Bridge Piers.” Proceedings of the Eighth International Conference on Creep, Shrinkage and Durability of Concrete and Concrete Structures. Ise-Shima. 2008. 1139-1146.

31. TxDOT. *Item 421 Hydraulic Cement Concrete*. Austin: Texas Department of Transportation, 2004.

32. TxDOT. *Special Provision 421-028 Portland Cement Concrete*. Austin: Texas Department of Transportation, 1995.